A THEORETICAL STUDY OF THE STABILITY OF DISK GALAXIES AND PLANETARY RINGS

by

SUGURU ARAKI

SUBMITTED TO THE DEPARTMENT OF PHYSICS
IN PARTIAL FULFILLMENT OF THE
REQUIREMENTS FOR THE
DEGREE OF
DOCTOR OF PHILOSOPHY

at the

MASSACHUSETTS INSTITUTE OF TECHNOLOGY
SEPTEMBER 1985

Signature of Author . . . . . /

Department of Physics
August 2, 1985

Certified by . . . . . .

Professor Scott Tremaine
Thesis Supervisor

Accepted by . . . . . .

Professor George F. Koster
Chairman, Department Committee

To Jun Araki (January 6, 1952 — May 20, 1984)

TABLE OF CONTENTS

A THEORETICAL STUDY OF THE STABILITY OF DISK GALAXIES AND PLANETARY RINGS

by

SUGURU ARAKI

Submitted to the Department of Physics on August 2, 1985
in partial fulfillment of the requirements for the
Degree of Doctor of Philosophy in Physics

ABSTRACT

My Ph.D. thesis research consists of three independent projects regarding highly flattened astrophysical systems.

In the first project I investigate the existence of the two-stream instability in stellar systems using the collisionless Boltzmann equation. Here I distinguish the two-stream instability from other possible instabilities using a physically plausible definition. I consider only systems which are time-reversal invariant. Systems which consist of a pair of uniformly rotating counterstreams are studied both numerically and analytically in terms of linear perturbation theory. The main results are as follows: In counterstreaming Kalnajs disks, there is almost no two-stream instability for any mode of perturbation except $(n, m)=(3, 1)$. It is found from numerical analysis that the onset of the two-stream instability in Kalnajs disks seems to set in through a neutral mode: $\omega = 0$. We further conjecture that the one-armed mode may be unstable to the two-stream instability also in counterstreaming disks with differential rotation.

In the second project, in collaboration with Prof. Toomre, I explore the possibility of the hose instability in disk galaxies also using the collisionless Boltzmann equation. It is shown that a small-scale bending instability originates when there is a large velocity dispersion in the disk plane. A major consequence of this work is that the hose instability arises in any thin stellar disk if the vertical velocity dispersion is much smaller than the horizontal velocity dispersion. In general the critical degree of anisotropy depends on the unperturbed distribution function. For a thin non-rotating stellar system with an anisotropic Gaussian velocity distribution, it is found from detailed numerical analyses that the hose instability can be avoided at all wavelengths if the ratio of the vertical to horizontal velocity dispersion exceeds 0.293.

In the third project I investigate collisional transport processes in differentially rotating dense particle disks in terms of kinetic theory. In contrast to the stellar disk systems treated in the first and second projects, planetary rings are collision-dominated systems which consist mainly of icy rocks. My objective is to extend particle disk models of previous workers by taking the effect of nonlocal collisions into account. The nonlocality gives rise to several novel features since the fractional volume occupied by the ring particles is not small and so the or-

dinary kinetic theory is not accurate. As a possible way to improve on this, I employ the Enskog theory of dense hard sphere gases to study the dynamics of particle disks. Results from this theory permit us to understand the structure and stability of optically thick regions in planetary rings, such as the Saturnian B ring. Particularly, the vertical density profile is determined and possibilities of the viscous instability and liquid-solid phase transition are discussed.

Thesis Supervisor: Dr. Scott Tremaine
Title: Professor of Physics

CHAPTER 1.

THE TWO-STREAM INSTABILITY IN STELLAR SYSTEMS

THE TWO-STREAM INSTABILITY IN STELLAR SYSTEMS

Suguru Araki

Department of Physics, Center for Theoretical Physics

and Center for Space Research,

Massachusetts Institute of Technology,

Cambridge, Massachusetts 02139

ABSTRACT

The two-stream instability of self-gravitating stellar systems has been studied in the infinite homogeneous case by many authors. We review previous analyses, whose conclusions are often conflicting, and show that there is no two-stream instability in infinite homogeneous gravitating systems. In more realistic models the effects of finite size and rotation must be taken into account. In this paper we extend the stability analysis to finite, disk-like systems (counterstreaming Kalnajs disks). By comparing the stability diagram of a counterstreaming disk with that of a reference single-stream disk we can separate the two-stream instability from the Jeans instability inherent in any self-gravitating system. We find that there is very little parameter space in which a counterstreaming Kalnajs disk can exhibit the two-stream instability for any mode except $(n, m) = (3, 1)$. Using a WKB dispersion relation we examine the asymptotic behavior of high order modes in the stability diagram and we find that the results roughly agree with those from numerical analysis of the exact dispersion relation. Studying the modes for which the two-stream instability is possible, we find it is likely that the two-stream instability sets in through a neutral mode: $\omega = 0$. We further conjecture that there may be unstable one-armed ($m = 1$) modes in counterstreaming stellar systems with differential rotation.

I. INTRODUCTION

This paper investigates the possibility of an instability in stellar systems which is analogous to the two-stream instability of plasma physics. The classical two-stream instability appears when a beam of electrons passes through a plasma at rest. Suppose for simplicity that both the beam and the plasma consist of cold electrons so that the thermal motion of the particles is negligible compared with the beam speed. An inert background of protons ensures overall neutrality. The system is assumed to be infinite and homogeneous: both the beam and the plasma extend throughout space and the beam velocity is the same everywhere. The dispersion relation is then given by

$$\frac{\omega_p^2}{\omega^2} + \frac{\omega_b^2}{(\omega - \vec{k}\cdot\vec{V})^2} = 1, \tag{1}$$

where the longitudinal oscillation frequencies for the plasma and the beam are $\omega_p = \sqrt{4\pi n_p e^2/m}$ and $\omega_b = \sqrt{4\pi n_b e^2/m}$, n_p and n_b are the corresponding number densities, m is the electron mass, and $\vec{V}$ is the beam velocity relative to the plasma. In most practical cases the beam density is small compared with the plasma density so that $n_p \gg n_b$ or $\omega_p \gg \omega_b$. Then the presence of the beam only slightly affects the principal mode of longitudinal plasma oscillations: $\omega \cong \pm\omega_p$. However, in addition to this mode, another mode $\omega \cong \vec{k}\cdot\vec{V}$ appears which we call the drift mode. In general when a group of particles move as a whole with a velocity $\vec{V}$, we can define a collective mode $(\omega, \vec{k})$ with $\omega \cong \vec{k}\cdot\vec{V}$ associated with such a drift motion. The beam-plasma instability can be explained in terms of a coupling between the above two modes. If the frequencies and the wave vectors of the two modes match each other and if there exists an imbalance of energy contents between them, the excessive amount of energy in one mode is spent to excite another mode through the mode coupling. If further this energy input exceeds the decay rate of the mode inherent in the plasma, we can establish an

instability. In the beam-plasma system the instability criterion is given by

$$\frac{|\vec{k}\cdot\vec{V}|}{\omega_p} < \left[1+\left(\frac{n_b}{n_p}\right)^{1/3}\right]^{3/2}$$

The growth rate is generally a function of $|\vec{k}\cdot\vec{V}|/\omega_p$ and n_b/n_p, but the maximum growth rate is attained when $|\vec{k}\cdot\vec{V}| = \omega_p$ and is given by Buneman (1958):

$$\gamma_{\max} = \frac{\sqrt{3}}{2}\left(\frac{n_b}{2n_p}\right)^{1/3}\omega_p. \tag{2}$$

The existence of this instability has led to the suggestion that stellar systems containing two or more streams of stars may be unstable. It must be stressed at the start, however, that the analogy between stellar systems and electrostatic plasmas has two major limitations:

1. The maximum growth rate of the two-stream instability due to an electron beam in a plasma is proportional to ω_p. To construct the analogous stellar system we replace $n_p e^2/m$ by $-G\rho$. Thus the growth rate γ becomes purely imaginary, and the instability disappears.

2. In an infinite, homogeneous, Maxwellian, electrostatic plasma oscillations of all wavelengths are damped, but in the corresponding stellar system oscillations are damped if $k > k_J$ but grow if $k < k_J$, where the Jeans wavenumber is

$$k_J = \sqrt{\frac{4\pi G\rho}{\sigma^2}} \tag{3}$$

and σ is the root mean square velocity dispersion in one dimension. Therefore, in stellar systems the Jeans instability is already present, and any instability appearing in stellar systems with two streams may be simply a modified Jeans instability rather than a two-stream instability.

In this paper we distinguish Jeans and two-stream instabilities using the following physically plausible definition. We consider only systems which are

time-reversal invariant, i.e., in which the phase space density of the stellar system containing two streams can be written

$$F_2(\vec{x},\vec{v}) = \frac{1}{2}\left[f(\vec{x},\vec{v}) + f(\vec{x},-\vec{v})\right]. \tag{4}$$

The analogous single-stream system is described by the phase space density

$$F_1(\vec{x},\vec{v}) = f(\vec{x},\vec{v}). \tag{5}$$

We shall say that there exists a two-stream instability if the system described by $F_2(\vec{x},\vec{v})$ is unstable or overstable but the system described by $F_1(\vec{x},\vec{v})$ is stable.[1]

There have been a number of earlier analyses of the two-stream instability in infinite homogeneous gaseous and stellar systems. We comment on and summarize these results in §II. In §III we extend these analyses to investigate the two-stream instability in uniformly rotating axisymmetric systems. §IV contains a summary and discussion of the relevance of the two-stream instability to differentially rotating stellar systems. We shall not discuss the two-stream instability between gaseous and stellar systems, which has been investigated in detail by Sweet (1963), Talwar and Kalra (1966), Suchkov (1969), Kato (1973), Ikeuchi, Nakamura and Takahara (1974) and others.

[1] A system is called stable if $\mathrm{Im}\omega \leq 0$ with respect to some mode $(\omega,\vec{k})$. If $\mathrm{Im}\omega > 0$, it is called unstable when $\mathrm{Re}\omega = 0$ and overstable when $\mathrm{Re}\omega \neq 0$.

II. INFINITE HOMOGENEOUS SYSTEM

II.1. Results

Unlike electrostatic plasmas, which can be neutral due to the cancellation of positive and negative charges, infinite homogeneous stellar systems can never be in static equilibrium. Nevertheless, it is useful to analyze their stability using the assumption that the unperturbed homogeneous system is in equilibrium. This is the so-called Jeans swindle. The analysis below has been given by a number of authors such as Sweet (1963), Lynden-Bell (1967) and Ikeuchi, Nakamura and Takahara (1974), but we repeat it here for reference.

Consider two infinite homogeneous stellar systems 1 and 2 whose mean velocities are $\vec{V}_1 = \vec{V}/2$ and $\vec{V}_2 = -\vec{V}/2$, respectively. Assume further that the unperturbed distribution function f_0 is the sum of two Gaussians f_{01}, f_{02} with unperturbed mass densities ρ_{01}, ρ_{02} and velocity dispersions c_1, c_2:

$$f_0(\vec{v}) = \sum_{i=1}^{2} f_{0i}(\vec{w}_i), \tag{6}$$

where

$$\vec{w}_i = \vec{v} - \vec{V}_i \tag{7}$$

and

$$f_{0i} = \frac{\rho_{0i}}{(\sqrt{2\pi}c_i)^3} \exp\left(-\frac{w_i^2}{2c_i^2}\right). \tag{8}$$

As stated before, the Jeans swindle consists of assuming that the unperturbed potential ψ_0=constant or $\nabla\psi_0 = 0$ (even though this apparently contradicts Poisson's equation $\nabla^2\psi_0 = 4\pi G\rho_0$). Then the linearized Boltzmann and Poisson equations read

$$\frac{\partial f_1}{\partial t} + (\vec{v}\cdot\nabla)f_1 - \left(\nabla\psi_1 \cdot \frac{\partial}{\partial \vec{v}}\right) f_0 = 0 \tag{9}$$

and

$$\nabla^2\psi_1 = 4\pi G\rho_1, \tag{10}$$

where the perturbed potential, distribution function, density are denoted by ψ_1, f_1, ρ_1, respectively and

$$\rho_1 = \int f_1 d\vec{v}. \tag{11}$$

Assuming perturbations of the form

$$A_1 \propto A\exp\left[i(\vec{k}\cdot\vec{x} - \omega t)\right], \tag{12}$$

where the frequency ω is generally complex and the wave vector $\vec{k}$ is real, we find the dispersion relation from equations (9), (10) and (11) as

$$k^2 = -4\pi G\int \frac{\vec{k}\cdot(\partial f_0/\partial\vec{v})}{\vec{k}\cdot\vec{v} - \omega}d\vec{v} = -4\pi G\sum_{i=1}^{2}\int \frac{\vec{k}\cdot(\partial f_{0i}/\partial\vec{w}_i)}{\vec{k}\cdot(\vec{w}_i + \vec{V}_i) - \omega}d\vec{w}_i. \tag{13}$$

Introducing the component of $\vec{w}_i$ parallel to $\vec{k}$ as $w_{i\|} = \vec{w}_i\cdot\hat{k}$, where $\hat{k} = \vec{k}/k$ and $|\vec{k}| = k \geq 0$, and carrying out the two-dimensional integration over the perpendicular component, we find

$$k^2 = -4\pi G\sum_{i=1}^{2}\int_{-\infty}^{\infty}\frac{k(\partial g_i/\partial w_{i\|})dw_{i\|}}{k(w_{i\|} + V_{i\|}) - \omega} = -4\pi G\sum_{i=1}^{2}\int_{-\infty}^{\infty}\frac{g_i(w_{i\|})dw_{i\|}}{(w_{i\|} + V_{i\|} - \omega/k)^2}, \tag{14}$$

where

$$g_i(w_{i\|}) = \frac{\rho_{0i}}{\sqrt{2\pi}c_i}\exp\left(-\frac{w_{i\|}^2}{2c_i^2}\right), \tag{15}$$

and

$$V_{i\|} = \vec{V}_i\cdot\hat{k}. \tag{16}$$

In terms of the plasma dispersion function[2] (Fried and Conte 1961)

$$Z(\varsigma) = \frac{1}{\sqrt{\pi}}\int_{-\infty}^{\infty}\frac{\exp(-z^2)}{z - \varsigma}dz, \tag{17}$$

[2] The integral representation (17) is valid only in the upper half ς plane, but it can be analytically continued into the real axis and lower half ς plane by deforming the integration contour in such a way that Z is well-defined in the whole ς plane.

the dispersion relation (14) is written as

$$-2k^2 = \sum_{i=1}^{2} k_{Ji}^2 Z'\left[\frac{1}{\sqrt{2}}\left(\frac{\omega}{kc_i} - \frac{V_{i\parallel}}{c_i}\right)\right], \tag{18}$$

where the Jeans wavenumber for each subsystem i ($i = 1, 2$) is defined by

$$k_{Ji}^2 = \frac{4\pi G\rho_{0i}}{c_i^2}. \tag{19}$$

The real and imaginary parts of equation (18) yield

$$-2k^2 = k_{J1}^2 \mathrm{Re}Z'\left(\frac{x - x_0 + iy}{\sqrt{2}}\right) + k_{J2}^2 \mathrm{Re}Z'\left(\beta\frac{x + x_0 + iy}{\sqrt{2}}\right), \tag{20-1}$$

$$0 = k_{J1}^2 \mathrm{Im}Z'\left(\frac{x - x_0 + iy}{\sqrt{2}}\right) + k_{J2}^2 \mathrm{Im}Z'\left(\beta\frac{x + x_0 + iy}{\sqrt{2}}\right), \tag{20-2}$$

where

$$x = \frac{\mathrm{Re}\omega}{kc_1}, \qquad y = \frac{\mathrm{Im}\omega}{kc_1}, \qquad x_0 = \frac{\vec{V}_1 \cdot \hat{k}}{c_1} = \frac{V}{2c_1}, \qquad \beta = \frac{c_1}{c_2}.$$

The system of equations (20) must be solved for x and y for fixed values of $(k/k_{J1})^2$, $(k/k_{J2})^2$, x_0 and β.

Assume, for simplicity, that $c_1 = c_2$ and $k_{J1} = k_{J2}$. Then we have a two-dimensional parameter space ($V/c_1 = 2x_0, [k/k_{J1}]^2$), which is to be divided into three regions as defined in footnote 1. The result is shown in Figure 1 (Fig. 3[3] in Ikeuchi, Nakamura and Takahara 1974).

---

[3] There is a mistake in Fig. 3 in Ikeuch, Nakamura and Takahara (1974): The curve corresponding to $x = y = 0$ is

$$\left(\frac{k}{k_{J1}}\right)^2 = 2 - 4\xi e^{-\xi^2}\int_0^{\xi} e^{t^2} dt,$$

where $\xi = x_0/\sqrt{2}$ and it has an intercept with the horizontal axis at $V/c_1 = 2.61$, above which value no unstable mode exists for any wavenumber.

Now we will show that, according to our definition given in §I, there is no two-stream instability in the counterstreaming stellar system described by equation (6). Our reference system with a single stream at a mean velocity $\vec{V}/2$ has a Gaussian velocity distribution $2f_{01}(\vec{w}_1)$ so that its dispersion relation is

$$-k^2 = k_{J1}^2 \mathrm{Re} Z'\left(\frac{x - x_0 + iy}{\sqrt{2}}\right), \tag{21-1}$$

$$0 = \mathrm{Im} Z'\left(\frac{x - x_0 + iy}{\sqrt{2}}\right). \tag{21-2}$$

This system has a Jeans wavenumber $\sqrt{2}k_{J1}$ since its mass is equal to the total mass of the counterstreaming system. The stability diagram of the single stream system is easily drawn in the $(V/c_1,\ [k/k_{J1}]^2)$ space. It has a neutral line $(k/k_{J1})^2 = 2$, on and above which the system is stable, and below which it is unstable for $V = 0$ and overstable for $V \neq 0$. Comparison between the two stability diagrams shows that the instability (either unstable or overstable) region in Figure 1 is completely contained by that in the single stream stability diagram. Thus, there is no two-stream instability in the counterstreaming system. It is to be stressed that, as the relative speed V becomes much larger than the velocity dispersion $c_1 = c_2$, the two streams become independent and all we see in Figure 1 is a convected Jeans instability.

II.2. Other Authors

A number of somewhat confusing claims about the existence of the two-stream instability in stellar systems have been made by other workers.

Sweet (1963) was the first to consider the stability of homogeneous, interpenetrating systems of gas and stars with relative streaming motions. He treated three cases:

1. gas moving through a Maxwellian stellar system at rest;

2. two Maxwellian stellar systems interpenetrating each other with equal and opposite mean velocities;

3. two Maxwellian stellar streams with equal and opposite velocities in the presence of a stationary gaseous background.

Most of Sweet's attention was directed to the interaction of gas and star streams (case 1 and case 3); we shall not examine these results since we are concerned with the two-stream instability in stellar systems. For case 2 Sweet derived the correct dispersion relation (18), but did not examine its consequences, as he was mainly concerned with the interactions of gaseous and stellar streams.

Lynden-Bell (1967) was the first to state clearly that no two-stream instability arose in a homogeneous stellar system consisting of two Maxwellian streams. He also investigated non-Maxwellian star streams, making use of Nyquist diagrams, and found that a two-stream instability could occur only when at least one of the streams had a very flat-topped velocity distribution.

Harrison (1970) also clearly understood that the only instability in a counterstreaming stellar system is the Jeans instability, and that star-streaming does not introduce any new form of instability although it affects the quantitative location of the stability boundary.

Hohl (1971) claimed to find a two-stream instability in a planar stellar system using analytic arguments and numerical experiments. His analytic results[4] are misleading because he uses the fluid equations rather than the Vlasov equation, and the instabilities of counterstreaming fluids are very different from collisionless

[4] There are some mistakes in Hohl's equation (3): it should read

$$\omega^{*2} = k^*\{[k^*(V^{*2}+1)-1] \pm [4V^{*2}k^*(k^*-1)+1]^{1/2}\},$$

with proper definitions $k_J = 2\pi GmN/\sigma^2$, $\omega_J = k_J\sigma$, $k^* = k/k_J$ and $\omega^* = \omega/\omega_J$.

systems (Ikeuchi, Nakamura and Takahara 1974). His numerical results appear to be correct, but Hohl's interpretation of them is misleading, and in fact they support our claim that there is no two-stream instability in homogeneous Maxwellian stellar systems: as the streaming velocity was increased Hohl found that instabilities parallel to the streaming direction were suppressed, leading to a filamentary structure caused by Jeans instabilities in the transverse direction.

Marochnik and Suchkov (1969), Mark (1976), Bertin and Mark (1980) all found a kind of two-stream instability between the disk and the halo, but this kind of instability is very different from what we discuss here, because their systems are not time-reversal invariant.

Mikhailovskii and Fridman (1972), and Polyachenko and Shukhman (1980) claimed to find a two-stream instability but in an extremely artificial system, i.e., collisionless particles which rotate uniformly in a cylinder of infinite length and finite radius and have a velocity distribution along the cylindrical axis consisting of a low density beam and a high density background.

Nakamura (1978) considered a two-component rotating disk model to find constraints on the velocity dispersion of the missing mass in the solar neighborhood, but his results are based on the gas dynamical approximation and there is no relative angular velocity between the observed mass component and the missing mass component so that his model is not adequate to study the two-stream instability of two-component stellar disks.

In conclusion, there is no two-stream instability for an infinite homogeneous stellar system containing two Maxwellian velocity distributions, but a two-stream instability is possible in some cases if the velocity distribution is non-Maxwellian (Lynden-Bell 1967).

III. STABILITY OF UNIFORMLY ROTATING STELLAR DISKS

In this section we analyze the linear dispersion relation of counterstreaming Kalnajs disks both numerically (§**III.1**) and analytically (§**III.2**), the latter in terms of the WKB approximation. Complete understanding of the stability of the system would be possible with the help of N-body experiments.

III.1. Numerical Analysis

Kalnajs (1972) disks have the surface density

$$\sigma_0(r) = \begin{cases} (3M/2\pi R^2)\sqrt{1-r^2/R^2} & r \le R; \\ 0 & r > R. \end{cases} \tag{22}$$

and potential

$$\mathcal{V}_0(r) = \frac{1}{2}\Omega_0^2 r^2 \quad \text{for} \quad r \le R, \tag{23}$$

where

$$\Omega_0 = \sqrt{\frac{3\pi GM}{4R^3}}, \tag{24}$$

G is the gravitational constant, M is the total mass of the disk and R is the radius of the outer edge. The mean angular speed, Ω, of the stars in a Kalnajs disk is independent of position, and relative to this mean speed, the stars have an isotropic velocity dispersion in the disk plane, whose components are

$$\langle c_r^2 \rangle = \langle c_\theta^2 \rangle = \frac{1}{3}(\Omega_0^2 - \Omega^2)(R^2 - r^2). \tag{25}$$

As an unperturbed distribution function Kalnajs chooses

$$\Psi_0(c_r, c_\theta, \Omega, r) = \begin{cases} \left[\sigma_0(r)/2\pi a(\Omega, r)\right]\left[a^2(\Omega, r) - \tau^2\right]^{-1/2} & \tau < a; \\ 0 & \tau \ge a. \end{cases} \tag{26}$$

where the polar coordinates (τ, s) are introduced in the two-dimensional velocity space:

$$c_r = R\Omega_0 \tau \cos s \qquad \text{and} \qquad c_\theta = R\Omega_0 \tau \sin s. \tag{27}$$

The maximum value of τ is given by

$$a(\Omega, r) = \varsigma\sqrt{1 - C^2}, \tag{28}$$

where

$$\varsigma = \sqrt{1 - \frac{r^2}{R^2}}, \tag{29}$$

and the coldness C of the disk is defined by

$$C = \frac{|\Omega|}{\Omega_0}. \tag{30}$$

Since Ω can take on any value between $-\Omega_0$ and Ω_0, the coldness parameter C ranges between zero and unity. The Ostriker-Peebles parameter[5] t is related to C by

$$t = \frac{1}{2}C^2. \tag{31}$$

It is easy to show that Ψ_0 is a self-consistent solution of the Vlasov and Poisson equations, with a surface density given by equation (22).

Kalnajs (1972) analyzed the stability of stellar disks using the linearized Vlasov equation. Just as for the fluid Maclaurin disks, the normal modes have potential distributions which are described by associated Legendre polynomials, $P_n^m(\varsigma)$. However, the dispersion relations are very different in the two cases. In particular, for a given (n, m) a Kalnajs disk has up to $(n+1)$ different modes with different frequencies, while a Maclaurin disk has only three.

Linear combinations of the functions defined by equation (26) for different Ω's can be constructed to form more general solutions; in particular, we can construct a composite model with the weighted distribution function

$$\widetilde{\Psi}_0 = \Psi_+ + \Psi_- \tag{32}$$

[5] t is defined as the ratio of the rotational kinetic energy T to minus the energy of self-gravitation W (Ostriker and Peebles 1973).

in order to determine whether the two-stream instability is present in Kalnajs disks. Here we have introduced the notation

$$\Psi_{\pm} = \frac{1}{2}\Psi_0(\pm\Omega). \tag{33}$$

It is clear that $\widetilde{\Psi}_0$ will also be a self-consistent solution of the Vlasov and Poisson equations. The dispersion relation for the distribution function (32) is given by

$$\frac{1}{2}\lambda(n,m,\Omega,\omega) + \frac{1}{2}\lambda(n,m,-\Omega,\omega) = 1, \tag{34}$$

where $\lambda(n,m,\Omega,\omega)$ is given by Kalnajs (1972):

$$\lambda(n,m,\Omega,\omega) = \frac{2}{\pi}\frac{\Gamma(l+1/2)\Gamma(m+1)}{\Gamma(l+m+1)2^m}\sum_{c=0}^{l}\sum_{d=-c}^{c}\sum_{k=-d}^{m-d}(-1)^{c+d}\frac{m\Omega/\Omega_0 - m + 2k}{\omega/\Omega_0 - m + 2k}$$
$$\times \frac{\Gamma(m+l+c+1/2)(1-\Omega/\Omega_0)^{c+d+k-1}(1+\Omega/\Omega_0)^{m+c-d-k-1}}{\Gamma(c-d+1)\Gamma(c+d+1)\Gamma(l-c+1)\Gamma(k+d+1)\Gamma(m-k-d+1)} \tag{35}$$

where

$$l = \frac{n-m}{2}, \tag{36}$$

and l, m, n are non-negative integers, but $n^2+m^2 \neq 0$. For convenience we define

$$\Lambda(n,m,\Omega,\omega) = \frac{1}{2}\lambda(n,m,\Omega,\omega) + \frac{1}{2}\lambda(n,m,-\Omega,\omega) - 1. \tag{37}$$

Λ is an even function of ω. If n is even, Λ has n simple poles at $\omega = -n, -(n-2), \ldots, -2, 2, \ldots, n-2, n$, and if n is odd, it has $n+1$ simple poles at $\omega = -n, -(n-2), \ldots, -1, 1, \ldots, n-2, n$. Therefore, for even n there are generally n complex roots which satisfy $\Lambda = 0$, whereas for odd n there are $n+1$ complex roots. Our goal is to determine the number of real roots of the equation $\Lambda(\omega) = 0$ as a function of the coldness C for various modes (n, m). If all the roots are real, the mode (n, m) is stable. We have determined the stability of all the modes with $l \leq 5$ and $m \leq 10$ numerically. [The modes with lowest and highest values of n examined are (1,1) and (20,10).] The regions of instability of the modes with

$l \leq 5$ and $m \leq 5$ are indicated by thick horizontal lines in Figure 2, which is to be compared with the instability regions for the single stream disk indicated by thin horizontal lines. (Compare Fig. 1 of Kalnajs 1972).

Here are some remarks on Figure 2. In general instability regions of the counterstreaming Kalnajs disk are much scarcer than those of its single stream counterpart, and localized around the cold end $C \approx 1$ except for the low l modes ($l = 0$ or 1) where there are short instability regions at the hot end $C \approx 0$. At the hot end instability regions have some complex structure when the azimuthal mode number m is smaller than 5, but after attaining a small maximum length they generally become shorter and seem to vanish asymptotically as m increases. As for the axisymmetric modes, the instability regions are identical with those of the single stream counterpart as they should be, because reversing the velocity of half the stars in the single stream disk does not affect the axisymmetric dynamics.

According to our definition of the two-stream instability, among the modes we have examined only the $(n, m) = (3,1)$, (9,1), (11,3), (11,1), (13,3) modes are unstable to the two-stream instability. The two-stream instability is present over the following intervals of C:

Mode (n, m)	Regions of Two-stream Instability
(3,1)	$0.7071 < C < 0.8029$
(9,1)	$0.8935 < C < 0.8942$
(11,1)	$0.9185 < C < 0.9198$
(11,3)	$0.8942 < C < 0.9107$
(13,3)	$0.9267 < C < 0.9319$

(38)

Each interval shown above is a part of an overstable or unstable interval of the counterstreaming Kalnajs disk. At the left endpoint of each interval a pair of frequencies merge to become zero while the other frequencies remain real and

finite. The fact that the number of real frequencies decreases by two at these left end points implies that the emerging pair of complex frequencies are purely imaginary since Λ is an even function of ω. It can be shown numerically that all the remaining roots stay real in the above intervals. Thus the counterstreaming Kalnajs disk is not overstable but unstable in all intervals shown in equation (38).

In the cases of the (3,1), (9,1), (11,1) modes, as we increase the coldness C, the two-stream instability sets in at $C = 0.7071, 0.8942, 0.9185$, respectively when a pair of real frequencies with the same magnitude become zero and then appear as a pair of purely imaginary frequencies. As C increases further, the growth rates become larger and reach 0.5150, 0.1665, 0.3172 (in units of Ω_0) at $C = 0.8029$, 0.8942, 0.9198, respectively. Above these values of C the two-stream instability is no longer considered to be present since the single stream stellar system is also unstable.

As for the (11,3), (13,3) modes each interval shown in equation (38) is completely contained by unstable intervals of the counterstreaming Kalnajs disk $0.8434 < C < 0.9296$, $0.8745 < C < 0.9540$, respectively. In each case, as C increases, a pair of purely imaginary frequencies appear at $C = 0.8434$, 0.8745, and disappear at $C = 0.9296, 0.9540$, respectively. In between there is an interval in which the single stream system is stable and only the counterstream system is unstable, and it is this interval which we identify in equation (38) as the region of two-stream instability. The growth rate of the two-stream instability decreases from 0.6604 to 0.5950 as C varies from 0.8942 to 0.9107 for the (11,3) mode, and from 0.9108 to 0.8873 as C varies from 0.9267 to 0.9319 for the (13,3) mode.

The above observations lead us to a conjecture that the occurrence of two-stream instability in our counterstreaming stellar system may be closely related to the presence of a neutral mode: $\omega = 0$. Although it is hard to prove this

conjecture, it seems more natural to assume $\mathrm{Re}\omega = 0$ rather than non-zero $\mathrm{Re}\omega$ at the onset of instability since we have confined ourselves to time-reversal invariant systems. Indeed, no two-stream instability was found within the unstable or overstable intervals with non-zero left endpoint frequencies.

III.2. Short Wavelength Perturbation Analysis

In the last section we carried out a normal mode analysis to investigate the stability of counterstreaming Kalnajs disks. In order to confirm and extend the above results, we here treat the same problem using the WKB approximation and obtain a dispersion relation which is valid for high order modes.

We impose a potential perturbation of the following form

$$\mathcal{V}_1(r,\theta,z=0,t) = A(r)\exp\{i[m\theta + \Phi(r,t) - \omega t]\}, \tag{39}$$

where $A(r)$ and $\Phi(r,t)$ are real functions. Equation (39) is identified as a gravitational potential with m identical spiral arms. Introducing the radial wavenumber

$$k(r,t) = \frac{\partial \Phi}{\partial r}, \tag{40}$$

we can write the condition under which the WKB approximation is valid as $|k|r \gg 2\pi$. If the spiral wave pattern is assumed to rotate in the positive θ direction, $k > 0$ corresponds to trailing waves and $k < 0$ to leading waves. If the arms are tightly wound, the radial distance between arms is approximately $2\pi/|k|$. In the WKB approximation, if we drop terms of the order of $1/(|k|r)$, the Poisson equation reduces to a simple relation between the potential perturbation and the density response:

$$\mathcal{S}_1 = -\frac{|k|}{2\pi G}\mathcal{V}_1. \tag{41}$$

Equation (41) shows that the surface density response must have the same sinusoidal dependence as the imposed potential. Thus we may write

$$S_1(r,\theta,t) = (\hat{\sigma}_+ + \hat{\sigma}_-)\exp\{i[m\theta + \Phi(r,t) - \omega t]\}, \tag{42}$$

where $\hat{\sigma}_\pm(r)$ are the real amplitudes of surface density perturbations for the stellar component with mean angular velocity $\pm\Omega$. Hereafter Ω is assumed to be positive.

In order to solve the linearized Vlasov equation and to find the perturbed distribution function, we also assume that the radial and tangential velocity dispersions are much smaller than the mean circular speed so that the unperturbed orbits satisfy the epicyclic approximation. Then, under both WKB and epicyclic approximations, the solution of the linearized Vlasov equation can be obtained analytically (Lin, Yuan and Shu 1969):

$$\hat{\sigma}_\pm = \int_0^a d\tau \int_0^{2\pi} ds\tau\Psi_{1\pm} = \frac{2A}{(R\Omega_0)^2}\int_0^a d\tau\int_0^{2\pi} ds\tau(1-q_\pm)\frac{\partial\Psi_0}{\partial(\tau^2)}, \tag{43}$$

where Ψ_0 is given by equation (26) and

$$\begin{aligned} q_\pm &= q(\alpha\tau, s, \nu_\pm) \\ &= \frac{1}{2\pi}\frac{\nu_\pm\pi}{\sin\nu_\pm\pi}\int_{-\pi}^{\pi} dx \exp\left\{i\left[\nu_\pm x + 2\alpha\tau\sin\left(s-\frac{x}{2}\right)\cos\frac{x}{2}\right]\right\}, \end{aligned} \tag{44}$$

$$\alpha = \frac{k(r)R}{2C}, \tag{45}$$

$$\nu_\pm = \frac{\omega \mp m\Omega}{\kappa}. \tag{46}$$

Here the epicyclic frequency $\kappa(r)$ is defined by

$$\kappa^2 = 2\Omega\left(2\Omega + r\frac{d\Omega}{dr}\right) \tag{47}$$

and $\kappa = 2\Omega$ in the case of uniform rotation. In order to remove the nonintegrable singularity of

$$\frac{\partial\Psi_0}{\partial(\tau^2)} = \frac{\Psi_0}{2(a^2-\tau^2)} \tag{48}$$

at the upper limit $\tau = a$, we approximate Ψ_0 by a sequence $\{\Psi_{0n}\}$ of distributions with continuous derivatives which converges to Ψ_0 in the limit $n \to \infty$ (Kalnajs 1972). We first integrate

$$\int_0^a \tau(1-q_\pm)\frac{\partial \Psi_{0n}}{\partial(\tau^2)}d\tau$$

by parts over τ^2, noting that

$$\Psi_{0n}(\tau = a) = 0 \qquad \text{and} \qquad q(\tau = 0) = 1, \tag{49}$$

and then take the limit to find

$$\hat{\sigma}_\pm = \frac{A}{(R\Omega_0)^2}\int_0^{2\pi} ds \int_0^a d\tau \Psi_0 \frac{\partial q}{\partial \tau}. \tag{50}$$

Integrating over s and then τ, we obtain the density response to the spiral gravitational perturbation

$$\hat{\sigma}_\pm = -\frac{A}{\pi^2 G R\varsigma(1-C^2)}\left[1 - \frac{\nu_\pm \pi}{\sin \nu_\pm \pi} H_{\nu_\pm}(2\alpha a)\right], \tag{51}$$

where

$$H_\nu(y) = \frac{2}{\pi}\int_0^{\pi/2} dx \cos(2\nu x)\cos(y\cos x) \tag{52}$$

and we have used the equations (22), (24) and (28). Combining equation (41) with equation (51), we reach the WKB dispersion relation for a pair of counterstreaming Kalnajs disks:

$$\frac{\pi}{2}\frac{y^2|k|R\varsigma}{y^2 + (|k|R\varsigma)^2} = 2 - \frac{\nu_+\pi}{\sin\nu_+\pi}H_{\nu_+}(y) - \frac{\nu_-\pi}{\sin\nu_-\pi}H_{\nu_-}(y), \tag{53}$$

where

$$y = 2\alpha a = kR\varsigma\sqrt{\frac{1}{C^2} - 1}. \tag{54}$$

It has been shown by Hunter (1963) that the elementary surface densities

$$\sigma_n^m = \frac{1}{\varsigma}P_n^m(\varsigma)\exp[i(m\theta - \omega t)] \tag{55}$$

or their corresponding elementary potentials

$$\Psi_n^m = 2\pi^2 G R \gamma_n^m P_n^m(\zeta) \exp[i(m\theta - \omega t)] \tag{56}$$

form a complete set of normal modes, where γ_n^m are constants depending on m and n. Since the associated Legendre polynomial $P_n^m(\zeta)$ has an asymptotic expansion

$$P_n^m(\zeta) = \frac{\Gamma(n+m+1/2)}{\Gamma(n+3/2)} \left(\frac{\pi}{2}\sqrt{1-\zeta^2}\right)^{-1/2} \times \cos\left[\left(n+\frac{1}{2}\right)\arccos\zeta - \frac{\pi}{4} + \frac{m\pi}{2}\right] + O\left(\frac{1}{n}\right), \tag{57}$$

where $0 < \arccos\zeta < \pi$ (Abramowitz and Stegun 1964), we have, by equation (44),

$$k(r) = \left(n+\frac{1}{2}\right)\frac{d}{dr}\arccos\zeta = \frac{n+1/2}{R\zeta}.$$

Therefore,

$$|k|R\zeta \approx n + \frac{1}{2} \qquad \text{for} \qquad n \gg 1. \tag{58}$$

According to the stability diagram shown in Figure 2 the onset of the two-stream instability in a counterstreaming Kalnajs disk seems to occur through a neutral mode. Therefore, we shall set $\omega = 0$ in equation (53) to look for the critical coldness parameter at the onset of instability. When $\omega = 0$ and $\kappa = 2\Omega$, we find $\nu_- = -\nu_+ = m/2$. Noting the symmetry properties of the function (52) $H_\nu(y) = H_{-\nu}(y) = H_\nu(-y)$, we can simplify equation (53):

$$\frac{\pi}{4}\frac{y^2(n+1/2)}{y^2+(n+1/2)^2} = 1 - \frac{m\pi/2}{\sin(m\pi/2)} H_{m/2}(y). \tag{59}$$

For each mode (n, m) we will solve equation (59) for y and thus for the critical value of C by

$$C_{crit} = \frac{n+1/2}{\sqrt{y^2+(n+1/2)^2}}, \tag{60}$$

which follows from equation (54).

The dimensionless frequency $\nu_{\pm}$ can take on only values between -1 and 1 since the density response cannot support the imposed potential perturbation for $|\nu_{\pm}| \geq 1$ in stellar disks. Since $\nu_{-} = -\nu_{+} = m/2$, only modes with $m = 0$ and $m = 1$ satisfy the condition for supporting the waves. According to the WKB analysis, therefore, the counterstreaming Kalnajs disk cannot support waves with $m \geq 2$ modes: they are evanescent. For $m = 0$ and $m = 1$ modes the roots of equation (59) are found numerically and the corresponding values of the critical coldness parameter are obtained from equation (60). Results are listed in the following:

Mode (n,m)	C_{crit} from Eqs. (59), (60)	Instability Regions shown in Figure 2
(4,0)	0.7781	$0.818 < C < 1$
(6,0)	0.8522	$0.852 < C < 1$
(8,0)	0.8923	$0.889 < C < 1$
(10,0)	0.9173	$0.914 < C < 1$
(3,1)	0.6393	$0.707 < C < 1$
(5,1)	0.7915	$0.794 < C < 1$
(7,1)	0.8598	$0.855 < C < 1$
(9,1)	0.8979	$0.894 < C < 1$
(11,1)	0.9218	$0.919 < C < 1$

(61)

For any mode equation (59) has an obvious root $y = 0$, i.e., $C_{crit} = 1$, but it is not shown in the table (61). The corresponding instability regions in Figure 2 which set in through neutral modes are also listed for comparison. The (2,0) and (1,1) modes are omitted because there are no instability regions to be compared in Figure 2 and also because these n's are so small that the short wavelength perturbation analysis is not good. While Figure 2 shows that the (11,3) and (13,3) modes have some instability regions, they are stable (evanescent) according

to the WKB analysis so that C_{crit} does not exist for these modes. As expected the agreement between the WKB and exact numerical results becomes better as n increases.

IV. SUMMARY AND DISCUSSION

The results from §III are summarized here briefly: We have found from numerical analysis of the linear dispersion relation that counterstreaming Kalnajs disks exhibit almost no two-stream instability except for five low order modes which are two-stream unstable in very short intervals of the coldness parameter C. The only exception is the (3,1) mode which has a two-stream unstable interval extending over about 10% of the entire C range. We have found that the two-stream instability seems to set in through the neutral mode. The complementary WKB analysis for the high order modes gives a fair agreement to the numerical analysis in §III.1. The WKB analysis also shows that only density waves for the $m = 0$ and 1 modes are supported in counterstreaming Kalnajs disks under the assumption that the instability to amplify these waves sets in through the neutral mode. A physical argument which makes this assumption plausible is as follows: If the two-stream instability sets in through the neutral mode, a certain density wave driven by this instability has zero pattern speed. Therefore, if this density wave is trailing as seen from one stellar stream, the same wave is leading as seen from the other stellar stream. Since these trailing and leading waves have angular momentum densities of equal magnitude but opposite sign, it is possible that by combining the two streams we can amplify the density wave at no extra cost.

Now how will the situation change in the more general case of differential rotation? Instead of developing a stability theory of differentially rotating stellar disks, we discuss the possibility of two-stream instability within kinematical arguments. The results for the differentially rotating stellar disks could be confirmed and improved by N-body experiments. In more general cases of counterstreaming disks with differential rotation, we have $\nu_- = m\Omega(r)/\kappa(r) = -\nu_+$ if we assume $\omega = 0$ at the onset of the two-stream instability. Since $d\Omega/dr < 0$ in general, we find $\kappa < 2\Omega$. Therefore, the condition on which density waves are supported:

$|\nu_{\pm}| < 1$ again implies that m cannot be 2 or larger. Since we are not interested in the axisymmetric mode, it turns out that the $m = 1$ mode is the only mode with zero pattern speed that can be supported in counterstreaming disks with differential rotation. It is conceivable, then, that the possibly unstable $m = 1$ mode in the counterstreaming model disks, such as Mestel disks (Mestel 1963) and isochrone disks (Hénon 1959), is also caused by the two-stream instability due to stellar counterstreams. The two-dimensional N-body experiments by Zang and Hohl (1978) seem to support this conjecture. As the percentage of retrograde stars at the initial time becomes higher, they find increasingly prominent one-armed feature in the later stage of evolution.

In real stellar systems counterstreaming motions by retrograde stars are observed in the central bulges of disk galaxies and in the elliptical galaxies, where the systematic rotation is overwhelmed by the random motion due to high velocity dispersions. In order to realize the internal motions of elliptical galaxies or central bulges of disk galaxies most simply, let us consider a disk galaxy which is flattened due to rotation. If we randomly choose half the stars and reverse their velocities, the overall mass distribution will not be affected by this operation so that the disk will keep an axisymmetric and flat shape. However, the disk has no net rotation now! This hypothetical system can be said to be flattened not because of rotation but because of its anisotropic velocity dispersion $\langle c_r^2 \rangle \approx \langle c_\theta^2 \rangle > \langle c_z^2 \rangle$, consistent with observations (Bertola and Capaccioli 1975, Illingworth 1977). The true situation in elliptical galaxies and central bulges in disk galaxies should not be so simple and three dimensional models are clearly necessary, but we may be right in spirit in the above simple model. Therefore, the counterstreaming stellar disk models we have considered in this paper may be of some use in understanding the stability of bulges in disk galaxies or ellipticals. These locations might be the only places to look for the two-stream instability in stellar systems.

ACKNOWLEDGEMENTS

I wish to thank Scott Tremaine for suggesting this topic, for valuable comments and for critically reading the manuscript. This research was supported in part by NSF grant AST84–12365.

REFERENCES

Abramowitz, M., and Stegun, I. A. (1964). *Handbook of Mathematical Functions* (National Bureau of Standards, Washington), p.336.

Bertin, G., and Mark, J. W-K. (1980). *Astron. Astrophys.* **88**, 289.

Bertola, F., and Capaccioli, M. (1975). *Ap. J.* **200**, 439.

Buneman, O. (1958). *Phys. Rev.* **115**, 503.

Harrison, E. R. (1970). *M. N. R. A. S.* **150**, 443.

Hénon, M. (1959). *Annales d'Astrophysique* **22**, 126.

Hohl, F. (1971). *Astron. J.* **76**, 202.

Hunter, C. (1963). *M. N. R. A. S.* **126**, 299.

Ikeuchi, S., Nakamura, T., and Takahara, F. (1974). *Prog. Theor. Phys.* **52**, 1807.

Illingworth, G. (1977). *Ap. J. Lett.* **218**, L43.

Kalnajs, A. J. (1972). *Ap. J.* **175**, 63.

Kato, S. (1973). *Publ. Astron. Soc. Japan* **25**, 231.

Lin, C. C., Yuan, C., and Shu, F. H. (1969). *Ap. J.* **155**, 721.

Lynden-Bell, D. (1967). *Relativity Theory and Astrophysics–2. Galactic Structure*, edited by J. Ehlers (Am. Math. Soc., Providence), p. 131.

Mark, J. W-K. (1976). *Ap. J.* **206**, 418.

Marochnik, L. S., and Suchkov, A. A. (1969). *Sov. Astron. –AJ* **13**, 252.

Mestel, L. (1963). *M. N. R. A. S.* **126**, 553.

Mikhailovskii, A. B., and Fridman, A. M. (1972). *Sov. Phys. JETP* **34**, 243.

Nakamura, T. (1978). *Prog. Theor. Phys.* **59**, 1129.

Ostriker, J. P., and Peebles, P. J. E. (1973). *Ap. J.* **186**, 467.

Suchkov, A. A. (1969). *Sov. Astron. –AJ* **13**, 418.

Sweet, P. A. (1963). *M. N. R. A. S.* **125**, 285.

Talwar, S. P., and Kalra, G. L. (1966). *Annales d'Astrophysique* **29**, 507.

Toomre, A. (1981). In *The Structure and Evolution of Normal Galaxies*, edited by S. M. Fall and D. Lynden-Bell (Cambridge University Press, Cambridge), p. 111.

Zang, T. A., and Hohl, F. (1978). *Ap. J.* **226**, 521.

FIGURE CAPTIONS

Figure 1:— The stability diagram of a pair of infinite homogeneous Maxwellian stellar systems counterstreaming with a relative speed V. Both counterstreams are assumed to have the same velocity dispersion and density so that the stability of the system is determined by two parameters: V/c_1 and $(k/k_{J1})^2$.

Figure 2:— Instability regions for the low order modes ($l \leq 5$ and $m \leq 5$) of the counterstreaming Kalnajs disk as a function of the coldness C are indicated by thick horizontal lines. Corresponding instability regions of the single stream reference disk are indicated by thin horizontal lines. The absolute value of a pair of real frequencies of the modes which become unstable at the onset of instability (endpoint frequency) is indicated on the right side of the diagram (in units of Ω_0) in the order in which it appears as the coldness C increases. The number of real frequencies in the associated instability region is shown in parentheses.

Figure 1

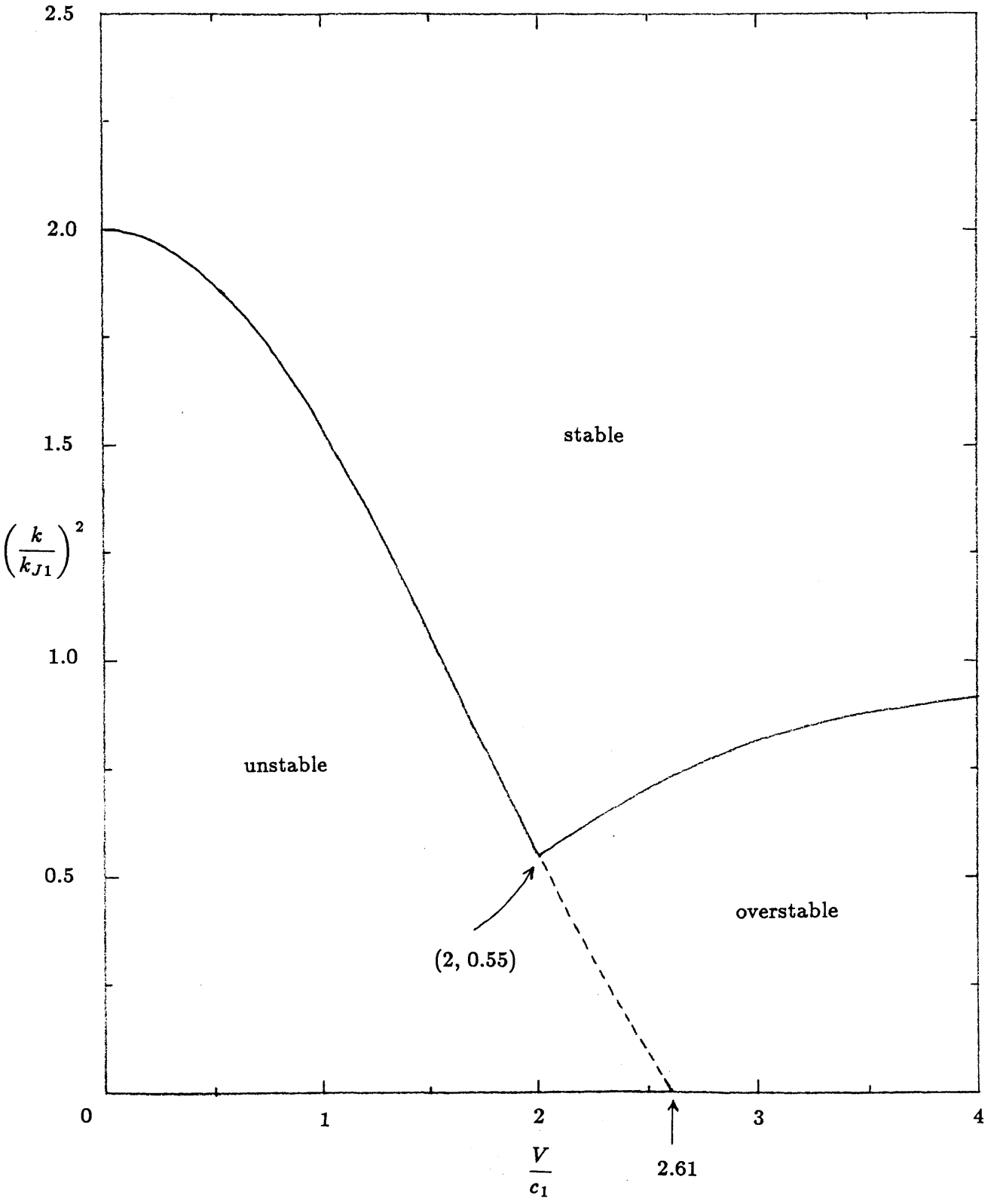
2.5
2.0
1.5
1.0
0.5
0
1
2
3
4
$\left(\frac{k}{k_{J1}}\right)^2$
$\frac{V}{c_1}$
stable
unstable
overstable
(2, 0.55)
2.61

Figure 2

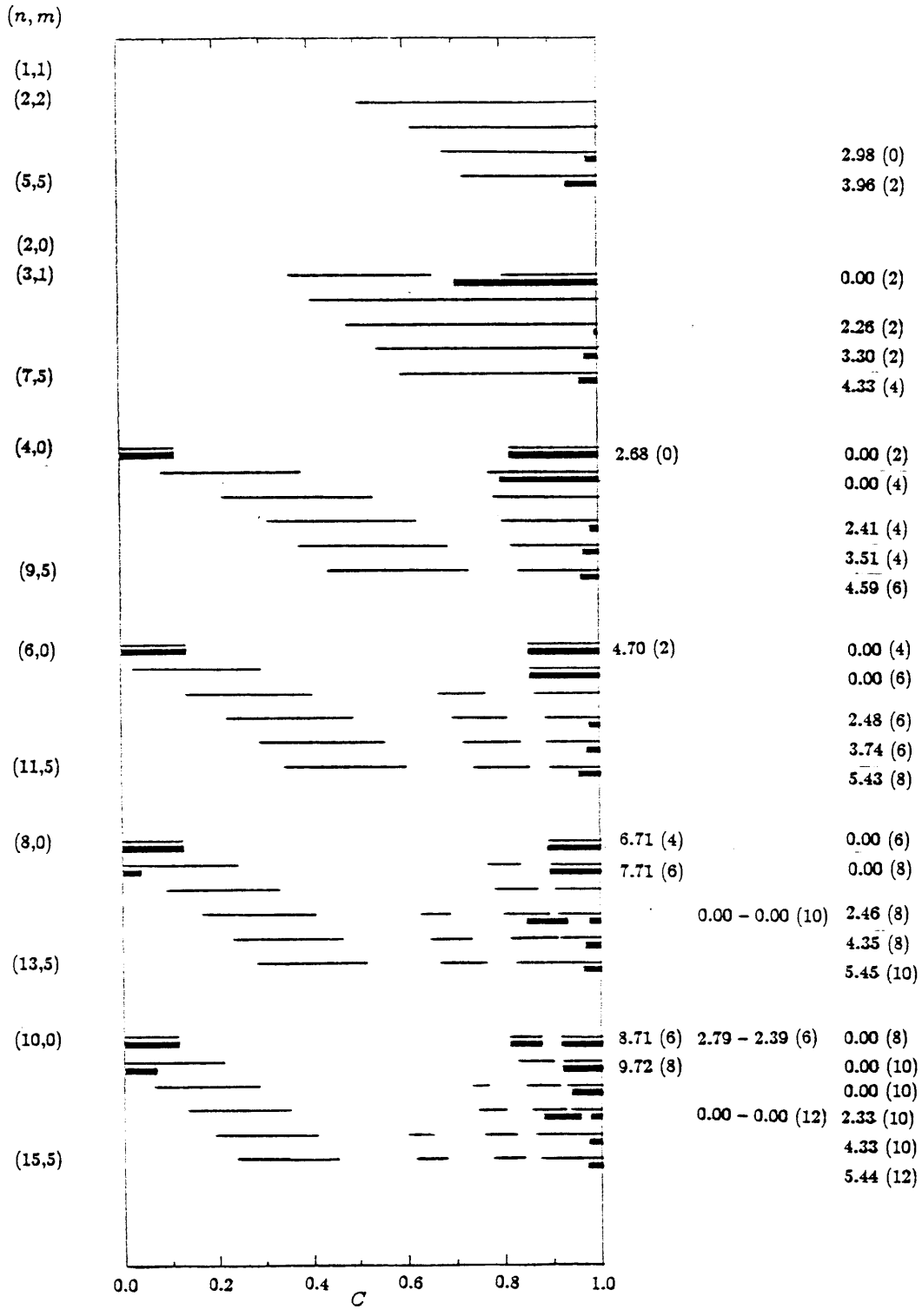
(n, m)
(1,1)
(2,2)
(5,5)
(2,0)
(3,1)
(7,5)
(4,0)
(9,5)
(6,0)
(11,5)
(8,0)
(13,5)
(10,0)
(15,5)
2.98 (0)
3.96 (2)
0.00 (2)
2.26 (2)
3.30 (2)
4.33 (4)
2.68 (0)
0.00 (2)
0.00 (4)
2.41 (4)
3.51 (4)
4.59 (6)
4.70 (2)
0.00 (4)
0.00 (6)
2.48 (6)
3.74 (6)
5.43 (8)
6.71 (4)
7.71 (6)
0.00 (6)
0.00 (8)
0.00 – 0.00 (10)
2.46 (8)
4.35 (8)
5.45 (10)
8.71 (6)
9.72 (8)
2.79 – 2.39 (6)
0.00 (8)
0.00 (10)
0.00 (10)
0.00 – 0.00 (12)
2.33 (10)
4.33 (10)
5.44 (12)
0.0
0.2
0.4
0.6
0.8
1.0
C

CHAPTER 2.

THE HOSE INSTABILITY IN HIGHLY FLATTENED STELLAR SYSTEMS

THE HOSE INSTABILITY
IN HIGHLY FLATTENED STELLAR SYSTEMS

Alar Toomre

Department of Mathematics, Massachusetts Institute of Technology

and

Suguru Araki

Center for Space Research, Center for Theoretical Physics,

and Department of Physics, Massachusetts Institute of Technology

ABSTRACT

We explore the possibility of the hose instability in disk galaxies using the collisionless Boltzmann equation. It is shown that a small-scale bending instability originates when there is a large velocity dispersion in the disk plane. A major consequence of this work is that the hose instability arises in any thin stellar disk if the vertical velocity dispersion is much smaller than the horizontal velocity dispersion. In general the critical degree of anisotropy depends on the unperturbed distribution function. For a thin non-rotating stellar system with an anisotropic Gaussian velocity distribution, we find from detailed numerical analysis that the hose instability can be avoided at all wavelengths if the ratio of the vertical to horizontal velocity dispersion exceeds 0.293.

I. INTRODUCTION

About 60% of bright galaxies in the general field are classified as spiral galaxies. Spiral galaxies are quite flat, having roughly a ten-to-one aspect ratio. Although there is a considerable central bulge, it seems that in the solar neghborhood the equal density surfaces are effectively parallel to each other at least to 0.5 kpc on both sides of the galactic plane. Studies of galactic rotation have revealed that $1.3 \times 10^{11} M_{\odot}$ are concentrated in the central bulge and $0.6 \times 10^{11} M_{\odot}$ are spread fairly uniformly in the disk (Oort 1927, Schmidt 1965, Mihalas and Binney 1981, Bahcall and Soneira 1980,1984). The attraction of the parallel layers of mass in the disk is mainly responsible for accelerations perpendicular to the galactic plane. The attraction of the central bulge also has a component perpendicular to the galactic plane, but this is relatively small up to distance of about 0.5 kpc from the galactic plane. Thus, we ignore the effect due to the bulge component in this paper.

According to the above considerations, it appears that the plane-parallel approximation to the stellar disks of spiral galaxies is an excellent one. The velocity distribution is independent of two space coordinates x and y in the galactic plane and consequently so are the density and the potential. There have been a number of investigations of the structure and stability of stellar disks as inhomogeneous collisionless systems in terms of the plane-parallel approximation, but they have assumed that the disks have no macroscopic motion in the vertical direction (e.g., Toomre 1964). In this paper we will fully treat the vertical equilibrium in order to investigate the vertical motion in the disks. The dynamical equilibrium in the disk plane will be left out, but consideration of this simpler one-dimensional equilibrium permits us to deal rigorously with analogs to real inhomogeneous and rotating systems. Our objective is to develop the stability analysis of highly flattened non-rotating stellar systems with an anisotropic Gaussian velocity distribution

by solving the collisionless Boltzmann and Poisson equations and to determine the regions of possible instabilities in their parameter space. Our results will be compared with observational data.

Before describing the more accurate derivation which we shall give later using the Boltzmann and Poisson equations, we first give a simple heuristic derivation of the dispersion relation for a bending mode which we shall call the "hose" mode later. We note here that the basic understanding and the following heuristic analysis have already appeared in Toomre (1966). We consider the stellar disk as a collection of interpenetrating plane-parallel streams with different streaming velocities. For simplicity, we assume that the disk has zero thickness, that all the stars stream along the x axis in the disk plane (the x-y plane), and that the system is uniform in the y direction.

Suppose that the sheet experiences a small displacement $h(x,t)$ in the z direction perpendicular to the disk plane, and assume that the streams are all constrained to have the same displacement. The vertical acceleration for stars of a given x velocity, u, is

$$a_z = \left(\frac{\partial}{\partial t} + u\frac{\partial}{\partial x}\right)^2 h(x,t). \tag{1}$$

If there were only two streams interpenetrating each other along the x axis with velocities $\pm U_0$, we would have

$$f(u) = \frac{1}{2}\left[\delta(u - U_0) + \delta(u + U_0)\right] \tag{2}$$

and thus

$$\langle a_z \rangle = \frac{\partial^2 h}{\partial t^2} + {U_0}^2 \frac{\partial^2 h}{\partial x^2}. \tag{3}$$

Our velocity distribution is instead given by

$$f(u) = \frac{1}{\sqrt{2\pi\sigma^2}} \exp\left(-\frac{u^2}{2\sigma^2}\right), \tag{4}$$

and the acceleration averaged over many streams is

$$\langle a_z \rangle = \frac{\partial^2 h}{\partial t^2} + \sigma^2 \frac{\partial^2 h}{\partial x^2}. \tag{5}$$

If we write $h(x,t) = H \exp\left[i(kx - \omega t)\right]$, the equilibrium potential at the height $h(x,t)$ is $-2\pi G\mu h(x,t)$, where μ is the constant surface density and G is the gravitational constant. Thus, the restoring force per unit mass acting on the displaced sheet is given by $-2\pi G\mu k h(x,t)$ since the perturbed potential depends on z as $\exp(-k\,|z|)$. Therefore, we obtain the equation of motion

$$\frac{\partial^2 h}{\partial t^2} + \sigma^2 \frac{\partial^2 h}{\partial x^2} = -2\pi G\mu k h, \tag{6}$$

and thus the dispersion relation for an infinitesimally thin sheet:

$$\omega^2 = 2\pi G\mu k - \sigma^2 k^2. \tag{7}$$

It is clear from equation (7) that the gravitational restoring force serves to stabilize the system, while a centrifugal force originating from the horizontal velocity promotes instability. The physical mechanism of the instability is understood as follows: Suppose that the stellar sheet is bent slightly due to gravitational perturbations. Since the stars are confined to the sheet, they exert centrifugal force on the stellar sheet and thus serve to enhance the original perturbation. The instability is rather similar to the hose instability in a magnetized plasma, where the dispersion relation is given by (Spitzer 1962)

$$\omega^2 = \sigma_\perp^2 k^2 + \frac{B^2 k^2}{4\pi\rho} - \sigma_\parallel^2 k^2, \tag{8}$$

where ρ is the mass density of the plasma, $\sigma_\perp$ and $\sigma_\parallel$ are the velocity dispersions of the plasma parallel and perpendicular to the magnetic field and $B^2/8\pi$ is the energy density of the magnetic field. There are, however, two main differences. First, both the tension of magnetic lines of force and the perpendicular

velocity dispersion work to stabilize the plasma whereas there is only a gravitational restoring force in the stellar system. Second, the hose instability in the plasma can occur at all wavelengths whereas in the stellar system the instability is avoided if the wavelength is longer than $\sigma^2/G\mu$ as is shown by equation (7). Despite the above differences it is appropriate to call the instability derived from the dispersion relation (7) the "hose instability" of the infinitesimally thin stellar system.

It turns out that in the infinitesimally thin stellar system the hose instability is exactly complementary to the Jeans instability: It has been shown (Toomre 1964) that an infinitesimally thin stellar sheet with horizontal velocity dispersion and without rotation is subject to the Jeans instability at all wavelengths longer than the Jeans wavelength

$$\lambda_J = \frac{\sigma^2}{G\mu}, \tag{9}$$

whereas the dispersion relation (7) indicates that ω has two complex roots for k greater than $2\pi G\mu/\sigma^2$ or for wavelengths shorter than $\sigma^2/G\mu$.

In the remainder of this chapter we generalize the above considerations to a more realistic disk of finite thickness. The most important influence of the disk thickness is to suppress the instability at wavelengths less than the disk thickness (Toomre 1966; Kulsrud, Mark, Caruso 1971; Bertin, Mark 1980). Since the thickness is of the order of ${\sigma_w}^2/G\mu$, where σ_w is the vertical velocity dispersion, it is predicted that the hose instability will stop operating when the speed ratio, σ_w/σ, becomes sufficiently large. Toomre (1966) has already given a rough estimate of 0.3 for the critical speed ratio, but we will determine it more accurately in an independent numerical analysis in §**IV**. The stabilizing effect of a finite disk thickness has simple physical interpretation. Although the self-gravity of the stars is a stabilizing force, it also serves as the source of vertical coupling which is a

prerequisite for instability. The vertical coupling among the different horizontal velocity classes of stars is stronger if the vertical velocity dispersion, σ_w, is smaller. As the vertical coupling gets weaker, the various classes of stars gradually cease to move together in the z direction and the collective instability vanishes.

We can use these arguments to estimate the smallest unstable wavelength. If a certain velocity class of stars were vertically displaced by a distance d from the neutral plane, they would feel an acceleration of the order of $4\pi G\rho_c d$, where ρ_c is the volume density in the central plane. If the associated vertical frequency, $\sqrt{4\pi G\rho_c}$, were much higher than the natural horizontal frequency, σk, the various velocity classes of stars within the disk would be constrained to move almost completely together in the z direction. The above condition would be satisfied if

$$k^2 \lesssim \frac{4\pi G\rho_c}{\sigma^2}, \tag{10}$$

or, introducing the thickness

$$z_0 \approx \frac{\mu}{\rho_c} \approx \frac{\sigma_w^2}{G\mu}. \tag{11}$$

Thus the hose instability should be present if

$$\lambda_* \gtrsim \sqrt{\pi} R, \tag{12}$$

where

$$R = \frac{\sigma_w}{\sigma} \tag{13}$$

is the ratio between the two velocity dispersions and λ_* is the wavelength λ expressed in units of the Jeans wavelength:

$$\lambda_* = \frac{\lambda}{\lambda_J}. \tag{14}$$

It is to be noted that the similar role of maintaining the vertical coupling among various parallel velocity classes of charged particles in magnetized plasmas is played by the magnetic field.

II. EQUILIBRIUM MODEL

As a simple equilibrium solution to the Boltzmann equation describing a stellar system which is infinite and homogeneous in the x-y plane, we choose the following distribution function:

$$f_0(z,u,v,w) = C\exp\left(-\frac{E-E_3}{\sigma^2} - \frac{E_3}{\sigma_w^2}\right), \tag{15}$$

where both the total energy per unit mass

$$E = \frac{1}{2}(u^2+v^2+w^2) + \phi_0(z) \tag{16}$$

and the partial energy in the z direction

$$E_3 = \frac{1}{2}w^2 + \phi_0(z) \tag{17}$$

are separately conserved. In our model system the unperturbed stellar motion in the vertical direction is exactly decoupled from that in the horizontal plane; in a real stellar disk the motions are approximately decoupled so long as the disk is thin. Integrating equation (15) over velocities, we find the equilibrium density distribution

$$\rho_0(z) = \int\int\int_{-\infty}^{\infty} f_0 du dv dw = 2\pi\sigma^2\sqrt{2\pi\sigma_w^2}C\exp\left[-\frac{\phi_0(z)}{\sigma_w^2}\right]. \tag{18}$$

Eliminating the equilibrium potential, $\phi_0(z)$, from equation (18) and the Poisson equation

$$\frac{d^2\phi_0}{dz^2} = 4\pi G\rho_0, \tag{19}$$

we get a differential equation for the equilibrium volume density:

$$\frac{d}{dz}\left(\frac{1}{\rho_0}\frac{d\rho_0}{dz}\right) = -\frac{4\pi G}{\sigma_w^2}\rho_0, \tag{20}$$

which is to be solved with the boundary conditions

$$\rho_0(0) = \rho_c \qquad \text{and} \qquad \rho_0'(0) = 0. \tag{21}$$

The solution is given by (Spitzer 1942, Camm 1950),

$$\rho_0(z) = \rho_c \,\mathrm{sech}^2\left(\sqrt{\frac{2\pi G\rho_c}{\sigma_w^2}}z\right) = \frac{\sigma_w^2}{2\pi G z_0^2}\,\mathrm{sech}^2\frac{z}{z_0}, \tag{22}$$

where

$$\rho_c = \frac{\sigma_w^2}{2\pi G z_0^2} \tag{23}$$

and z_0 is a typical thickness of the system since the vertical scale height is given by $z_0/2$ as z tends to infinity. From equations (18) and (22) we obtain the equilibrium potential

$$\phi_0(z) = 2\sigma_w^2 \ln\cosh\frac{z}{z_0}. \tag{24}$$

Then, the normalization constant, C, is determined:

$$C = \frac{\sigma_w}{(2\pi)^{5/2} G z_0^2 \sigma^2}. \tag{25}$$

Integrating equation (22) over z, we get the surface density

$$\mu = \int_{-\infty}^{\infty} \rho_0(z)dz = \frac{\sigma_w^2}{\pi G z_0}, \tag{26}$$

which shows that only two out of the three quantities μ, z_0, σ_w can be chosen independently. From equation (23) we also have

$$\rho_c = \frac{\mu}{2z_0}. \tag{27}$$

In §**III** we develop the linear perturbation analysis for this equilibrium system and solve the Boltzmann and Poisson equations in order to determine the regions of stability and instability in parameter space. The modes considered in this paper are labeled as "hose" modes or "Jeans" modes according to whether the density perturbation is antisymmetric or symmetric in the vertical cordinate z.

III. LINEAR PERTURBATION ANALYSIS

First, we introduce dimensionless variables:

$$\begin{aligned} x_* = \frac{x}{z_0}, y_* = \frac{y}{z_0}, z_* = \frac{z}{z_0}, \\ u_* = \frac{u}{\sigma_w}, v_* = \frac{v}{\sigma_w}, w_* = \frac{w}{\sigma_w}, \\ t_* = \frac{t}{t_0}, \end{aligned} \tag{28}$$

where the time scale, t_0, is given by

$$t_0 = \frac{z_0}{\sigma_w} = \sqrt{\frac{z_0}{\pi G \mu}}. \tag{29}$$

Using the above dimensionless variables, we express the equilibrium density, potential and velocity distribution function as follows:

$$\rho_0(z_*) = \frac{\mu}{2z_0} \mathrm{sech}^2 z_*, \tag{30}$$

$$\phi_0(z_*) = 2\sigma_w^2 \ln \cosh z_*, \tag{31}$$

$$f_0(z_*, u_*, v_*, w_*) = \frac{\rho_0(z_*)}{2\pi\sigma^2\sqrt{2\pi\sigma_w^2}} \exp\left[-\frac{1}{2}(R^2 u_*^2 + R^2 v_*^2 + w_*^2)\right], \tag{32}$$

where the ratio R between the two velocity dispersions is defined by equation (13). We now consider a small perturbation which we write as

$$\rho'(x_*, z_*, t_*) = \frac{\mu}{2z_0} \rho_*(x_*, z_*, t_*), \tag{33}$$

$$\phi'(x_*, z_*, t_*) = \sigma_w^2 \phi_*(x_*, z_*, t_*), \tag{34}$$

$$f'(x_*, z_*, t_*, u_*, v_*, w_*) = f_0(z_*, u_*, v_*, w_*) f_*(x_*, z_*, t_*, u_*, v_*, w_*), \tag{35}$$

where we have assumed without loss of generality that the perturbation propagates along the x axis in the x-y plane:

$$\frac{\partial \rho_*}{\partial y_*} = \frac{\partial \phi_*}{\partial y_*} = \frac{\partial f_*}{\partial y_*} = 0. \tag{36}$$

Now the basic equations which must be satisfied by the above perturbed quantities are the Boltzmann equation

$$\frac{Df_*}{Dt_*} = -R^2 u_* \frac{\partial \phi_*}{\partial x_*} - w_* \frac{\partial \phi_*}{\partial z_*}, \tag{37}$$

where the convective derivative is defined as

$$\frac{D}{Dt_*} = \frac{\partial}{\partial t_*} + u_* \frac{\partial}{\partial x_*} + v_* \frac{\partial}{\partial y_*} + w_* \frac{\partial}{\partial z_*} - 2 \tanh z_* \frac{\partial}{\partial w_*}, \tag{38}$$

and the Poisson equation

$$\frac{\partial^2 \phi_*}{\partial x_*^2} + \frac{\partial^2 \phi_*}{\partial z_*^2} = 2\rho_*. \tag{39}$$

These are supplemented by the relation between the distribution function and the density:

$$\rho_* = \frac{R^2}{(2\pi)^{3/2}} \operatorname{sech}^2 z_* \int\int\int_{-\infty}^{\infty} f_* \exp\left[-\frac{1}{2}(R^2 u_*^2 + R^2 v_*^2 + w_*^2)\right] du_* dv_* dw_*. \tag{40}$$

First we solve the Boltzmann equation for f_*. Integrating equation (37) along the stellar orbit from the remote past to the present time, t_*, and assuming that f_* vanishes in the remote past, we get

$$f_*(x_*, z_*, t_*, u_*, v_*, w_*) = -\int_{-\infty}^{t_*} \left(R^2 u'_* \frac{\partial}{\partial x'_*} + w'_* \frac{\partial}{\partial z'_*} \right) \phi_*(x'_*, z'_*, t'_*) dt'_*, \tag{41}$$

where x'_*, z'_*, u'_*, w'_* are the position and velocity at time t'_* of the orbit which passes through the phase space point x_*, z_*, u_*, w_* at t_*. Since the projection of the stellar motion onto the x-y plane is constant in velocity, we have

$$u'_* = u_*,$$

$$v'_* = v_*,$$

$$x'_* = x_* - u_*(t_* - t'_*). \tag{42}$$

Since the perturbation propagates along the x axis, we may write

$$\phi_*(x_*, z_*, t_*) = \Phi(z_*, t_*) \cos \frac{2R^2 x_*}{\lambda_*}, \tag{43}$$

where λ_* is the wavelength in units of the Jeans wavelength, λ_J, as defined by equation (14). For future convenience we also define a parameter

$$\alpha = \frac{2R^2}{\lambda_*}. \tag{44}$$

Making use of equations (41), (42), (43), we can now integrate equation (40) over u_* and v_* to obtain

$$\rho_*(x_*, z_*, t_*) = (2\pi)^{-1/2} \mathrm{sech}^2 z_* \cos \alpha x_* \int_{-\infty}^{\infty} \exp\left(-\frac{1}{2} {w_*}^2\right) H(w_*, z_*, t_*) dw_*, \tag{45}$$

where

$$H(w_*, z_*, t_*) = -\int_{-\infty}^{t_*} \exp\left[-\frac{\alpha^2 (t_* - t'_*)^2}{2R^2}\right] \left[\alpha^2 (t_* - t'_*) + w'_* \frac{\partial}{\partial z'_*}\right] \Phi(z'_*, t'_*) dt'_*. \tag{46}$$

Noting the relation

$$w'_* \frac{\partial}{\partial z'_*} \Phi(z'_*, t'_*) = \left(\frac{D}{Dt'_*} - \frac{\partial}{\partial t'_*}\right) \Phi(z'_*, t'_*) \tag{47}$$

and integrating the term with $D\Phi/Dt'_*$ by parts, we rewrite equation (46) as follows:

$$\begin{aligned} H(w_*, z_*, t_*) = -\Phi(z_*, t_*) + \int_{-\infty}^{t_*} \exp\left[-\frac{\alpha^2}{2R^2}(t_* - t'_*)^2\right] \\ \times \left[\frac{\partial}{\partial t'_*} + \left(\frac{1}{R^2} - 1\right) \alpha^2 (t_* - t'_*)\right] \Phi(z'_*, t'_*) dt'_*, \end{aligned} \tag{48}$$

where the w_* dependence of H is hidden in z'_* through the equation of motion in the vertical direction

$$\frac{d^2 z'_*}{{dt'_*}^2} = -2 \tanh z'_*, \tag{49}$$

and the boundary conditions

$$z'_*(t_*) = z_* \qquad \text{and} \qquad \frac{dz'_*}{dt'_*}(t_*) = w_*. \tag{50}$$

Without loss of generality we may write

$$\Phi(z'_*, t'_*) = \exp(2Rst'_*)\mathcal{P}(z'_*), \tag{51}$$

where s is the dimensionless growth rate of the perturbation in units of $2\pi\sigma/\lambda_J$. The perturbed density can also be written in the form

$$\rho_*(x'_*, z'_*, t'_*) = \mathcal{D}(z'_*)\cos\alpha x'_* \exp(2Rst'_*). \tag{52}$$

Due to the Poisson equation (39), $\mathcal{P}(z_*)$ is connected with $\mathcal{D}(z_*)$ by

$$\left(-\alpha^2 + \frac{d^2}{dz_*^2}\right)\mathcal{P}(z_*) = 2\mathcal{D}(z_*), \tag{53}$$

or

$$\mathcal{P}(z_*) = -\frac{1}{\alpha}\int_{-\infty}^{\infty} \exp(-\alpha\,|z_* - \varsigma|)\mathcal{D}(\varsigma)d\varsigma. \tag{54}$$

Also, $\mathcal{P}(z_*)$ and $\mathcal{D}(z_*)$ are related to each other through equations (45) and (48):

$$\mathcal{D}(z_*) = (2\pi)^{-1/2}\mathrm{sech}^2 z_* \int_{-\infty}^{\infty} \exp\left(-\frac{1}{2}w_*^2\right) H(w_*, z_*)dw_*, \tag{55}$$

where

$$H(w_*, z_*) = -\mathcal{P}(z_*) + \int_0^{\infty} \exp\left(-\frac{\alpha^2\tau^2}{2R^2} - 2Rs\tau\right)\left[2Rs + \left(\frac{1}{R^2} - 1\right)\alpha^2\tau\right]\mathcal{P}(z'_*)d\tau. \tag{56}$$

In order to solve these coupled integral equations (54), (55) and (56), we expand $\mathcal{D}(z_*)$ in terms of a set of orthogonal functions

$$\mathcal{D}(z_*) = \sum_{k=1}^{\infty} c_k \mathcal{D}_k(z_*), \tag{57}$$

and impose a single component perturbation $\mathcal{D}_k(z_*)$. The corresponding imposed potential perturbation is given by

$$\mathcal{P}_k(z_*) = -\frac{1}{\alpha}\int_{-\infty}^{\infty} \exp(-\alpha\,|z_* - \zeta|)\,\mathcal{D}_k(\zeta)\,d\zeta. \tag{58}$$

Substituting (58) into (56), we find

$$H_k(w_*, z_*) = -\mathcal{P}_k(z_*) + \int_0^{\infty} \exp\left(-\frac{\alpha^2\tau^2}{2R^2} - 2Rs\tau\right)\left[2Rs + \left(\frac{1}{R^2} - 1\right)\alpha^2\tau\right]\mathcal{P}_k(z'_*)\,d\tau. \tag{59}$$

Thus, we obtain the resulting density perturbation

$$\widetilde{\mathcal{D}}_k(z_*) = (2\pi)^{-1/2}\mathrm{sech}^2 z_* \int_{-\infty}^{\infty} \exp\left(-\frac{1}{2}w_*^2\right) H_k(w_*, z_*)\,dw_*, \tag{60}$$

which is in general not $\mathcal{D}_k(z_*)$ but a linear combination:

$$\widetilde{\mathcal{D}}_k(z_*) = \sum_{m=1}^{\infty} A_{km}\mathcal{D}_m(z_*). \tag{61}$$

The matrix A_{km} tells us how much of the density component $\mathcal{D}_m(z_*)$ is excited by imposing an initial density perturbation $\mathcal{D}_k(z_*)$. Our objective is to determine the boundary between stability and instability regions in the three-dimensional parameter space (λ_*, R, s), which is equivalent to finding the set of parameter values (λ_*, R, s) for which the largest eigenvalue of A_{km} is equal to unity. Not second or third largest ones but the largest, because in order for this system to be unstable it is only necessary that we have one eigen-perturbation which grows in the system.

To proceed further we need an explicit expression for the density perturbation, $\mathcal{D}_k(z_*)$. There exist two distinct modes according to the parity of $\mathcal{D}_k(z_*)$, that is, the hose mode if

$$\mathcal{D}_k(-z_*) = -\mathcal{D}_k(z_*), \tag{62}$$

and the Jeans mode if

$$\mathcal{D}_k(-z_*) = \mathcal{D}_k(z_*). \tag{63}$$

We choose to impose the following density perturbations:

$$\mathcal{D}_k(z_*) = \operatorname{sech}^{2-\alpha} z_* \times \begin{cases} P_{2k-1}(\tanh z_*) & \text{hose} \\ P_{2k-2}(\tanh z_*) & \text{Jeans,} \end{cases} \tag{64}$$

where $k = 1, 2, 3, \ldots$ and $P_n(x)$ is the Legendre polynomial of order n. The particular choice of the exponent, $2 - \alpha$, caused a rapid convergence in the eigenvalue series as a function of the order of the matrix A_{km}. Acknowledgement is due to Alar Toomre for this neat technical improvement. The function (64) satisfies the orthogonality condition

$$\int_{-\infty}^{\infty} \operatorname{sech}^{2\alpha-2} z_* \mathcal{D}_m(z_*) \mathcal{D}_n(z_*) dz_* = \frac{\delta_{mn}}{C_m}, \tag{65}$$

where

$$C_m = \begin{cases} 2m - (1/2) & \text{hose} \\ 2m - (3/2) & \text{Jeans.} \end{cases} \tag{66}$$

From equations (60), (61), (65) we find the following expression for the response matrix:

$$A_{km} = \frac{C_m}{\sqrt{2\pi}} \int_{-\infty}^{\infty} dz_* \int_{-\infty}^{\infty} dw_* \operatorname{sech}^{2\alpha} z_* \exp\left(-\frac{1}{2} w_*^2\right) \mathcal{D}_m(z_*) H_k(w_*, z_*). \tag{67}$$

Recalling that z energy is conserved:

$$\frac{1}{2} w_*^2 + 2 \ln \cosh z_* \equiv \frac{1}{2} w_0^2, \tag{68}$$

where $w_0 \equiv w_*(0)$ is the dimensionless maximum velocity attained when the star passes through the neutral plane ($z_* = 0$), we make a change of variables from (z_*, w_*) to (t_*, w_0). The corresponding Jacobian is

$$\begin{aligned} \frac{\partial(z_*, w_*)}{\partial(t_*, w_0)} &= w_* \left(\frac{\partial w_*}{\partial w_0}\right)_{t_*} - \left(\frac{\partial z_*}{\partial w_0}\right)_{t_*} (-2 \tanh z_*) \\ &= \left[\frac{\partial}{\partial w_0}\left(\frac{1}{2} w_0^2 - 2 \ln \cosh z_*\right)\right]_{t_*} + 2 \tanh z_* \left(\frac{\partial z_*}{\partial w_0}\right)_{t_*} \\ &= w_0. \end{aligned} \tag{69}$$

Thus

$$dz_* dw_* = w_0 dw_0 dt_*. \tag{70}$$

The range of the new variables is $0 \leq w_0 < \infty$ and $0 \leq t_* \leq T(w_0)$, where the dimensionless period associated with the stellar vertical motion, $T(w_0)$, is given by

$$\begin{aligned} T(w_0) &= 4 \int_{w_0}^{0} \frac{dw_*}{-2 \tanh z_*} \\ &= 2w_0 \int_0^{\pi/2} \left[1 - \exp\left(-\frac{1}{2} w_0^2 \cos^2 \theta \right) \right]^{-1/2} \cos\theta d\theta \end{aligned} \tag{71}$$

and behaves asymptotically like

$$T \sim \sqrt{2}\pi \quad \text{as} \quad w_0 \to 0 \qquad \text{and} \qquad T \sim 2w_0 \quad \text{as} \quad w_0 \to \infty.$$

Thus, equation (67) is replaced by

$$\begin{aligned} A_{km} &= (2\pi)^{-1/2} C_m \int_0^{\infty} \exp\left(-\frac{1}{2} w_0^2 \right) S_{km}(w_0) w_0 dw_0 \\ &= (2\pi)^{-1/2} C_m \int_0^{\infty} e^{-x} S_{km}(\sqrt{2x}) dx, \end{aligned} \tag{72}$$

where

$$\begin{aligned} S_{km}(w_0) &= -V_{km}(w_0, 0) \\ &+ \int_0^{\infty} \left[2Rs + \left(\frac{1}{R^2} - 1 \right) \alpha^2 \tau \right] \exp\left(-2Rs\tau - \frac{\alpha^2 \tau^2}{2R^2} \right) V_{km}(w_0, \tau) d\tau \end{aligned} \tag{73}$$

and

$$V_{km}(w_0, \tau) = \int_0^{T(w_0)} \operatorname{sech}^{2\alpha - 2} z_*(t_*) \mathcal{D}_m\left[z_*(t_*) \right] \mathcal{P}_k\left[z_*(t_* - \tau) \right] dt_*. \tag{74}$$

This completes the prescription for calculating the matrix elements, A_{km}. In order to actually evaluate the three-fold integral in equations (72), (73), (74) we have to resort to numerical analysis, which will be developed in the following section.

IV. NUMERICAL ANALYSIS AND RESULTS

In this section we describe the numerical techniques used to solve the equation of motion (49) and to evaluate the integrals in equations (58), (72), (73) and (74). Here we declare that our general goal of accuracy should be to obtain seven significant digits for elements and eigenvalues of the response matrix A_{km}.

IV.1. Fast Potential Integrator

First, we use equation (58) or

$$P_k(z_*) = -\frac{1}{\alpha}\int_0^\infty e^{-\alpha x}\left[D_k(z_* + x) + D_k(z_* - x)\right]dx \tag{75}$$

to solve the Poisson equation. We evaluate the integral using the Euler-Maclaurin summation formula and a step size $\Delta x = 0.02$; the error is of order $(\Delta x)^8 \approx 10^{-13}$. After specifying the value of α, we tabulate $P_k(z_*)$ for $k = 1, 2, \ldots, 8$ and $-9.98 \leq z_* \leq 9.98$ at intervals of $\Delta z_* = 0.02$. We need not keep terms $P_k(z_*)$ for $k \geq 9$, because it turns out by experiment that we can obtain sufficiently accurate eigenvalues as we increase the order of the response matrix A_{km} towards eight.

IV.2. Orbit Determination

Next we solve the equation of motion (49) to determine z_* as a function of t_*. We consider equation (49) as a pair of first-order differential equations

$$\frac{dz_*}{dt_*} = w_* \qquad \text{and} \qquad \frac{dw_*}{dt_*} = -2\tanh z_*, \tag{76}$$

impose initial conditions

$$z_*(0) = 0 \qquad \text{and} \qquad w_*(0) = w_0 \tag{77}$$

and use the fourth-order Runge-Kutta method, which involves errors of order $h^5 \approx 10^{-8}$, when the step size is chosen to be $h \approx 0.025$. Although w_0 varies continually between zero and infinity, we only have to integrate equation (76) for a small number of values of w_0, because we shall employ the N-point Laguerre integration formula for the w_0 integration (Abramowitz and Stegun 1972). After trying various N points, we find that we typically need $N = 32$ to establish secure answers. Moreover, in order to obtain seven significant figures we need to deal with only 15 out of 32 values of w_0 since the rest have weight factors smaller than 10^{-8}. Therefore, the initial velocities to be chosen are

$$w_0(i) = \sqrt{2x_i}, \tag{78}$$

where $i = 1, 2, \ldots, 15$ and x_i is the ith zero of the Laguerre polynomial of order 32, $L_{32}(x)$. Numerical values of $w_0(i)$ are given in Table 1. It is to be noted that the maximum height reached by a star in the fifteenth orbit is given by $z_0(15) = 9.339374$ and is within the range for which values of $P_k(z_*)$ are tabulated. Once we know the initial velocities it is straightforward to compute the periods (71) by the trapezoidal rule. Since the stellar orbit has the symmetry properties

$$z_*(T - t_*) = -z_*(t_*) \qquad \text{and} \qquad z_*\big[(T/2) - t_*\big] = z_*(t_*), \tag{79}$$

we have only to integrate equation (76) for one quarter period.

IV.3. Three-fold Integral

Since the first term in equation (73) does not involve z_* at different times, we can evaluate its contribution to A_{km} more efficiently without change of integration variables from (z_*, w_*) to (t_*, w_0), that is,

$$A_{km}^{(1)} = -(2\pi)^{-1/2} C_m \int_0^\infty \exp\left(-\frac{1}{2} w_0^2\right) V_{km}(w_0, 0) w_0 dw_0$$

$$= -2C_m \int_0^\infty \mathrm{sech}^{2\alpha} z_* \mathcal{D}_m(z_*) \mathcal{P}_k(z_*) dz_*. \tag{80}$$

Using the values of $\mathcal{D}_m(z_*)$ and $\mathcal{P}_k(z_*)$ listed in the table, we can easily evaluate the above integral by the trapezoidal rule. It can be shown analytically that $A_{km}^{(1)} = 0$ if $m < k$.

The second term in equation (73) involves more work since we require the product of $\mathcal{D}_m$ and $\mathcal{P}_k$ at different times. However, the integration over t_* in equation (74) is simplified if we decompose $\mathrm{sech}^{2\alpha-2} z_*(t_*) \mathcal{D}_m\left[z_*(t_*)\right]$ and $\mathcal{P}_k\left[z_*(t_*-\tau)\right]$ into Fourier components:

$$\mathrm{sech}^{2\alpha-2} z_*(t_*) \mathcal{D}_m\left[z_*(t_*)\right] = \sum_{i=1}^{\infty} d_i \times \begin{cases} \sin(2i-2)\omega t_* & \text{hose} \\ \cos(2i-2)\omega t_* & \text{Jeans,} \end{cases} \tag{81}$$

and

$$\mathcal{P}_k\left[z_*(t_*-\tau)\right] = \sum_{i=1}^{\infty} p_i \times \begin{cases} \sin(2i-2)\omega(t_*-\tau) & \text{hose} \\ \cos(2i-2)\omega(t_*-\tau) & \text{Jeans,} \end{cases} \tag{82}$$

where

$$\omega = \frac{2\pi}{T(w_0)}. \tag{83}$$

The density and potential Fourier coefficients are given by

$$d_i(m, w_0, \alpha) = \frac{8}{T} \int_0^{T/4} dt\, \mathrm{sech}^{2\alpha-2} z_*(t) \mathcal{D}_m\left[z_*(t)\right] \times \begin{cases} \sin(2i-2)\omega t & \text{hose} \\ \left[1 - (\delta_{i1}/2)\right] \cos(2i-2)\omega t & \text{Jeans} \end{cases} \tag{84}$$

and

$$p_i(k, w_0, \alpha) = \frac{8}{T} \int_0^{T/4} dt\, \mathcal{P}_k\left[z_*(t)\right] \times \begin{cases} \sin(2i-2)\omega t & \text{hose} \\ \left[1 - (\delta_{i1}/2)\right] \cos(2i-2)\omega t & \text{Jeans.} \end{cases} \tag{85}$$

It turns out that we need only the first several Fourier coefficients for equations (81) and (82) to retain the necessary accuracy. Thus, $i = 1, 2, \ldots, 5$, m and $k = 1, 2, \ldots, 8$ and $w_0 = w_0(1), w_0(2), \ldots, w_0(15)$, and for a fixed value of α we

typically require a table of $5 \times 8 \times 15 = 600$ density and potential Fourier coefficients. Integration in equations (84) and (85) is easily done by the centered rectangle rule without loss of accuracy, because the integrands are periodic functions of t with a period T. The necessary values of $P_k(z_*)$ at a certain time along the stellar orbit have been computed by the use of the table of $P_k(z_*)$ and the Lagrange four-point interpolation formula. The remaining integration over τ and w_0 is carried out by the Euler-Maclaurin summation formula and by the 32-point Laguerre integration formula, respectively.

IV.4. Results

Now we shall show the actual procedure to obtain some typical values on the hose neutral curve. We set the growth rate $s = 0$. We first choose a certain speed ratio, say, $R = 0.1$ and then vary the wavelength λ_*. (At some places where the hose neutral curve has a small gradient we should rather fix λ_* and vary R.) At $\lambda_* = 1.00$ the response matrix A_{km} is evaluated as shown in Table 2. By inspection we realize a few features of this matrix. First, it is almost diagonal and the diagonal element becomes progressively smaller as k gets larger. Second, for a fixed k or m higher order elements are progressively smaller than lower ones except around the diagonal element. Third, it is not symmetric. Once we have known that the contribution from higher order density perturbations is progressively smaller, it is expected that we can accurately estimate major eigenvalues of this actually infinite dimensional matrix in the following way. We evaluate the eigenvalues of M dimensional submatrices (See Table 2. $M = 1, 2, \ldots, 8$) using subroutine GREV in the VAXMATH subroutine library. The result is shown in Table 3. It turns out by numerical experiments that all the eigenvalues are real positive and the second largest eigenvalue is always smaller than the largest one

by roughly one order of magnitude. We also realize that the series for the largest eigenvalues as a function of the order M of submatrices in most cases converge rapidly as M approaches 6 to 8. Typical CPU time for this evaluation of the largest eigenvalue for fixed s, R and λ_* is 1.7 to 1.9 seconds in our VAX computer. It is a phenomenally short time for this much of computation. Were it not for the elaborate choice of any of the computational methods described in §**IV.1**, §**IV.2** and §**IV.3**, the CPU time would easily blow up to hours. By trial and error we know that, for $R = 0.1$, as λ_* increases from 0, the largest eigenvalue increases, becomes unity between 0.25 and 0.26, reach the maximum and keeps decreasing while getting unity again somewhere between 1.07 and 1.08. The largest eigenvalues are found at $\lambda_* = 1.06$, 1.07, 1.08, 1.09 as 1.000600, 1.000273, 0.999959, 0.999659, respectively. The wavelength giving the largest eigenvalue of unity is found by the Lagrange four-point interpolation formula as $\lambda = 1.0787$.

We have arrived at the elements of the response matrix, A_{km}. For each set of parameters (λ_*, R, s) we have computed the largest eigenvalue of the matrix A_{km}. In Figure 1 and Figure 2 we have plotted in the λ_*-R plane those points at which the largest eigenvalue is equal to unity for four fixed values of s. Each mode has its neutral curve, corresponding to $s = 0$, which divides the whole parameter plane into stable and unstable regions.

Two particular points along the Jeans neutral curve correspond to systems which have been investigated in the literature. The first point ($\lambda_* = 1$, $R = 0$) is the neutral wavelength for a planar stellar system with infinitesimal thickness. This wavelength, shown in equation (9). A given velocity dispersion in the system can thus stabilize only those disturbances whose typical dimensions are smaller than λ_J. The second point ($\lambda_* = 2$, $R = 1$) represents the neutral wavelength for a plane-parallel stellar system with isotropic velocity distribution. Ledoux (1951) investigated the stability of the corresponding gaseous system. He showed that

Jeans' criterion was still valid provided that the density ρ in the standard Jeans wavelength (Jeans 1928)

$$\lambda_J^{(3)} = \sqrt{\frac{\pi\sigma^2}{G\rho}} \tag{86}$$

for an infinite homogeneous medium is replaced by half the density in the central plane, $\rho_c/2$. Combining equations (9), (14), (22), (26) and (86) we can show that the above statement is also true for the stellar system:

$$\sqrt{\frac{\pi\sigma^2}{G\rho_c/2}} = \frac{2\sigma^2}{G\mu} = 2\lambda_J \qquad \text{or} \qquad \lambda_* = 2. \tag{87}$$

For the hose neutral curve, note that there exists a maximum speed ratio $R = 0.293$ at the wavelength $\lambda_* = 1.22$, beyond which the system is stable for all wavelengths. That is, there is no hose instability if the vertical velocity dispersion exceeds 29% of the horizontal velocity dispersion (Toomre 1966, Toomre 1983). There is a small overlapping region where both the Jeans instability and the hose instability are possible (Figure 3).

In Figure 1 and Figure 2 three more curves are shown in the instability region of each mode. These correspond to finite growth rates $s = 0.1, 0.2, 0.3$. Each of these three curves divides the instability region into two subregions according to whether the horizontal disturbances can grow faster than at a given growth rate or not.

Finally, we can check the numerical results by investigating the limiting case of an infinitesimally thin system ($R = 0$). For the hose mode, replacing ω in the dispersion relation (7) by $is(2\pi\sigma/\lambda_J)$, we obtain

$$-s^2 = \frac{1}{\lambda_*} - \frac{1}{\lambda_*^2}. \tag{88}$$

Solving this for λ_*, we find

$$\lambda_* = \frac{2}{1 + \sqrt{1 + 4s^2}}. \tag{89}$$

Another obvious root is $\lambda_* = 0$ as indicated by equation (12). For the Jeans mode, similar arguments through equation (56) in §III lead us to the following equation for the critical wavelength:

$$\frac{1}{\lambda_*} = 1 - \sqrt{\pi}\frac{s\lambda_*}{\sqrt{2}} \exp\left(\frac{s^2\lambda_*^2}{2}\right)\left[1 - \mathrm{erf}\left(\frac{s\lambda_*}{\sqrt{2}}\right)\right] \tag{90}$$

where $\mathrm{erf}(x)$ is the error function

$$\mathrm{erf}(x) = \frac{2}{\sqrt{\pi}} \int_0^x e^{-t^2}\, dt. \tag{91}$$

Numerical values of λ_* are given in Table 4 for different growth rates. The growth rate for the hose instability can be arbitrarily large, which occurs at around ($\lambda_* = 0$, $R = 0$), whereas there exists a maximum growth rate, $s = 0.3468$, for the Jeans instability which is attained at ($\lambda_* = 3.349$, $R = 0$).

V. CONCLUSIONS

We have determined the regions of the hose instability and the Jeans instability in the parameter space (λ_*, R) for a non-rotating stellar system with an anisotropic Gaussian velocity distribution in the vertical and horizontal directions. Our conclusion is that in this system the hose instability is avoided at all wavelengths if the vertical velocity dispersion exceeds 29% of the horizontal velocity dispersion.

These calculations can be extended in a number of ways. The critical ratio of the two velocity dispersions generally depends on the choice of the equilibrium distribution function. What is more important, in a more realistic model, the effect of rotation must be taken into account. If the growth rate s is much larger than the angular frequency of rotation, we can neglect the effect of rotation and thus the equilibrium in the horizontal direction. Toomre (1966) has done a more complicated numerical calculation involving the epicyclic motion of disk stars and has found that its effect would not alter the critical ratio by more than 10%. However, the self-consistent treatment of the rotational effect may require inclusion of both epicyclic motion and galactic rotation through proper choice of a more complicated equilibrium model.

Observational data show us that the ratio of vertical to radial velocity dispersion ranges between 0.45 and 0.65 for various velocity classes of disk stars at the solar neighborhood (e.g., Wielen 1974). The ratio of vertical to tangential velocity dispersion is even larger. Thus it is unlikely that the hose instability is operating in our Galaxy at the present time.

However, it is an established observational fact that the random velocities of disk stars in our Galaxy increase with increasing age. The most natural class of explanations is based on the hypothesis that there exist mechanisms to progressively

increase the velocity dispersions of disk stars with time. Moreover, the observed velocity dispersions as a function of stellar age rise most rapidly for young stars and change relatively more slowly for old stars. Thus, we cannot exclude the possibility that the axial ratios of the velocity ellipsoid may also depend on the stellar age. In fact, according to Fig. 4. and TABLE V of Wielen (1974), Group $6d$ stars on or near the main sequence with $B-V$ color less than 0.05 (spectral types $\leq$A1) have mean age $\langle\tau\rangle = 0.2 \times 10^9$ years, speed ratio $R = \sigma_w/\sigma_u = 0.29$ while Group $6c$ stars on or near the main sequence with $0.05 \leq B-V \leq 0.2$ (A2 $\leq$ spectral types $\leq$ A6) have $\langle\tau\rangle = 0.4 \times 10^9$ years, $R = 0.24$. For each main-sequence group, the mean age is assumed to be about half the main-sequence lifetime of the appropriate stellar type, that is, a constant star-formation rate is assumed. The above two groups of young stars also show a significant vertex deviation of about $+20°$. Therefore, it may be possible that the hose instability was present in our Galaxy in the past. We wish to make more definite statements in this respect in our future works.

ACKNOWLEDGEMENTS

S. Araki would like to thank Scott Tremaine for first awakening his interest in the subject and for the critical reading of the manuscript. This research was in part supported by NASA grants NSG–7643 and NGL–22–009–638.

REFERENCES

Abramowitz, M., and Stegun, I. A. 1964, *Handbook of Mathematical Functions* (Washington: National Bureau of Standards), p.890.

Bahcall, J. N., and Soneira, R. M. 1980, *Ap. J. Suppl.*, **44**, 73.

Bahcall, J. N., and Soneira, R. M. 1984, *Ap. J. Suppl.*, **55**, 67.

Bertin, G., and Mark, J. W. K. 1980, *Astron. Astrophys.*, **88**, 289.

Camm, G. L. 1950, *M. N. R. A. S.*, **110**, 305.

Jeans, J. H. 1928, *Astronomy and Cosmogony* (London: Cambridge University Press), p.348.

Kulsrud, R. M., Mark, J. W. K., and Caruso, A. 1971, *Astrophys. Sp. Sci.*, **14**, 52.

Ledoux, P. 1951, *Annales d'Astrophysique*, **14**, 438.

Mihalas, D., and Binney, J. 1981, *Galactic Astronomy* (San Francisco: Freeman), pp.477-483.

Oort, J. H. 1927, *Bull. Astron. Inst. Netherlands*, **3**, 275.

Schmidt, M. 1965, *Galactic Structure*, ed. A. Blaauw and M. Schmidt (Chicago: University of Chicago Press), p.513-530.

Spitzer, L., Jr. 1942, *Ap. J.*, **95**, 329.

Spitzer, L., Jr. 1962, *Physics of Fully Ionized Gases* (New York: Wiley-Interscience), p.106.

Toomre, A. 1964, *Ap. J.*, **139**, 1217.

Toomre, A. 1966, *Notes on the 1966 Summer Study Program in Geophysical Fluid Dynamics at the Woods Hole Oceanographic Institution*, pp.111-115.

Toomre, A. 1983, *IAU Symposium No. 100, Internal Kinematics and Dynamics*

of Galaxies, ed. E. Athanassoula (Dordrecht: Reidel), pp.177-186.

Wielen, R. 1974, *Highlights of Astronomy* (Dordrecht: Reidel), pp.395-407

FIGURE AND TABLE CAPTIONS

Figure 1:— The region of the hose instability for a non-rotating stellar system with a finite thickness and an anisotropic Gaussian velocity distribution in vertical and horizontal directions. Boundary curves corresponding to growth rates (in units of $2\pi\sigma/\lambda_J$) $s = 0, 0.1, 0.2, 0.3$ are drawn in the parameter space (λ_*, R), where $\lambda_* = \lambda/\lambda_J$ is the wavelengh in units of the Jeans wavelength and $R = \sigma_w/\sigma$ is the ratio of the vertical to the horizontal velocity dispersion.

Figure 2:— The region of the Jeans instability for a non-rotating stellar system with a finite thickness and an anisotropic Gaussian velocity distribution in vertical and horizontal directions. Boundary curves corresponding to growth rates (in units of $2\pi\sigma/\lambda_J$) $s = 0, 0.1, 0.2, 0.3$ are drawn in the prameter space (λ_*, R), where $\lambda_* = \lambda/\lambda_J$ is the wavelength in units of the Jeans wavelength and $R = \sigma_w/\sigma$ is the ratio of the vertical to the horizontal velocity dispersion.

Figure 3:— The mutual relationship between hose and Jeans boundary curves. The part of the parameter space (λ_*, R) where both the hose instability and the Jeans instability are possible.

Table 1:— The vertical components of stellar velocities (in units of the vertical velocity dispersion) when they pass through the neutral plane, which are necessary to accomplish the w_0 integration in Equation (72) by the 32-point Laguerre integration formula. The first fifteen values of w_0 are actually necessary since the rest have too small weight factors.

Table 2:— The lower order ($k, m \leq 8$) elements of a typical response matrix A_{km} when $s = 0$, $R = 0.1$ and $\lambda_* = 1$.

Table 3:— Eigenvalues of $i \times i$ submatrices ($i \leq 8$) shown in Table 2.

Table 4:— The critical wavelengths (in units of the Jeans wavelength) in the limiting case of a non-rotating infinitesimally thin stellar system: $R = 0$. The

hose critical wavelengths, other than an obvious solution $\lambda_* = 0$, are analytically given by Equation (89). The Jeans critical wavelengths are found numerically from Equation (90). Numerical values of these critical wavelengths are shown for reduced growth rates $s = 0, 0.1, 0.2, 0.3$.

Figure 1

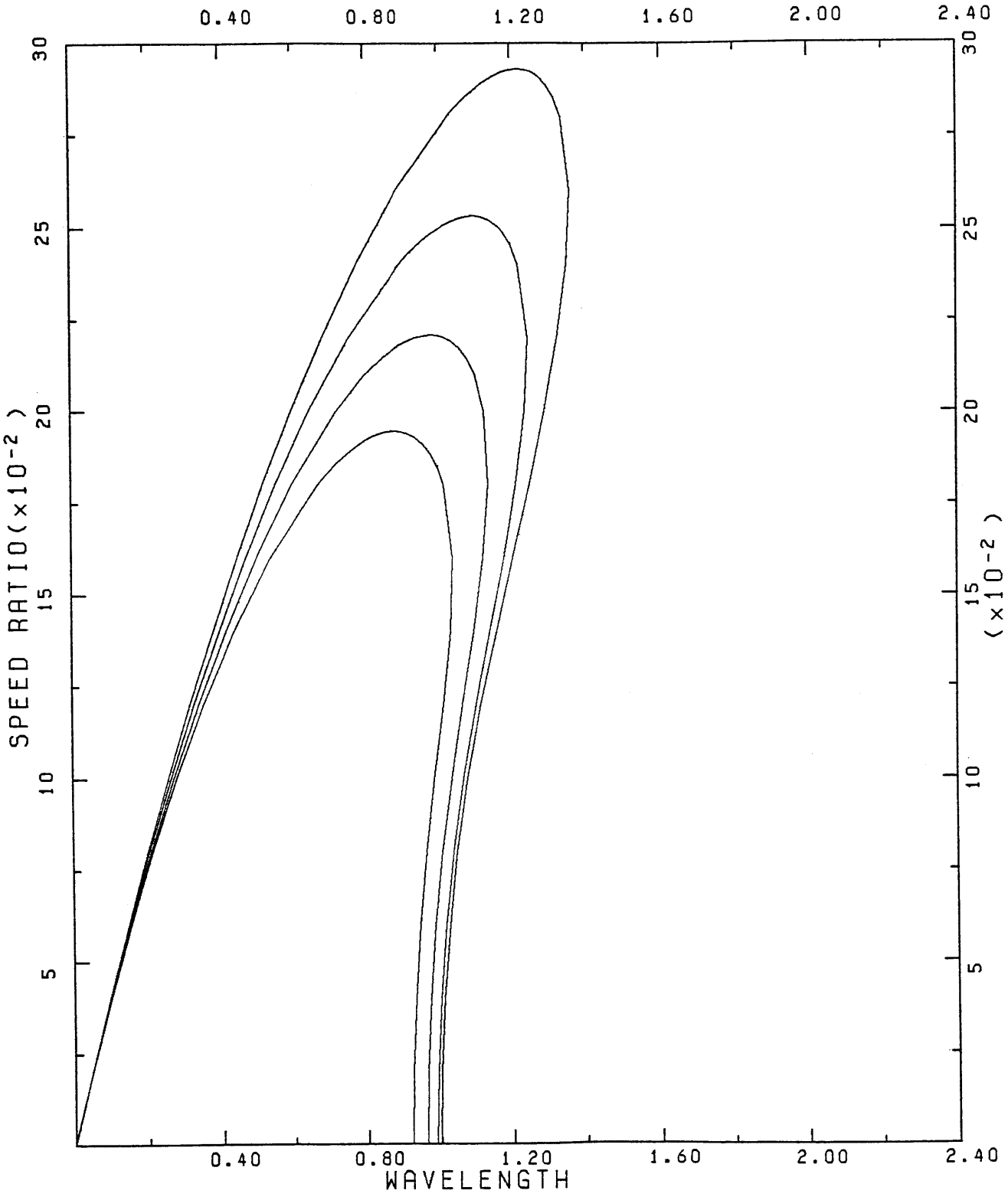
0.40
0.80
1.20
1.60
2.00
2.40
30
25
20
15
10
5
SPEED RATIO(x10-2)
(x10-2)
WAVELENGTH

Figure 2

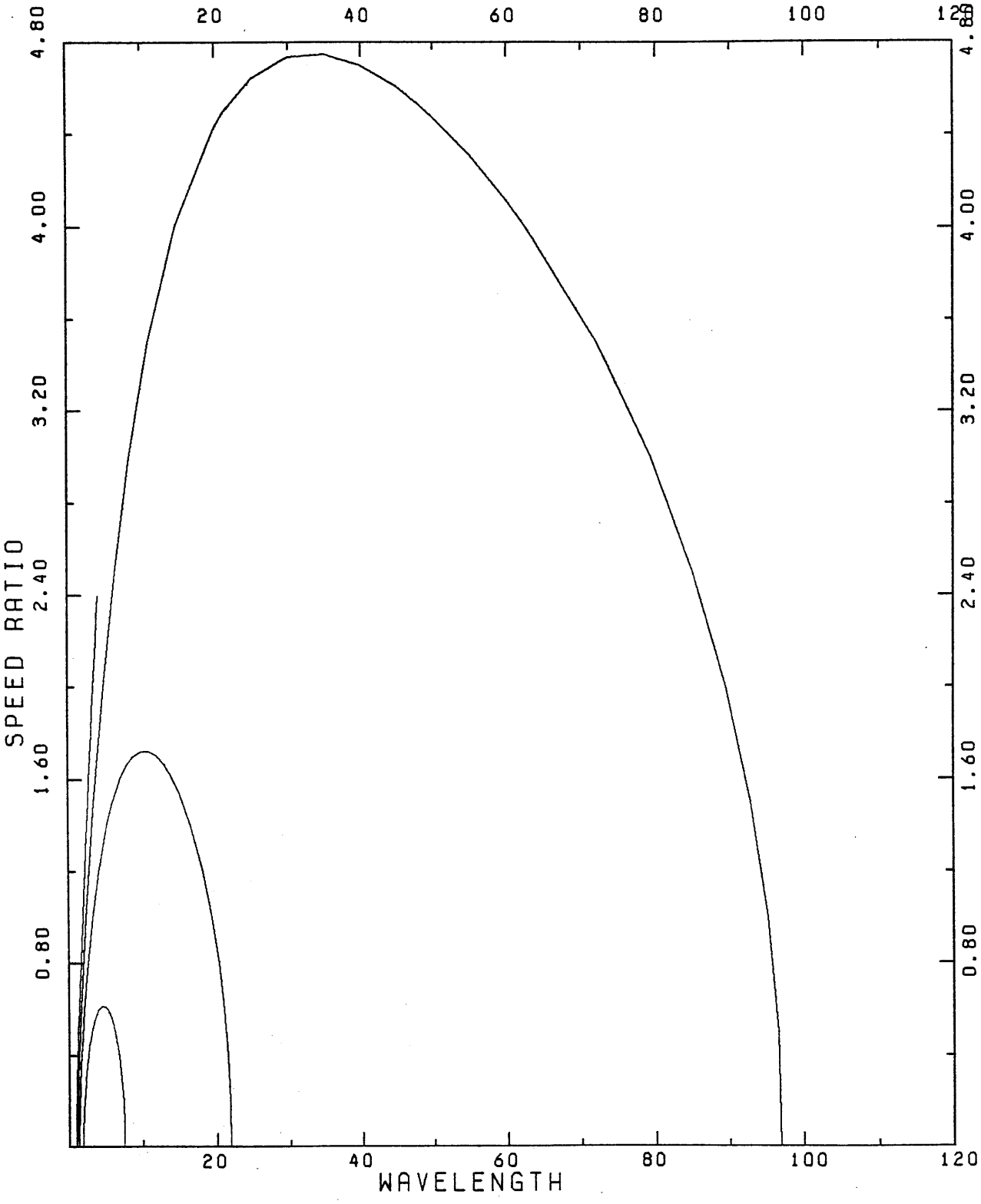
20
40
60
80
100
120
4.80
4.00
3.20
2.40
1.60
0.80
SPEED RATIO
WAVELENGTH

Figure 3

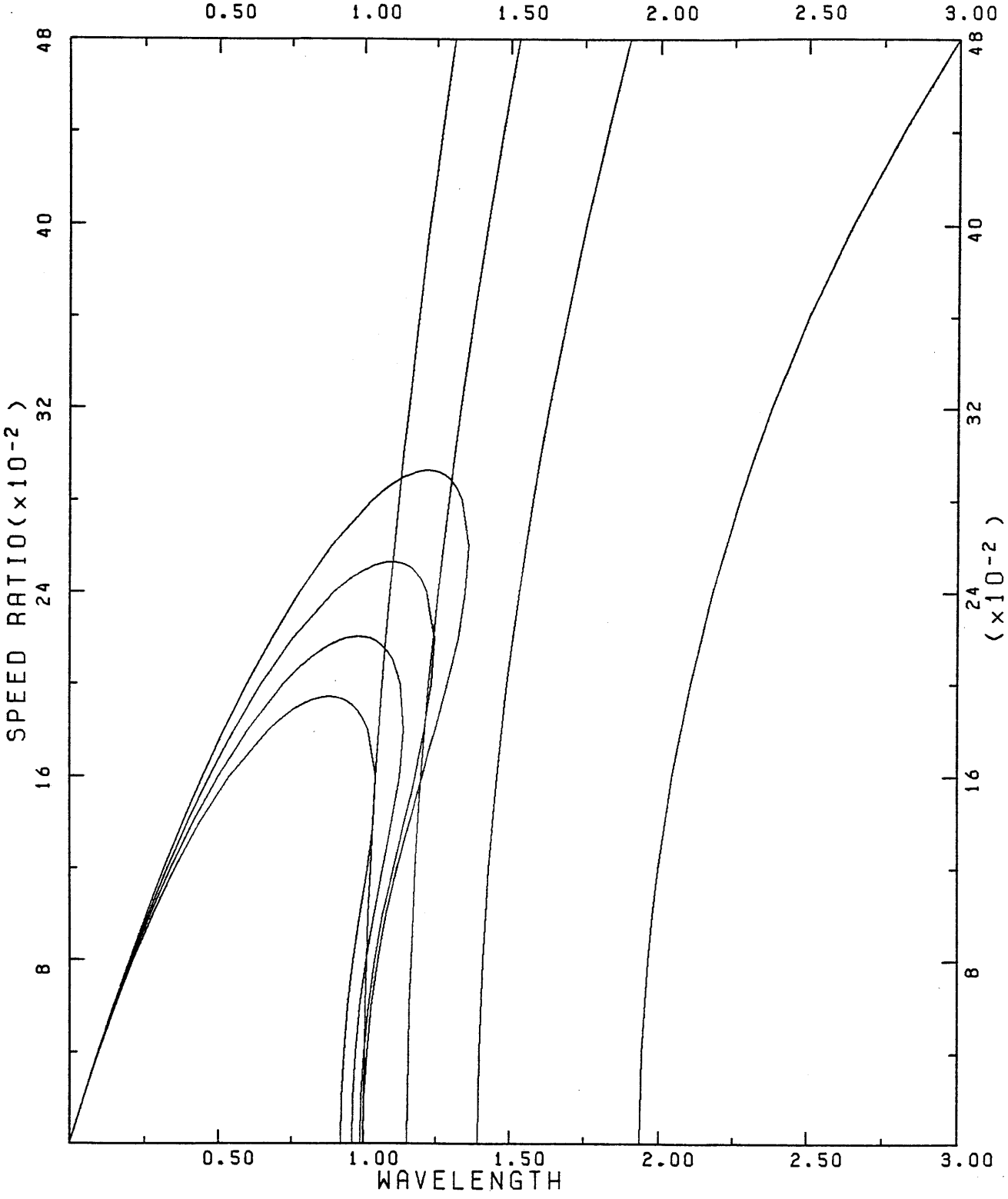
0.50
1.00
1.50
2.00
2.50
3.00
48
40
32
24
16
8
SPEED RATIO(x10-2)
(x10-2)
WAVELENGTH

Table 1

i	$w_0(i)$
1	0.298293
2	0.684874
3	1.074137
4	1.464547
5	1.856022
6	2.248705
7	2.642807
8	3.038571
9	3.436265
10	3.836177
11	4.238618
12	4.643925
13	5.052464
14	5.464639
15	5.880894

Table 2

$$A_{km} =$$

1.002919	−0.009102	−0.005071	−0.003341	−0.002400	−0.001824	−0.001411	−0.001278
0.001029	0.169159	−0.000308	−0.000305	−0.000253	−0.000206	−0.000171	−0.000099
0.000178	0.000555	0.067653	0.000065	−0.000006	−0.000025	−0.000014	−0.000105
0.000054	0.000153	0.000312	0.036205	0.000082	0.000037	−0.000016	0.000094
0.000022	0.000059	0.000111	0.000191	0.022506	0.000052	0.000079	−0.000033
0.000011	0.000028	0.000050	0.000081	0.000118	0.015355	0.000021	0.000013
0.000006	0.000015	0.000027	0.000035	0.000075	0.000070	0.011100	0.000069
0.000003	0.000009	0.000011	0.000032	0.000020	0.000038	0.000084	0.008424

Table 3

1	1.002919							
2	1.002908	0.169170						
3	1.002907	0.169168	0.067656					
4	1.002907	0.169168	0.067657	0.036205				
5	1.002907	0.169168	0.067657	0.036206	0.022505			
6	1.002907	0.169168	0.067657	0.036206	0.022506	0.015354		
7	1.002907	0.169168	0.067657	0.036206	0.022507	0.015354	0.011099	
8	1.002907	0.169168	0.067657	0.036206	0.022506	0.015354	0.011101	0.008422

Table 4

s	Hose Mode	Jeans Mode
0	$0, 1$	$1, \infty$
0.1	$0, 0.990195$	$1.152106, 96.967545$
0.2	$0, 0.962912$	$1.396445, 21.835955$
0.3	$0, 0.923280$	$1.938289, 7.510781$

CHAPTER 3.

THE DYNAMICS OF DENSE PARTICLE DISKS

THE DYNAMICS OF DENSE PARTICLE DISKS

Suguru Araki and Scott Tremaine*

Department of Physics, Center for Theoretical Physics
and Center for Space Research,
Massachusetts Institute of Technology,
Cambridge, Massachusetts 02139

* Alfred P. Sloan Research Fellow

ABSTRACT

We investigate the mechanical equilibrium and collisional transport processes in differentially rotating dense particle disks in which the filling factor is not small, so that the ordinary Boltzmann kinetic theory is not accurate. Our treatment is based on the Enskog theory of dense hard sphere gases, except that the spheres are inelastic. We show that the viscous instability which has been suggested as a source of the structure in Saturn's B ring does not arise in our models. However, the ring may be subject to a liquid-solid phase transition so that alternating "frozen" and "melted" zones may be present.

I. INTRODUCTION

Since the celebrated work by Maxwell (1890) there have been a number of theoretical attempts at understanding the structure and stability of planetary rings, using both hydrodynamical and kinetic theoretical approaches. Hydrodynamical treatments would be accurate if the collision frequency were much higher than the orbital frequency, whereas the equations of stellar dynamics would apply if the collision frequency were much lower than the orbital frequency. However, neither theory can accurately account for the behavior of planetary rings since the two frequencies are comparable with each other in particulate rings with optical depth near unity. Therefore, we must solve the Boltzmann equation with an appropriate collision term. In general it is a difficult task to determine the collision term for a many-particle system and various approximate methods have been developed to evaluate the collision term by various authors.

Cook and Franklin (1964) solved the Boltzmann equation for a differentially rotating disk, using the relaxation-time approximation to the collision term (Krook model): $(\partial f/\partial t)_c = -\nu_c(f - f_0)$ where ν_c is the collision frequency and f_0 is the equilibrium distribution function. Unfortunately the Krook model works best for collisions of elastic particles, and Cook and Franklin had to introduce the energy loss in inelastic collisions in an *ad hoc* way.

Recently Shu and Stewart (1985) have discussed an elegant modification to the Krook model in which different velocity dispersions are assigned to the phase space distribution function and its equilibrium counterpart. This modification provides a natural way for the Krook approximation to handle inelastic collisions. However, although the relaxation-time approximation is very useful and helps us avoid the complications involved in a detailed account of particle collisions, it is difficult to estimate the errors involved and to know how to improve on this

assumption in a systematic way.

Goldreich and Tremaine (1978) constructed a model of collisional particle disks in which the collision term was evaluated by assuming that the velocity distribution was a triaxial Gaussian. Their results are probably more accurate than results based on the Krook model. However, this treatment still neglects spin degrees of freedom and the finite size of the particles.

Brahic (1977) was the first to stress the importance of the finite size of the ring particles. He showed that nonlocal effects in collisions led to a minimum velocity dispersion of the ring particles which was comparable with the difference in orbital velocities between radially adjacent particles.

Recently the generalization to include the spin degrees of freedom and the effect of nonlocal collisions has been investigated by Shukhman (1984).

All the above analytic treatments have assumed low filling factors, but it is also important to deal with high filling factors. A dense particle disk is not expected to behave like a gas but like a liquid and therefore liquid models are essential for understanding the features of rings with high optical depths, such as the Saturnian B ring. It is even conceivable that parts of the ring may be in a solid phase. Thus it is important to study the possibility of a phase transition between the two phases. A crude model of dense disks, based on a granular flow model due to Haff (1983), was investigated by Borderies *et al.* (1985).

In this paper we generalize the kinetic theory of differentially rotating particle disks to the case where the filling factor is not small by employing the Enskog theory of dense hard sphere gases (Enskog, 1922). In §**II** we derive the Boltzmann equation and its moment equations in cylindrical coordinates and apply them to the axially symmetric steady state. Particle spins are included in the derivation. §**III** is devoted to the construction and evaluation of the Enskog collision term and

to the definition of the momentum flux density tensor. We consider actual ring models and present numerical results in §**IV**. Spin degrees of freedom are neglected in the present numerical analysis, but they will be included in a subsequent paper. A discussion is given in §**V**.

II. THE BOLTZMANN EQUATION AND ITS MOMENTS

II.1. The Boltzmann Equation in Cylindrical Coordinates

In our analysis of particle disks at high optical depths we make the following assumptions:

(i) The particles are identical hard spheres of mass m, diameter a and moment of inertia I. Thus, we neglect the effects of the particle size distribution.

(ii) Collisions are inelastic so that, after each collision, the magnitude of the normal component of the relative velocity decreases by a factor equal to the normal restitution coefficient ϵ_n, $0 \leq \epsilon_n \leq 1$, while the tangential component changes by a factor equal to the tangential restitution coefficient ϵ_t, $-1 \leq \epsilon_t \leq 1$. Perfectly smooth spheres have $\epsilon_t = 1$ while perfectly rough spheres have $\epsilon_t = -1$. These coefficients are assumed to be independent of the magnitude of the incident relative velocity. In most materials the normal restitution coefficient decreases as the relative velocity increases; we have neglected this dependence since it does not play a central role in the models we examine here.

(iii) Gravitational scattering is neglected, although the overall self-gravitational field of the ring will be included.

(iv) The velocity ellipsoid is assumed to be independent of the vertical coordinate z. (Within the other assumptions of our model, this can be proved to be true in the limit of high optical depths; see equation [141] in §**IV.3**). The spin pressure tensor (equation [17] below) is also assumed to be independent of z.

We begin by deriving the Boltzmann equation which governs the distribution function of the ring particles. Many of the results in this section were first obtained by Shukhman (1984).

Let the center of mass of a ring particle have the radius vector $\vec{x}$. The orientation of the body is specified by the three Euler angles, which together with the three components of the vector $\vec{x}$ make six coordinates. The continuity equation for the system of particles is given by

$$\frac{\partial F}{\partial t} + \frac{\partial}{\partial \vec{q}} \cdot \left(F \frac{d\vec{q}}{dt} \right) + \frac{\partial}{\partial \vec{p}} \cdot \left(F \frac{d\vec{p}}{dt} \right) = \left(\frac{\partial F}{\partial t} \right)_c . \tag{1}$$

Here the distribution function F is defined so that $F(\vec{p}, \vec{q}, t) d\vec{p} d\vec{q}$ is the number of particles at time t whose generalized momenta are within an element $d\vec{p}$ around $\vec{p}$ and whose generalized coordinates are within $d\vec{q}$ around $\vec{q}$, where $\vec{q} = (q_1, \ldots, q_6)$ and $\vec{p} = (p_1, \ldots, p_6)$. The term $(\partial F/\partial t)_c$ is the rate of change of F due to collisions. Using Hamilton's equations

$$\frac{d\vec{q}}{dt} = \frac{\partial H}{\partial \vec{p}}, \qquad \frac{d\vec{p}}{dt} = -\frac{\partial H}{\partial \vec{q}},$$

we can express equation (1) as

$$\frac{\partial F}{\partial t} + \frac{\partial H}{\partial \vec{p}} \cdot \frac{\partial F}{\partial \vec{q}} - \frac{\partial H}{\partial \vec{q}} \cdot \frac{\partial F}{\partial \vec{p}} = \left(\frac{\partial F}{\partial t} \right)_c . \tag{2}$$

We write $\vec{q} = (r, \theta, z, \alpha, \beta, \gamma)$ where r, θ, z are the usual cylindrical coordinates and α, β, γ are the Euler angles of a particle (See Figure 1 for definitions). The particle Hamiltonian is

$$H = \frac{1}{2m} \left(p_r^2 + \frac{p_\theta^2}{r^2} + p_z^2 \right) + \frac{1}{2I} \left(p_\alpha^2 + \frac{p_\beta^2 + p_\gamma^2 - 2 p_\beta p_\gamma \cos \alpha}{\sin^2 \alpha} \right) + mU(r, \theta, z), \tag{3}$$

where p_r, p_θ, p_z, p_α, p_β, p_γ are the generalized momenta corresponding to r, θ, z, α, β, γ, respectively, and U is the gravitational potential per unit mass. Due to the spherical symmetry of the particle the potential is independent of the Euler angles. Substituting equation (3) into equation (2), we find

$$\frac{\partial F}{\partial t} + \frac{p_r}{m} \frac{\partial F}{\partial r} + \frac{p_\theta}{m r^2} \frac{\partial F}{\partial \theta} + \frac{p_z}{m} \frac{\partial F}{\partial z}$$

$$-\left(-\frac{p_\theta^2}{mr^3}+m\frac{\partial U}{\partial r}\right)\frac{\partial F}{\partial p_r}-m\frac{\partial U}{\partial \theta}\frac{\partial F}{\partial p_\theta}-m\frac{\partial U}{\partial z}\frac{\partial F}{\partial p_z}$$
$$+\frac{p_\alpha}{I}\frac{\partial F}{\partial \alpha}+\frac{p_\beta-p_\gamma\cos\alpha}{I\sin^2\alpha}\frac{\partial F}{\partial \beta}+\frac{p_\gamma-p_\beta\cos\alpha}{I\sin^2\alpha}\frac{\partial F}{\partial \gamma}$$
$$-\frac{(p_\beta-p_\gamma\cos\alpha)(p_\gamma-p_\beta\cos\alpha)}{I\sin^3\alpha}\frac{\partial F}{\partial p_\alpha}=\left(\frac{\partial F}{\partial t}\right)_c. \tag{4}$$

We now wish to use (v_r, v_θ, v_z) instead of (p_r, p_θ, p_z) and $(\omega_r, \omega_\theta, \omega_z)$ instead of $(p_\alpha, p_\beta, p_\gamma)$, where $\vec{v} = v_r\hat{r} + v_\theta\hat{\theta} + v_z\hat{z}$ is the velocity of the center of mass of the sphere and $\vec{\omega} = \omega_r\hat{r} + \omega_\theta\hat{\theta} + \omega_z\hat{z}$ is its angular velocity about its center of mass. The relations between the old and new variables are

$$v_r = \frac{p_r}{m}, \qquad v_\theta = \frac{p_\theta}{mr}, \qquad v_z = \frac{p_z}{m},$$
$$\omega_r = \frac{p_\alpha}{I}\cos(\theta-\beta) + \frac{p_\beta\cos\alpha - p_\gamma}{I\sin\alpha}\sin(\theta-\beta),$$
$$\omega_\theta = -\frac{p_\alpha}{I}\sin(\theta-\beta) + \frac{p_\beta\cos\alpha - p_\gamma}{I\sin\alpha}\cos(\theta-\beta),$$
$$\omega_z = \frac{p_\beta}{I}. \tag{5}$$

We define a new distribution function f so that

$$f(\vec{x},\vec{\phi},\vec{v},\vec{\omega},t)d\vec{x}d\vec{\phi}d\vec{v}d\vec{\omega} = F(\vec{p},\vec{q},t)d\vec{p}d\vec{q},$$

where $\vec{\phi} = (\alpha,\beta,\gamma)$ and $d\vec{\phi} = d\alpha d\beta d\gamma$. The relation between F and f is given by

$$f(\vec{x},\vec{\phi},\vec{v},\vec{\omega},t) = (mI)^3\sin\alpha F(\vec{q},\vec{p},t). \tag{6}$$

Using equations (5) and (6), we can express all the derivatives in equation (4) in terms of the new variables. Consequently, the Boltzmann equation for f is

$$\frac{\partial f}{\partial t}+v_r\frac{\partial f}{\partial r}+\frac{v_\theta}{r}\frac{\partial f}{\partial \theta}+v_z\frac{\partial f}{\partial z}$$
$$+\left(-\frac{\partial U}{\partial r}+\frac{{v_\theta}^2}{r}\right)\frac{\partial f}{\partial v_r}+\left(-\frac{1}{r}\frac{\partial U}{\partial \theta}-\frac{v_r v_\theta}{r}\right)\frac{\partial f}{\partial v_\theta}-\frac{\partial U}{\partial z}\frac{\partial f}{\partial v_z}$$
$$+\frac{v_\theta\omega_\theta}{r}\frac{\partial f}{\partial \omega_r}-\frac{v_\theta\omega_r}{r}\frac{\partial f}{\partial \omega_\theta}$$

$$+\left[\omega_r\cos(\theta-\beta)-\omega_\theta\sin(\theta-\beta)\right]\left(\frac{\partial f}{\partial\alpha}-f\cot\alpha\right)$$
$$+\left\{\omega_z+\cot\alpha\left[\omega_r\sin(\theta-\beta)+\omega_\theta\cos(\theta-\beta)\right]\right\}\frac{\partial f}{\partial\beta}$$
$$-\csc\alpha\left[\omega_r\sin(\theta-\beta)+\omega_\theta\cos(\theta-\beta)\right]\frac{\partial f}{\partial\gamma}=\left(\frac{\partial f}{\partial t}\right)_c. \tag{7}$$

If the spheres are randomly oriented, then F does not depend on the Euler angles. Thus, f is proportional to $\sin\alpha$ and independent of β and γ. In this case, which we assume from now on, the last three terms on the left hand side of equation (7) drop out.

II.2. Moment Equations

The number density, the mean velocity and the pressure tensors of second and third ranks are defined by the lowest order velocity moments of the distribution function:

$$n(\vec{x},t)=\int f(\vec{x},\vec{v},\vec{\omega},t)d\vec{v}d\vec{\omega}, \tag{8}$$

$$nu_A(\vec{x},t)=\int v_A f d\vec{v}d\vec{\omega}, \tag{9}$$

$$p_{AB}(\vec{x},t)=\int(v_A-u_A)(v_B-u_B)f d\vec{v}d\vec{\omega}, \tag{10}$$

$$p_{ABC}(\vec{x},t)=\int(v_A-u_A)(v_B-u_B)(v_C-u_C)f d\vec{v}d\vec{\omega}, \tag{11}$$

where suffixes A, B and C denote r, θ or z.

Next, velocity moments of the collision term are defined by

$$T_A(\vec{x},t)=\int v_A\left(\frac{\partial f}{\partial t}\right)_c d\vec{v}d\vec{\omega}, \tag{12}$$

and

$$Q_{AB}(\vec{x},t)=\int(v_A-u_A)(v_B-u_B)\left(\frac{\partial f}{\partial t}\right)_c d\vec{v}d\vec{\omega}. \tag{13}$$

Note that T_A would vanish if collisions were assumed to be local, i.e., if the finite size of the constituent particles were neglected. Local collisions would ensure local conservation of momentum regardless of whether collisions are elastic or inelastic and thus T_A would vanish; however, in a nonlocal collision model momentum can be transferred across a boundary via sound waves travelling through particles which straddle the boundary ("collisional" momentum transfer as opposed to the usual "translational" transfer). Thus we cannot neglect the difference $\delta\vec{U}$ in the mean orbital velocity Ωr between adjacent particles with a radial separation of order a. Since $\delta U \approx r\Omega' a \approx \Omega a$, it turns out that the effect of nonlocal collisions is important if the velocity dispersion becomes comparable to or smaller than Ωa, i.e., if the ring is a monolayer. The effect of particle size can be neglected when the velocity dispersion is much larger than Ωa.

The spin counterparts of equations (9), (10), (12), (13) are defined in a similar manner by the angular velocity moments:

$$n\mu_A(\vec{x},t) = \int \omega_A f d\vec{v} d\vec{\omega}, \tag{14}$$

$$\nu_{AB}(\vec{x},t) = \int (\omega_A - \mu_A)(\omega_B - \mu_B) f d\vec{v} d\vec{\omega}, \tag{15}$$

$$M_A(\vec{x},t) = \int \omega_A \left(\frac{\partial f}{\partial t}\right)_c d\vec{v} d\vec{\omega}, \tag{16}$$

$$H_{AB}(\vec{x},t) = \int (\omega_A - \mu_A)(\omega_B - \mu_B)\left(\frac{\partial f}{\partial t}\right)_c d\vec{v} d\vec{\omega}. \tag{17}$$

The continuity equation, Euler's equation, the viscous-stress equation and the spin counterparts of the latter two equations are now obtained by multiplying equation (7) by 1, v_A, $(v_A - u_A)(v_B - u_B)$, ω_A, $(\omega_A - \mu_A)(\omega_B - \mu_B)$, respectively, and then by integrating over $\vec{v}$ and $\vec{\omega}$.

The continuity equation reads

$$\frac{\partial n}{\partial t} + \frac{\partial (n u_r)}{\partial r} + \frac{1}{r}\frac{\partial (n u_\theta)}{\partial \theta} + \frac{\partial (n u_z)}{\partial z} + \frac{n u_r}{r} = 0, \tag{18}$$

where we have used the fact that the number density is not changed by collisions:

$$\int \left(\frac{\partial f}{\partial t}\right)_c d\vec{v}d\vec{\omega} = 0. \tag{19}$$

Euler's equation reads

$$n\frac{Du_A}{Dt} + n\left(\frac{\partial U}{\partial r}\delta_{Ar} + \frac{1}{r}\frac{\partial U}{\partial \theta}\delta_{A\theta} + \frac{\partial U}{\partial z}\delta_{Az}\right) + \frac{\partial p_{Ar}}{\partial r} + \frac{1}{r}\frac{\partial p_{A\theta}}{\partial \theta} + \frac{\partial p_{Az}}{\partial z}$$
$$-\delta_{Ar}\frac{nu_\theta{}^2 + p_{\theta\theta}}{r} + \delta_{A\theta}\frac{nu_\theta u_r + p_{r\theta}}{r} + \frac{p_{Ar}}{r} = T_A, \tag{20}$$

where equation (19) has been used and the convective derivative is defined by

$$\frac{D}{Dt} = \frac{\partial}{\partial t} + u_r\frac{\partial}{\partial r} + \frac{u_\theta}{r}\frac{\partial}{\partial \theta} + u_z\frac{\partial}{\partial z}. \tag{21}$$

The viscous-stress equation reads

$$\frac{Dp_{AB}}{Dt} + \left(\frac{\partial u_r}{\partial r} + \frac{u_r}{r} + \frac{1}{r}\frac{\partial u_\theta}{\partial \theta} + \frac{\partial u_z}{\partial z}\right)p_{AB}$$
$$+\left(\frac{\partial u_B}{\partial r} + \delta_{B\theta}\frac{u_\theta}{r}\right)p_{Ar} + \left(\frac{\partial u_A}{\partial r} + \delta_{A\theta}\frac{u_\theta}{r}\right)p_{Br}$$
$$+\left(\frac{1}{r}\frac{\partial u_B}{\partial \theta} - \delta_{Br}\frac{2u_\theta}{r} + \delta_{B\theta}\frac{u_r}{r}\right)p_{A\theta} + \left(\frac{1}{r}\frac{\partial u_A}{\partial \theta} - \delta_{Ar}\frac{2u_\theta}{r} + \delta_{A\theta}\frac{u_r}{r}\right)p_{B\theta}$$
$$+\frac{\partial u_B}{\partial z}p_{Az} + \frac{\partial u_A}{\partial z}p_{Bz}$$
$$+\frac{\partial p_{ABr}}{\partial r} + \frac{p_{ABr}}{r} + \frac{1}{r}\frac{\partial p_{AB\theta}}{\partial \theta} + \frac{\partial p_{ABz}}{\partial z}$$
$$+\frac{1}{r}(\delta_{A\theta}p_{Br\theta} + \delta_{B\theta}p_{Ar\theta} - \delta_{Ar}p_{B\theta\theta} - \delta_{Br}p_{A\theta\theta}) = Q_{AB}. \tag{22}$$

Since we assume that the random speeds are much smaller than the mean orbital speeds, all the pressure tensors of the third rank in equation (22) will be dropped from now on except $\partial p_{ABz}/\partial z$, which is formally of the same order as the terms we keep (however, as we shall see this term never contributes to our final answer).

In deriving the spin counterparts of equations (20) and (22), we assume, following Shukhman, that it is possible to separate variables in the distribution function:

$$f(\vec{x}, \vec{v}, \vec{\omega}) = f_T(\vec{x}, \vec{v})f_S(\vec{\omega}). \tag{23}$$

Then, we find

$$n\frac{D\mu_A}{Dt} - \delta_{Ar}\frac{nu_\theta\mu_\theta}{r} + \delta_{A\theta}\frac{nu_\theta\mu_r}{r} = M_A, \tag{24}$$

where equation (19) has been used again, and

$$\frac{D\nu_{AB}}{Dt} + \left(\frac{\partial u_r}{\partial r} + \frac{u_r}{r} + \frac{1}{r}\frac{\partial u_\theta}{\partial \theta} + \frac{\partial u_z}{\partial z}\right)\nu_{AB}$$
$$+\frac{u_\theta}{r}(\delta_{A\theta}\nu_{Br} + \delta_{B\theta}\nu_{Ar} - \delta_{Ar}\nu_{B\theta} - \delta_{Br}\nu_{A\theta}) = H_{AB}. \tag{25}$$

II.3. Axially Symmetric Steady State Solutions

From now on we specialize to axially symmetric systems: $\partial/\partial\theta = 0$, and focus on the steady-state solutions: $\partial/\partial t = 0$.

Axial symmetry and time-independence imply that the mean orbital motion is circular so that

$$\vec{u} = u_\theta\hat{\theta} = r\Omega(r)\hat{\theta}, \tag{26}$$

where $\Omega(r)$ is the mean angular speed of circular motion. Axial symmetry also implies that the mean spin motion is given by

$$\vec{\mu} = \mu_z\hat{z} = \mu\hat{z}. \tag{27}$$

At any location in the central plane $z = 0$

$$p_{zr} = p_{z\theta} = \nu_{zr} = \nu_{z\theta} = p_{rrz} = p_{r\theta z} = p_{\theta\theta z} = p_{zzz} = 0. \tag{28}$$

Since, according to assumption (iv), the velocity ellipsoid is independent of z, equation (28) must be true in our model for arbitrary z.

From the above considerations, equations (20), (22), (24) and (25) are simplified to read (Shukhman, 1984, equations [8], [9], [10] and [11])

$$n\frac{\partial U}{\partial r} - nr\Omega^2 = T_r - \frac{\partial p_{rr}}{\partial r} - \frac{p_{rr}}{r} + \frac{p_{\theta\theta}}{r}, \tag{29-1}$$

$$0 = T_\theta - \frac{\partial p_{r\theta}}{\partial r} - \frac{2p_{r\theta}}{r}, \tag{29-2}$$

$$n\frac{\partial U}{\partial z} = T_z - \frac{\partial p_{zz}}{\partial z}, \tag{29-3}$$

$$0 = M_r, \qquad 0 = M_\theta, \qquad 0 = M_z, \tag{30}$$

$$-4\Omega p_{r\theta} = Q_{rr}, \tag{31-1}$$

$$\frac{\kappa^2}{\Omega} p_{r\theta} = Q_{\theta\theta}, \tag{31-2}$$

$$0 = Q_{zz}, \tag{31-3}$$

$$\frac{\kappa^2}{2\Omega} p_{rr} - 2\Omega p_{\theta\theta} = Q_{r\theta}, \tag{31-4}$$

$$0 = Q_{\theta z}, \tag{31-5}$$

$$0 = Q_{zr}, \tag{31-6}$$

$$-2\Omega\nu_{r\theta} = H_{rr}, \tag{32-1}$$

$$2\Omega\nu_{r\theta} = H_{\theta\theta}, \tag{32-2}$$

$$0 = H_{zz}, \tag{32-3}$$

$$\Omega(\nu_{rr} - \nu_{\theta\theta}) = H_{r\theta}, \tag{32-4}$$

$$0 = H_{\theta z}, \tag{32-5}$$

$$0 = H_{zr}, \tag{32-6}$$

where κ is the epicyclic frequency, defined by

$$\kappa^2(r) = 2\Omega(r)\left[2\Omega(r) + r\frac{d\Omega}{dr}\right]. \tag{33}$$

For each position there exist principal axes $(\hat{1}, \hat{2}, \hat{3})$ of the pressure tensor p which are in general tilted with respect to $(\hat{r}, \hat{\theta}, \hat{z})$. We can choose $\hat{3} = \hat{z}$ because

of equation (28). Then we introduce the transformation angle δ by $\hat{z}\sin\delta = \hat{r} \times \hat{1}$, where we can require δ to be between 0 and $\pi/2$ without loss of generality. In the new coordinate system p_{12} vanishes, and equation (31) is given by (Shukhman, 1984, equation [30])

$$-2Ap_{11}\sin 2\delta = Q_{11}, \tag{34-1}$$

$$2Ap_{22}\sin 2\delta = Q_{22}, \tag{34-2}$$

$$0 = Q_{33}, \tag{34-3}$$

$$(2\Omega - A - A\cos 2\delta)p_{11} - (2\Omega - A + A\cos 2\delta)p_{22} = Q_{12}, \tag{34-4}$$

$$0 = Q_{23}, \tag{34-5}$$

$$0 = Q_{31}, \tag{34-6}$$

where Oort's constant A is defined by

$$A(r) = -\frac{r}{2}\frac{d\Omega}{dr}. \tag{35}$$

Similarly, there exist principal axes ($\hat{a}$, $\hat{b}$, $\hat{c}$) of the spin pressure tensor ν. We can take $\hat{c} = \hat{3}$ because of equation (28). We introduce another transformation angle Δ by $\hat{3}\sin\Delta = \hat{1} \times \hat{a}$, where Δ also ranges between 0 and $\pi/2$. In the new coordinate system ν_{ab} vanishes, and equation (32) is given by (Shukhman, 1984, equation [31])

$$0 = H_{aa}, \tag{36-1}$$

$$0 = H_{bb}, \tag{36-2}$$

$$0 = H_{cc}, \tag{36-3}$$

$$\Omega(\nu_{aa} - \nu_{bb}) = H_{ab}, \tag{36-4}$$

$$0 = H_{bc}, \tag{36-5}$$

$$0 = H_{ca}. \tag{36-6}$$

Both the pressure tensor p and the spin pressure tensor ν are symmetric. It is to be noted that Q_{12} and H_{ab} may remain finite even though p_{12} and ν_{ab} vanish.

III. THE ENSKOG COLLISION TERM

III.1. Mechanics of Inelastic Two-Body Collisions

Suppose that two identical spheres with initial velocities $(\vec{v},\vec{\omega})$ and $(\vec{v}_1,\vec{\omega}_1)$ collide with each other and leave the collision site with final velocities $(\vec{v}\,',\vec{\omega}\,')$ and $(\vec{v}_1\,',\vec{\omega}_1')$, respectively. The centers of the two spheres at the instant of collision define a unit vector

$$\hat{\lambda} = \frac{\vec{x} - \vec{x}_1}{a}, \tag{37}$$

where a is the diameter of the sphere. $\hat{\lambda}$ is normal to the tangential plane of the two spheres. The initial and final relative velocities are given by

$$\vec{g} = \vec{v}_1 - \vec{v}, \tag{38}$$

$$\vec{g}\,' = \vec{v}_1\,' - \vec{v}\,'. \tag{39}$$

Conservation of momentum requires

$$\vec{v} + \vec{v}_1 = \vec{v}\,' + \vec{v}_1\,'. \tag{40}$$

The velocity change in the collision is

$$\vec{v}\,' - \vec{v} = \frac{\Delta\vec{P}}{m} = -(\vec{v}_1\,' - \vec{v}_1), \tag{41}$$

where

$$\Delta\vec{P} = \frac{m}{2}(\vec{g} - \vec{g}\,') \tag{42}$$

is the impulse exerted on the sphere with initial velocities $(\vec{v},\ \vec{\omega})$ during the collision. Since the changes of the angular momenta due to collision are given by

$$I(\vec{\omega}\,' - \vec{\omega}) = \frac{-a\hat{\lambda}}{2} \times \Delta\vec{P}, \tag{43}$$

$$I(\vec{\omega}_1\,' - \vec{\omega}_1) = \frac{a\hat{\lambda}}{2} \times (-\Delta\vec{P}), \tag{44}$$

we get

$$\vec{\omega}' - \vec{\omega} = -\frac{a}{2I}\hat{\lambda} \times \Delta\vec{P} = \vec{\omega}_1{}' - \vec{\omega}_1 \tag{45}$$

and

$$\vec{s}' = \vec{s} - \frac{a}{I}\hat{\lambda} \times \Delta\vec{P}, \tag{46}$$

where

$$\vec{s} = \vec{\omega} + \vec{\omega}_1 \tag{47}$$

and

$$\vec{s}' = \vec{\omega}' + \vec{\omega}_1{}'. \tag{48}$$

Introducing the relative velocities of the two contacting points before and after the collision:

$$\vec{W} = \left(\vec{v}_1 + \vec{\omega}_1 \times \frac{a\hat{\lambda}}{2}\right) - \left(\vec{v} + \vec{\omega} \times \frac{-a\hat{\lambda}}{2}\right) = \vec{g} + \frac{a}{2}\vec{s} \times \hat{\lambda}, \tag{49}$$

$$\vec{W}' = \vec{g}' + \frac{a}{2}\vec{s}' \times \hat{\lambda}, \tag{50}$$

and their normal and tangential components to the tangent plane:

$$\vec{W}_n = \vec{g}_n, \tag{51}$$

$$\vec{W}_t = \vec{g}_t + \frac{a}{2}\vec{s} \times \hat{\lambda}, \tag{52}$$

$$\vec{W}_n' = \vec{g}_n{}', \tag{53}$$

$$\vec{W}_t' = \vec{g}_t{}' + \frac{a}{2}\vec{s}' \times \hat{\lambda}, \tag{54}$$

where

$$\vec{W}_n = (\vec{W} \cdot \hat{\lambda})\hat{\lambda}, \qquad \vec{W}_t = \vec{W} - \vec{W}_n, \tag{55}$$

$$\vec{g}_n = (\vec{g} \cdot \hat{\lambda})\hat{\lambda}, \qquad \vec{g}_t = \vec{g} - \vec{g}_n, \tag{56}$$

etc., we can now define the normal and tangential restitution coefficients by

$$\vec{W}_n' = -\epsilon_n \vec{W}_n \qquad (0 \leq \epsilon_n \leq 1) \tag{57}$$

and

$$\vec{W}_t' = \epsilon_t \vec{W}_t \qquad (-1 \leq \epsilon_t \leq 1). \tag{58}$$

$\epsilon_t = 1$ corresponds to perfectly smooth spheres, whose spin motions are decoupled from translational motions. This case was treated by Goldreich and Tremaine (1978). $\epsilon_t = -1$ corresponds to perfectly rough spheres. When two rough spheres collide, the points which come into contact will not, in general, possess the same velocity. It is supposed that the two spheres grip each other without slipping. First each sphere is strained by each other, and then the strain energy is reconverted into kinetic energy of translation and spin, no energy being lost. The effect is that the tangential relative velocity of the spheres at their point of contact is reversed by the impact. In the extreme cases above ($\epsilon_t = +1$ or $\epsilon_t = -1$), there is no energy loss due to tangential friction, while $\epsilon_t = 0$ corresponds to maximum energy loss due to tangential friction (the latter case was treated by Shukhman, 1984). From equations (42), (46), (49) and (50) we get

$$\Delta\vec{P} = \frac{m}{2}\left[\vec{W} - \vec{W}' - \frac{a^2}{2I}(\hat{\lambda} \times \Delta\vec{P}) \times \hat{\lambda}\right]. \tag{59}$$

Taking the normal and tangential components of equation (59) and using the definitions (57) and (58), we find

$$\Delta\vec{P}_n = m\kappa_n \vec{W}_n \tag{60}$$

and

$$\Delta\vec{P}_t = m\kappa_t \vec{W}_t, \tag{61}$$

where

$$\kappa_n = \frac{1 + \epsilon_n}{2} \tag{62}$$

and

$$\kappa_t = \frac{1 - \epsilon_t}{2}\left(1 + \frac{ma^2}{4I}\right)^{-1}. \tag{63}$$

Note that our κ_t and ϵ_t are different from Shukhman's:

$$\kappa_t^S = \kappa_t(\epsilon_t = 0) = \frac{1}{2}\left(1 + \frac{ma^2}{4I}\right)^{-1}, \qquad \epsilon_t^S = 1 - 2\kappa_t^S = \left(1 + \frac{4I}{ma^2}\right)^{-1};$$

Shukhman's notation is unfortunate in that ϵ_t^S has nothing to do with the tangential restitution coefficient.

Thus we have

$$\frac{\Delta\vec{P}}{m} = \kappa_n\vec{W}_n + \kappa_t\vec{W}_t = -\frac{\kappa_n}{\epsilon_n}\vec{W}_n' + \frac{\kappa_t}{\epsilon_t}\vec{W}_t'. \tag{64}$$

Substituting equation (64) into equations (41) and (45), we obtain the final velocities expressed in terms of the initial velocities and the initial velocities in terms of the final velocities (Shukhman, 1984, equation [16]):

$$\vec{v}' = \vec{v} + \kappa_n\vec{W}_n + \kappa_t\vec{W}_t, \tag{65-1}$$

$$\vec{v}_1{}' = \vec{v}_1 - \kappa_n\vec{W}_n - \kappa_t\vec{W}_t, \tag{65-2}$$

$$\vec{\omega}' = \vec{\omega} - \frac{1 - \epsilon_t - 2\kappa_t}{a}\hat{\lambda} \times \vec{W}, \tag{65-3}$$

$$\vec{\omega}_1{}' = \vec{\omega}_1 - \frac{1 - \epsilon_t - 2\kappa_t}{a}\hat{\lambda} \times \vec{W} \tag{65-4}$$

and

$$\vec{v} = \vec{v}' + \frac{\kappa_n}{\epsilon_n}\vec{W}_n' - \frac{\kappa_t}{\epsilon_t}\vec{W}_t', \tag{66-1}$$

$$\vec{v}_1 = \vec{v}_1{}' - \frac{\kappa_n}{\epsilon_n}\vec{W}_n' + \frac{\kappa_t}{\epsilon_t}\vec{W}_t', \tag{66-2}$$

$$\vec{\omega} = \vec{\omega}' + \frac{1 - \epsilon_t - 2\kappa_t}{a\epsilon_t}\hat{\lambda} \times \vec{W}', \tag{66-3}$$

$$\vec{\omega}_1 = \vec{\omega}_1{}' + \frac{1 - \epsilon_t - 2\kappa_t}{2\epsilon_t}\hat{\lambda} \times \vec{W}'. \tag{66-4}$$

We can evaluate the amount of energy dissipated by the inelastic collision. From equations (38), (41) and (64) we find the change in the translational energy per unit mass

$$\Delta E^{(T)} = \frac{1}{2}(v'^2 + v_1'^2 - v^2 - v_1^2) = \kappa_n(\kappa_n - 1)W_n^2 - \kappa_t(\vec{g}_t \cdot \vec{W}_t) + \kappa_t^2 W_t^2. \tag{67}$$

Similarly, from equations (45), (47), (49), (63) and (64) the change in the spin energy per unit mass is:

$$\Delta E^{(S)} = \frac{I}{2m}(\omega'^2 + \omega_1'^2 - \omega^2 - \omega_1^2) = \kappa_t\left(\vec{g}_t \cdot \vec{W}_t - \frac{1+\epsilon_t+2\kappa_t}{2}W_t^2\right). \quad (68)$$

Thus, the change in the energy per unit mass is given by

$$\Delta E = \Delta E^{(T)} + \Delta E^{(S)} = -\frac{1}{4}\left[(1-\epsilon_n^2)g_n^2 + 2\kappa_t(1+\epsilon_t)W_t^2\right], \quad (69)$$

which is always negative and vanishes only when $\epsilon_n = 1$ and $\epsilon_t = \pm 1$. The first case corresponds to perfectly elastic and perfectly smooth spheres, whereas the second case corresponds to perfectly elastic and perfectly rough spheres.

We can see from equations (65) that the spin equations are decoupled from the translation equations if and only if

$$\epsilon_t = 1. \quad (70)$$

In this case collisions do not affect the spins on the spheres and the spin energy of the system is kept constant as seen from equation (68).

There is an interesting case which corresponds to complete concentration of the mass at the centers of the spheres. In this case I tends to zero and thus κ_t tends to zero even if $\epsilon_t \neq 1$. Equations (65–1) and (65–2) become identical with the analogous equations for smooth spheres, and the spin energy and translational energy cease to be interconvertible, as seen from equation (68). Thus the translational motion is completely unaffected by the spins, although the spins are still affected by translational motion through equations (65–3) and (65–4).

III.2. Construction of the Enskog Collision Term

In this section we derive a form for the collision term $(\partial f/\partial t)_c$, which takes into account the effects of (i) inelastic collisions, (ii) spin degrees of freedom, (iii) finite particle size and (iv) filling factor near unity. The original form of the collision term derived by Boltzmann was valid for elastic collisions of point particles with no spin degrees of freedom. Generalizations which include inelastic collisions have been considered by a number of authors (see Stewart *et al.* [1984] for a review). The generalization to include spin degrees of freedom and finite particle size is due to Shukhman (1984). In this section we rederive Shukhman's results and generalize them to the case where the filling factor $\pi n a^3/6$ is not small.

The Boltzmann collision term is constructed under the following two fundamental assumptions:

B1: There are only binary collisions and these collisions are instantaneous in time and local in space. This assumption is valid if the spatial extension of particles is negligible or, more exactly, if the particle size is much smaller than the mean free path at low densities ($na^3 \ll 1$). With this assumption we may write

$$\left(\frac{\partial f}{\partial t}\right)_c = P^+ - P^-, \tag{71}$$

where

$$N^- = P^- d\vec{x} d\vec{v} d\vec{\omega} dt \tag{72}$$

is the number of binary collisions in the time interval dt, where one particle with location $(\vec{x}, \vec{x} + d\vec{x})$, velocities $(\vec{v}, \vec{v} + d\vec{v})$ and $(\vec{\omega}, \vec{\omega} + d\vec{\omega})$ is deflected to any other velocities $\vec{v}'$ and $\vec{\omega}'$, and

$$N^+ = P^+ d\vec{x} d\vec{v} d\vec{\omega} dt \tag{73}$$

is the number of binary collisions in the time interval dt, where one particle lying in the element $d\vec{x}$ around $\vec{x}$, with arbitrary initial velocities $\vec{v}'$ and $\vec{\omega}'$, ends up after the collision with a velocity in the given range $(\vec{v}, \vec{v} + d\vec{v})$ and $(\vec{\omega}, \vec{\omega} + d\vec{\omega})$.

B2: The number of pairs of particles in the volume element $d\vec{x}$ and in the time interval dt with respective velocities in the range $(\vec{v}, \vec{v} + d\vec{v}), (\vec{\omega}, \vec{\omega} + d\vec{\omega})$ and $(\vec{v}_1, \vec{v}_1 + d\vec{v}_1), (\vec{\omega}_1, \vec{\omega}_1 + d\vec{\omega}_1)$, which are able to participate in a collision, is given by the product

$$f(\vec{x}, \vec{v}, \vec{\omega}, t) d\vec{x} d\vec{v} d\vec{\omega} f(\vec{x}_1, \vec{v}_1, \vec{\omega}_1, t) d\vec{x}_1 d\vec{v}_1 d\vec{\omega}_1. \tag{74}$$

This assumption, also called the "Molecular chaos assumption" or "Stosszahlansatz," is very hard to justify rigorously since it introduces statistical arguments into a purely mechanical problem. It claims that in a dilute particle system a binary collision between two particles which have already interacted, either directly or indirectly through a common set of other particles, is an extremely unlikely event. More precisely, it is equivalent to assuming the complete absence of correlations, both in position and in velocities, of two particles which are going to collide. Mathematically, this is the statement that the pair distribution function $f_2(\vec{x}, \vec{v}, \vec{\omega}, \vec{x}_1, \vec{v}_1, \vec{\omega}_1, t)$ is equal to the product $f(\vec{x}, \vec{v}, \vec{\omega}, t) f(\vec{x}_1, \vec{v}_1, \vec{\omega}_1, t)$.

With these two assumptions, it is rather straightforward to formulate the Boltzmann collision term. The Boltzmann collision term provides a successful description of many-particle systems as long as the filling factor is very small, but as the density increases, the Boltzmann collision term ceases to be valid and processes involving more than two particles start to play an important role. A systematic extension of the theory, which would take many-body effects into account, is extremely difficult to develop on the basis of Boltzmann's original arguments. A systematic generalization can be attained with the help of the distribution function method developed by Bogolyubov (1962). As Cohen (1983) remarks, however, this generalization is plagued by divergences, and the ensuing necessary rearrangements have severely restricted its usefulness in understanding the properties of even moderately dense gases.

Therefore, it is remarkable that Enskog (1922) was able to propose an *ad hoc* generalization of the Boltzmann equation which could successfully describe the properties of a dense fluid consisting of hard sphere particles. This theory still provides a very useful first approximation to the behavior of dense systems. Its principal virtue is that Boltzmann's binary collision term is modified in such a way that the simplicity of the binary collision dynamics of the Boltzmann equation is maintained. Boltzmann's assumptions were modified by Enskog in the following way:

E1: Enskog completely neglects multiple collisions and describes the dynamics by two-body events as in the Boltzmann theory. Enskog theory has had only limited success in the study of molecular dynamics because molecules are not hard spheres and multiple collisions cannot be neglected; however, it is ideally suited for the study of particulate systems like planetary rings.

E2: In the Enskog theory the equation for the one-particle distribution function is exactly the same as the Boltzmann equation except that the calculation of the collision term is modified. Since the spheres have finite diameter a, collisions are not local and collisions involve the two distribution functions at points $\vec{x}$ and $\vec{x}_1$ separated by the distance a. This entails a new transport mechanism of momentum and energy that is absent in the Boltzmann collision term, namely, the "collisional" transfer of momentum and energy. This is the essentially instantaneous — actually at the speed of sound in the particles — transfer of momentum and energy from the center of one particle to the center of the other via the interatomic potential, as opposed to the "translational" transfer of momentum and energy due to free flight over a mean free path which is the only tranfer mechanism in the Boltzmann theory. Collisional transfer leads to an instantaneous flux of momentum and energy through an arbitrary surface between two centers of colliding members, and hence to an increase in pressure. The collisional transfer

becomes important as the density becomes higher and it completely dominates the translational transfer at high densities.

E3: Enskog also takes into account that the frequency of binary collisions is modified by a geometrical effect: The particles of diameter a occupy a finite fraction of the total volume of the system so that the effective volume accessible to their motion is reduced. Therefore, the collision frequency in a system of dense hard spheres is enhanced by a factor $Y(n)$ as compared with that in a system of particles whose size is much smaller than the average interparticle distance. In this paper we call $Y(n)$ the "Enskog factor." Note that Y is a function of position through the density n but is independent of velocity, because the Enskog theory takes "position correlations" into account but completely ignores "velocity correlations."

This assumption is justified only in thermal equilibrium in which the created velocity correlations are destroyed through collisions in such a way that the Maxwellian velocity distribution is maintained. In an non-equilibrium system the value of Y may also involve the space derivatives of the density, but in planetary rings at high filling factors the density is expected to be almost uniform except at edges so that in the first approximation the value for Y in thermal equilibrium can be used.

In a uniform and isotropic system the average number of pairs of particles with one particle in a volume element $d\vec{x}$ and the other in $d\vec{x}_1$, $n_2(\vec{x}, \vec{x}_1)d\vec{x}d\vec{x}_1$, depends only on the radial distance $|\vec{x} - \vec{x}_1| = r_2$. A dimensionless function, called the radial distribution function, can be defined by $g(r_2) = n_2(r_2)/n^2$, where n is the uniform number density of single particles. It can be shown that the Enskog factor is identified as the radial distribution function for the two particles in contact

(Kirkwood *et al.*, 1950):

$$Y(n) = \lim_{r_2 \to a+0} g(r_2).$$

The Enskog factor approaches unity as the density becomes low, and increases with increasing density, becoming infinite as the system approaches the state in which the spheres are packed so closely that motion is impossible. The Enskog factor cannot be calculated directly in the context of Enskog theory; it must be determined separately, e.g., from molecular dynamics experiments (cf. §**III.4**).

The influence of nonlocal collisions (**E2**) on the dynamics of planetary rings was first noticed by Brahic (1977) in his numerical simulations. Recently Shukhman (1984) has taken this effect into account in his analysis, but he did not include the enhanced collision rates (**E3**).

With this background we now construct the Enskog collision term. Let us first find the formula for N^-. We consider a given particle located in a volume element $d\vec{x}$ and having velocities $\vec{v}$ and $\vec{\omega}$ and we observe scattering events in a frame fixed to this particle. This particle plays a role of the "target." Particles with velocities in the range $(\vec{v}_1, \vec{v}_1 + d\vec{v}_1)$ and $(\vec{\omega}_1, \vec{\omega}_1 + d\vec{\omega}_1)$ which can collide with this target are uniformly and randomly distributed, and at time t and at location $\vec{x}_1 = \vec{x} - a\hat{\lambda}$ they form a homogeneous incident "beam" with a number flux $dS = gf(\vec{x}_1, \vec{v}_1, \vec{\omega}_1, t) d\vec{v}_1 d\vec{\omega}_1$, where g is the magnitude of the initial relative velocity. The number of particles deflected by the target in the solid angle $d\mathbf{\Omega}$ in the time interval dt is

$$dS\sigma(\mathbf{\Omega}, g) d\mathbf{\Omega} dt, \tag{75}$$

where σ is the scattering cross section and is generally a function of $\mathbf{\Omega}$ as well as g. In terms of the scattering angle ψ, defined by $\psi = \arccos\left[(\vec{g} \cdot \vec{g}')/gg'\right]$, we have $d\mathbf{\Omega} = \sin\psi d\psi d\phi$, where ϕ is the azimuthal angle around the initial velocity

$\vec{g}$. Transforming to another angle θ, defined by

$$\theta = \arccos\left(\frac{\vec{g}\cdot\hat{\lambda}}{g}\right), \tag{76}$$

we can write $d\Omega = 4\left[(\vec{g}\cdot\hat{\lambda})/g\right]d\hat{\lambda}$, where

$$d\hat{\lambda} = \sin\theta d\theta d\phi.$$

Therefore, formula (75) now reads

$$dS4\sigma(\theta,\phi,g)\frac{\vec{g}\cdot\hat{\lambda}}{g}d\hat{\lambda}dt, \tag{77}$$

which has the advantage over formula (75) that it is independent of any particular frame of reference. For hard spheres we simply have $\sigma = a^2/4$ for $\theta < \pi/2$ and $\sigma = 0$ for $\theta > \pi/2$. Generally for repulsive interactions θ cannot exceed $\pi/2$. Therefore, we introduce the Heaviside function

$$\Theta(x) = \begin{cases} 1, & \text{if } x > 0; \\ 0, & \text{if } x < 0. \end{cases}$$

in order to take this geometrical constraint into account. Thus, for hard sphere systems formula (77) becomes

$$f(\vec{x}_1,\vec{v}_1,\vec{\omega}_1,t)d\vec{v}_1 d\vec{\omega}_1 a^2(\vec{g}\cdot\hat{\lambda})\Theta(\vec{g}\cdot\hat{\lambda})d\hat{\lambda}dt. \tag{78}$$

We see that N^- is obtained by multiplying formula (78), first, by the number of target particles $f(\vec{x},\vec{v},\vec{\omega},t)d\vec{x}d\vec{v}d\vec{\omega}$, second, by the Enskog factor Y evaluated at the point of contact $(\vec{x}+\vec{x}_1)/2 = \vec{x} - a\hat{\lambda}/2$ of the two colliding spheres and by integrating over all solid angles and all velocities $\vec{v}_1$ and $\vec{\omega}_1$. Thus, we find

$$\begin{aligned} N^-(\vec{x},\vec{v},\vec{\omega},t) = a^2 d\vec{x}d\vec{v}d\vec{\omega}dt \int d\vec{v}_1 \int d\vec{\omega}_1 \int d\hat{\lambda}(\vec{g}\cdot\hat{\lambda})\Theta(\vec{g}\cdot\hat{\lambda}) \\ \times Y\left[n(\vec{x}-a\hat{\lambda}/2)\right] f(\vec{x},\vec{v},\vec{\omega},t) f(\vec{x}-a\hat{\lambda},\vec{v}_1,\vec{\omega}_1,t). \end{aligned} \tag{79}$$

N^+ will be given by an expression similar to equation (79), but now we can no longer take $d\vec{v}$ and $d\vec{\omega}$ outside the integral. The number of binary collisions in

the time interval dt, where one particle in the volume element $d\vec{x}$ around $\vec{x}$, with arbitrary initial velocities $\vec{v}$ and $\vec{\omega}$, ends up with final velocities in the given range $(\vec{v}\,', \vec{v}\,' + d\vec{v}\,')$ and $(\vec{\omega}', \vec{\omega}' + d\vec{\omega}')$ is given by

$$N^+(\vec{x}, \vec{v}\,', \vec{\omega}', t) = a^2 d\vec{x} dt \int d\vec{v} \int d\vec{\omega} \int d\vec{v}_1 \int d\vec{\omega}_1 \int d\hat{\lambda} (\vec{g} \cdot \hat{\lambda}) \Theta(\vec{g} \cdot \hat{\lambda}) \times Y\left[n(\vec{x} - a\hat{\lambda}/2)\right] f(\vec{x}, \vec{v}, \vec{\omega}, t) f(\vec{x} - a\hat{\lambda}, \vec{v}_1, \vec{\omega}_1, t), \tag{80}$$

where the integrations are carried out under the constraints

$$\vec{v}\,' < \vec{v} + \kappa_n \vec{W}_n + \kappa_t \vec{W}_t < \vec{v}\,' + d\vec{v}\,' \quad \text{and} \quad \vec{\omega}' < \vec{\omega} - \frac{1 - \epsilon_t - 2\kappa_t}{a} \hat{\lambda} \times \vec{W} < \vec{\omega}' + d\vec{\omega}'.$$

We now make a change of integration variables from initial velocities to final velocities. The corresponding Jacobian is defined by

$$J = \frac{\partial(\vec{v}\,', \vec{\omega}', \vec{v}_1\,', \vec{\omega}_1\,')}{\partial(\vec{v}, \vec{\omega}, \vec{v}_1, \vec{\omega}_1)}. \tag{81}$$

If ϵ_n and ϵ_t are independent of $\vec{W}$, we have $J = -\epsilon_n {\epsilon_t}^2$. Thus

$$d\vec{v}\,' d\vec{\omega}' d\vec{v}_1\,' d\vec{\omega}_1\,' = |J| d\vec{v} d\vec{\omega} d\vec{v}_1 d\vec{\omega}_1. \tag{82}$$

From (57) we also note that

$$(\vec{g} \cdot \hat{\lambda}) = -\frac{1}{\epsilon_n} (\vec{g}\,' \cdot \hat{\lambda}). \tag{83}$$

Therefore, equation (80) is transformed to

$$N^+(\vec{x}, \vec{v}\,', \vec{\omega}', t) = a^2 d\vec{x} d\vec{v}\,' d\vec{\omega}' dt \int d\vec{v}_1\,' \int d\vec{\omega}_1\,' \int d\hat{\lambda} \frac{1}{|J|} (-\vec{g}\,' \cdot \hat{\lambda}/\epsilon_n) \Theta(-\vec{g}\,' \cdot \hat{\lambda}/\epsilon_n) \times Y\left[n(\vec{x} - a\hat{\lambda}/2)\right] f(\vec{x}, \vec{v}, \vec{\omega}, t) f(\vec{x} - a\hat{\lambda}, \vec{v}_1, \vec{\omega}_1, t), \tag{84}$$

where $\vec{v}, \vec{\omega}, \vec{v}_1, \vec{\omega}_1$ are given in terms of $\vec{v}\,', \vec{\omega}', \vec{v}_1\,', \vec{\omega}_1\,'$ by equations (66). Making the variable transformations: $\vec{v}\,', \vec{\omega}', \vec{v}_1\,', \vec{\omega}_1\,' \Longrightarrow \vec{v}, \vec{\omega}, \vec{v}_1, \vec{\omega}_1$ and $\hat{\lambda} \Longrightarrow -\hat{\lambda}$, we arrive at

$$N^+(\vec{x}, \vec{v}, \vec{\omega}, t) = a^2 d\vec{x} d\vec{v} d\vec{\omega} dt \int d\vec{v}_1 \int d\vec{\omega}_1 \int d\hat{\lambda} \frac{1}{\epsilon_n |J|} (\vec{g} \cdot \hat{\lambda}) \Theta(\vec{g} \cdot \hat{\lambda}) \times Y\left[n(\vec{x} + a\hat{\lambda}/2)\right] f(\vec{x}, \vec{v}^\star, \vec{\omega}^\star, t) f(\vec{x} + a\hat{\lambda}, \vec{v}_1^\star, \vec{\omega}_1^\star, t), \tag{85}$$

where

$$\vec{v}^{\star} = \vec{v} + \frac{\kappa_n}{\epsilon_n}\vec{W}_n - \frac{\kappa_t}{\epsilon_t}\vec{W}_t^{\star},$$
$$\vec{v}_1^{\star} = \vec{v}_1 - \frac{\kappa_n}{\epsilon_n}\vec{W}_n + \frac{\kappa_t}{\epsilon_t}\vec{W}_t^{\star},$$
$$\vec{\omega}^{\star} = \vec{\omega} - \frac{1-\epsilon_t-2\kappa_t}{a\epsilon_t}\hat{\lambda}\times\vec{W}_t^{\star},$$
$$\vec{\omega}_1^{\star} = \vec{\omega}_1 - \frac{1-\epsilon_t-2\kappa_t}{a\epsilon_t}\hat{\lambda}\times\vec{W}_t^{\star},$$
$$\vec{W}_t^{\star} = \vec{g}_t - \frac{a}{2}\vec{s}\times\hat{\lambda}. \tag{86}$$

The Enskog collision term is finally given by

$$\left(\frac{\partial f}{\partial t}\right)_c = a^2\int d\vec{v}_1\int d\vec{\omega}_1\int d\hat{\lambda}(\vec{g}\cdot\hat{\lambda})\Theta(\vec{g}\cdot\hat{\lambda})$$
$$\times\left\{\frac{Y\left[n(\vec{x}+a\hat{\lambda}/2)\right]}{\epsilon_n|J|}f(\vec{x},\vec{v}^{\star},\vec{\omega}^{\star},t)f(\vec{x}+a\hat{\lambda},\vec{v}_1^{\star},\vec{\omega}_1^{\star},t)\right.$$
$$\left.-Y\left[n(\vec{x}-a\hat{\lambda}/2)\right]f(\vec{x},\vec{v},\vec{\omega},t)f(\vec{x}-a\hat{\lambda},\vec{v}_1,\vec{\omega}_1,t)\right\}. \tag{87}$$

If the spin degrees of freedom and the effect of finite particle size are neglected, equation (87) reduces to equation (19) of Trulsen (1971), while if the spin degrees of freedom are neglected and perfectly elastic collisions are assumed, equation (87) reduces to equation (16.3,4) of Chapman and Cowling (1970).

Finally, from equation (87) we can calculate the following integral which will be useful later:

$$\int\Psi(\vec{v},\vec{\omega})\left(\frac{\partial f}{\partial t}\right)_c d\vec{v}d\vec{\omega}$$
$$=a^2\int d\vec{v}\int d\vec{\omega}\int d\vec{v}_1\int d\vec{\omega}_1\int d\hat{\lambda}(\vec{g}\cdot\hat{\lambda})\Theta(\vec{g}\cdot\hat{\lambda})Y\left[n(\vec{x}-a\hat{\lambda}/2)\right]$$
$$\times f(\vec{x},\vec{v},\vec{\omega},t)f(\vec{x}-a\hat{\lambda},\vec{v}_1,\vec{\omega}_1,t)\left[\Psi(\vec{v}',\vec{\omega}')-\Psi(\vec{v},\vec{\omega})\right]. \tag{88}$$

Here $\Psi(\vec{v},\vec{\omega})$ is an arbitrary function of velocities, and $\vec{v}'$ and $\vec{\omega}'$ are given by equations (65–1) and (65–3), respectively.

III.3. The Choice of Distribution function

To make further progress we assume that the distribution function is the product of a translational part and spin part as in equation (23), and that each of them is a triaxial Gaussian in the corresponding principal axis system (Goldreich and Tremaine, 1978; Shukhman, 1984):

$$f_T(\vec{x},\vec{v}) = n(\vec{x})(2\pi)^{-3/2}(c_1c_2c_3)^{-1}\exp\left\{-\sum_{i=1}^{3}\frac{\left[v_i-u_i(\vec{x})\right]^2}{2c_i^2}\right\}, \quad (89\text{–}1)$$

$$f_S(\vec{\omega}) = (2\pi)^{-3/2}(D_aD_bD_c)^{-1}\exp\left\{-\sum_{\alpha=a,b,c}\frac{(\omega_\alpha-\mu_\alpha)^2}{2D_\alpha^2}\right\}. \quad (89\text{–}2)$$

Here (c_1,c_2,c_3) are the velocity dispersions along the principal axes $(\hat{1},\hat{2},\hat{3})$ of p_{ij}, and (D_a,D_b,D_c) the angular velocity dispersions along the principal axes $(\hat{a},\hat{b},\hat{c})$ of $\nu_{\alpha\beta}$. The components of the mean velocities are given by

$$\begin{aligned} u_1 &= r\Omega(r)\sin\delta \\ u_2 &= r\Omega(r)\cos\delta \\ u_3 &= 0, \end{aligned} \quad (90)$$

$$\begin{aligned} \mu_a &= 0 \\ \mu_b &= 0 \\ \mu_c &= \mu. \end{aligned} \quad (91)$$

Introducing the velocity of the center of mass relative to the mean velocity

$$\vec{V}_c = \vec{V} - \vec{u} = \vec{v} + \frac{1}{2}\vec{g} - \vec{u}, \quad (92)$$

and substituting equations (89–1) and (89–2) into equation (88), we find

$$\begin{aligned} \int \Psi(\vec{v},\vec{\omega})\left(\frac{\partial f}{\partial t}\right)_c d\vec{v}d\vec{\omega} &= a^2\int d\vec{V}_c\int d\vec{g}\int d\vec{s}\int d\vec{\omega}\int d\hat{\lambda}\,(\vec{g}\cdot\hat{\lambda})\Theta(\vec{g}\cdot\hat{\lambda}) \\ \times Y\left[n(\vec{x}-a\hat{\lambda}/2)\right]n(\vec{x})n(\vec{x}-a\hat{\lambda})F(\vec{V}_c,\hat{\lambda})G(\vec{g},\hat{\lambda})S(\vec{s})W(\vec{\omega},\vec{s}) \\ \times\left\{\Psi\left[\vec{V}_c+\vec{u}-\frac{1}{2}\vec{g}+\kappa_n\vec{W}_n+\kappa_t\vec{W}_t,\vec{\omega}-\frac{1-\epsilon_t-2\kappa_t}{a}\hat{\lambda}\times\vec{W}\right]\right. \\ \left. -\Psi\left[\vec{V}_c+\vec{u}-\frac{1}{2}\vec{g},\vec{\omega}\right]\right\}, \end{aligned} \quad (93)$$

where

$$F(\vec{V}_c,\hat{\lambda}) = \pi^{-3/2}(c_1c_2c_3)^{-1}\exp\Big\{-\sum_{i=1}^{3}\frac{\left[V_{ci}-\delta u_i(\hat{\lambda})/2\right]^2}{c_i^2}\Big\},$$

$$G(\vec{g},\hat{\lambda}) = (4\pi)^{-3/2}(c_1c_2c_3)^{-1}\exp\Big\{-\sum_{i=1}^{3}\frac{\left[g_i-\delta u_i(\hat{\lambda})\right]^2}{4c_i^2}\Big\},$$

$$S(\vec{s}) = (4\pi)^{-3/2}(D_aD_bD_c)^{-1}\exp\Big[-\sum_{\alpha=a,b,c}\frac{(s_\alpha-2\mu_\alpha)^2}{4D_\alpha^2}\Big],$$

$$W(\vec{\omega},\vec{s}) = \pi^{-3/2}(D_aD_bD_c)^{-1}\exp\Big[-\sum_{\alpha=a,b,c}\frac{(\omega_\alpha-s_\alpha/2)^2}{D_\alpha^2}\Big]. \tag{94}$$

Here we define the difference of mean orbital velocities between the colliding particles by

$$\delta\vec{u} = \vec{u}(\vec{x}-a\hat{\lambda}) - \vec{u}(\vec{x}). \tag{95}$$

Since in planetary rings the particle size is much smaller than the orbital radius, equation (95) can be expanded in terms of a/r. For the Saturnian B ring $a/r \approx 10^{-9}$. To the lowest order in a/r, we have

$$\delta u_r = \Omega a\lambda_\theta, \qquad \delta u_\theta = \frac{1}{2}\Omega a\lambda_r, \qquad \delta u_z = 0. \tag{96}$$

In the principal axis system we obtain

$$\begin{aligned}
\delta u_1 &= \frac{1}{4}\Omega a\big[3\lambda_1\sin 2\delta + \lambda_2(1+3\cos 2\delta)\big],\\
\delta u_2 &= \frac{1}{4}\Omega a\big[\lambda_1(3\cos 2\delta - 1) - 3\lambda_2\sin 2\delta\big],\\
\delta u_3 &= 0.
\end{aligned} \tag{97}$$

Making use of equation (93) and integrating over $\vec{V}_c$, $\vec{\omega}$ and $\vec{s}$, we obtain a set of general expressions for the moments T_i, M_α, Q_{ij} and $H_{\alpha\beta}$:

$$\begin{aligned}
T_i = a^2\int d\hat{\lambda}\int d\vec{g}\,Y\left[n(\vec{x}-a\hat{\lambda}/2)\right]n(\vec{x})n(\vec{x}-a\hat{\lambda})\\
\times(\vec{g}\cdot\hat{\lambda})\Theta(\vec{g}\cdot\hat{\lambda})G(\vec{g},\hat{\lambda})(\kappa_n\vec{g}_n+\kappa_t\vec{Y})_i,
\end{aligned} \tag{98}$$

$$M_\alpha = -a^2 \int d\hat{\lambda} \int d\vec{g}\, Y\left[n(\vec{x} - a\hat{\lambda}/2)\right] n(\vec{x}) n(\vec{x} - a\hat{\lambda})$$
$$\times (\vec{g}\cdot\hat{\lambda})\Theta(\vec{g}\cdot\hat{\lambda}) G(\vec{g},\hat{\lambda}) \frac{1-\epsilon_t - 2\kappa_t}{a} \left[\hat{\lambda}\times\vec{g} + a\vec{\mu} - a(\vec{\mu}\cdot\hat{\lambda})\hat{\lambda}\right]_\alpha, \qquad (99)$$

$$Q_{ij} = a^2 \int d\hat{\lambda} \int d\vec{g}\, Y\left[n(\vec{x} - a\hat{\lambda}/2)\right] n(\vec{x}) n(\vec{x} - a\hat{\lambda}) (\vec{g}\cdot\hat{\lambda})\Theta(\vec{g}\cdot\hat{\lambda}) G(\vec{g},\hat{\lambda})$$
$$\times \Big\{ X_i(\kappa_n g_{nj} + \kappa_t Y_j) + X_j(\kappa_n g_{ni} + \kappa_t Y_i) + \kappa_n^2 g_{ni} g_{nj}$$
$$+ \kappa_n\kappa_t(g_{ni}Y_j + g_{nj}Y_i) + \kappa_t^2 \Big[g_{ti}g_{tj} + a g_{ti}(\vec{\mu}\times\hat{\lambda})_j$$
$$+ a g_{tj}(\vec{\mu}\times\hat{\lambda})_i + \frac{a^2}{4} \sum_{k,l,m,n} e_{ikl} e_{jmn} \chi_{km} \lambda_l \lambda_n \Big] \Big\}, \qquad (100)$$

$$H_{\alpha\beta} = a^2 \int d\hat{\lambda} \int d\vec{g}\, Y\left[n(\vec{x} - a\hat{\lambda}/2)\right] n(\vec{x}) n(\vec{x} - a\hat{\lambda}) (\vec{g}\cdot\hat{\lambda})\Theta(\vec{g}\cdot\hat{\lambda}) G(\vec{g},\hat{\lambda})$$
$$\times \Big[\frac{1-\epsilon_t - 2\kappa_t}{2} (D_\alpha^2 + D_\beta^2)(\delta_{\alpha\beta} + \lambda_\alpha\lambda_\beta) + \left(\frac{1-\epsilon_t - 2\kappa_t}{a}\right)^2$$
$$\times \Big\{ (\hat{\lambda}\times\vec{g})_\alpha (\hat{\lambda}\times\vec{g})_\beta + \frac{a^2}{4}\psi_{\alpha\beta} + \frac{a^2}{4}\lambda_\alpha\lambda_\beta \left[4(\vec{\mu}\cdot\hat{\lambda})^2 + 2\sum_\gamma D_\gamma^2 \lambda_\gamma^2\right]$$
$$+ a\left[\mu_\alpha(\hat{\lambda}\times\vec{g})_\beta + \mu_\beta(\hat{\lambda}\times\vec{g})_\alpha\right] - a(\vec{\mu}\cdot\hat{\lambda})\left[(\hat{\lambda}\times\vec{g})_\alpha\lambda_\beta + (\hat{\lambda}\times\vec{g})_\beta\lambda_\alpha\right]$$
$$- a^2(\vec{\mu}\cdot\hat{\lambda})(\lambda_\alpha\mu_\beta + \lambda_\beta\mu_\alpha) - \frac{a^2}{2}\lambda_\alpha\lambda_\beta(D_\alpha^2 + D_\beta^2) \Big\} \Big]. \qquad (101)$$

Equations (98) – (101) yield the right hand sides of the moment equations (29), (30), (34) and (36). Here,

$$X_i = \frac{1}{2}(\delta u_i - g_i),$$
$$Y_i = g_{ti} + a(\vec{\mu}\times\hat{\lambda})_i,$$
$$\chi_{ij} = \begin{bmatrix} 2D_a^2\cos^2\Delta + 2D_b^2\sin^2\Delta & (2D_a^2 - 2D_b^2)\sin\Delta\cos\Delta & 0 \\ (2D_a^2 - 2D_b^2)\sin\Delta\cos\Delta & 2D_a^2\sin^2\Delta + 2D_b^2\cos^2\Delta & 0 \\ 0 & 0 & 2D_c^2 + 4\mu^2 \end{bmatrix},$$
$$\psi_{\alpha\beta} = \begin{pmatrix} 2D_a^2 & 0 & 0 \\ 0 & 2D_b^2 & 0 \\ 0 & 0 & 2D_c^2 + 4\mu^2 \end{pmatrix}. \qquad (102)$$

III.4. The Equation of State and the Phase Transition

The Enskog factor $Y(n)$ is closely related to the equation of state of a system of elastic hard spheres. We assume that the Enskog factor is the same for a system of inelastic spheres as it is for elastic spheres. This assumption is unlikely to be exactly correct but should capture the qualitative behavior of the Enskog factor in the inelastic system. The equation of state for an elastic hard sphere gas is

$$\frac{p}{nkT} = 1 + bY, \tag{103}$$

where p, n, T, k are the pressure, number density, temperature and Boltzmann's constant and

$$b = \frac{2}{3}\pi n a^3 \tag{104}$$

is four times the filling factor and is related to the second virial coefficient B_2 by $b = nB_2$.

There have been a number of investigations of the equation of state for the elastic hard sphere gas. In the low density limit the compressibility factor p/nkT can be represented by the virial expansion

$$\frac{p}{nkT} = \sum_{i=1}^{\infty} B_i n^{i-1} = \sum_{i=1}^{\infty} C_i b^{i-1}, \tag{105}$$

where the B_i are the virial coefficients and are related to the reduced virial coefficients C_i by

$$B_i = {B_2}^{i-1} C_i \qquad (i = 1, 2, 3, \ldots). \tag{106}$$

For hard spheres the first seven virial coefficients have been evaluated. Therefore, in the low density limit the Enskog factor can be represented by

$$Y(b) = \sum_{i=2}^{7} C_i b^{i-2}, \tag{107}$$

where (Ree and Hoover, 1967; Devore, 1984)

$$C_2 = 1.00000, \qquad C_3 = 0.62500, \qquad C_4 = 0.28695,$$

$$C_5 = 0.11025, \qquad C_6 = 0.03894, \qquad C_7 = 0.01376.$$

At high densities, however, equation (107) becomes progessively less and less accurate. This is hardly surprising since Y must diverge when the density approaches the close-packing density $n_0 = \sqrt{2}/a^3$ (for a face centered cubic lattice). At this density $b = 2\sqrt{2}\pi/3 = 2.96$ and the filling factor is $\sqrt{2}\pi/6 = 0.74$. Even well before this density is reached, the virial expansion becomes inapplicable because the system undergoes a liquid-solid phase transition (Hoover and Ree, 1968; de Llano and Ramírez, 1975; Young and Alder, 1980). Computer experiments show that the phase transition starts to occur at $x = 0.67$ where $x = n/n_0$, corresponding to $b = 1.98$.

To represent $Y(b)$ in the range $0 \leq b < 1.98$ we will employ a polynomial fit to the molecular dynamics data by Alder and Wainwright (Ree and Hoover, 1967). The advantage of this "pseudo" virial expansion is that it permits us to calculate part of the collision integrals analytically while it reproduces the molecular dynamics data throughout the entire liquid phase.

From Table IV of Ree and Hoover (1967) we choose five points $(b,\ Y) =$ (0.2962, 1.2154), (0.9873, 2.0764), (1.4810, 3.3019), (1.7423, 4.3563), (1.8512, 4.9535) and look for a fifth order polynomial which satisfies $Y(0) = 1$. Thus we find

$$Y(b) = \sum_{i=2}^{7} D_i b^{i-2}, \tag{108}$$

where

$$D_2 = +1.0000, \qquad D_3 = +0.8874, \qquad D_4 = -1.1764,$$

$$D_5 = +2.5828, \qquad D_6 = -1.5909, \qquad D_7 = +0.3974.$$

Note that the Enskog factor reaches $Y(1.98) = 5.84$ at the crystallization density $b = 1.98$. Equation (108) yields values of $Y(b)$ which agree with the formula given by Carnahan and Starling (1969) within 2% error.

III.5. The Momentum Flux Density Tensor

As we mentioned in §**II.2** and §**III.2**, there are two modes of momentum transfer in dense particle disks, "collisional" and "translational" transfer. The momentum flux density tensor due to translational transfer is simply the pressure tensor p_{ij}. In this section we derive the analogous momentum flux density tensor p_{ij}^{NL} due to collisional or "nonlocal" transfer (cf. equation [A1.4] of Shukhman, 1984).

Consider the principal axis coordinate system $(\hat{1},\hat{2},\hat{3})$ of the pressure tensor p_{ij} evaluated at a given location $\vec{x}$. Suppose we have two colliding spheres whose centers straddle a plane perpendicular to $\hat{i}$. One particle with velocities $(\vec{v},\vec{\omega})$ has its center above the plane at $\vec{x}$, and the other with velocities $(\vec{v}_1,\vec{\omega}_1)$ has its center below the plane at $\vec{x}_1 = \vec{x} - a\hat{\lambda}$: $x_{1i} < x_i$. The condition that the two centers straddle the plane is that $\hat{\lambda}\cdot\hat{i} = \lambda_i > 0$, and that the center of the first sphere $\vec{x}$ must lie within a skew cylinder on the surface element dS (across which momentum is transferred) in the plane, with generators parallel to $\hat{\lambda}$ and of length a; the volume of this cylinder is $a\lambda_i dS$. Hence the average number of such collisions per unit time, in which $\vec{v},\vec{v}_1,\vec{\omega},\vec{\omega}_1,\hat{\lambda}$ lie in their respective ranges is

$$Y\left[n(\vec{x}-a\hat{\lambda}/2)\right]f(\vec{x},\vec{v},\vec{\omega})f(\vec{x}_1,\vec{v}_1,\vec{\omega}_1)a^2(\vec{g}\cdot\hat{\lambda})\Theta(\vec{g}\cdot\hat{\lambda})d\hat{\lambda}\Theta(\lambda_i)a\lambda_i dS.$$

Each such collision causes a sphere on the upper side of dS to gain momentum per unit mass $\vec{v}\,' - \vec{v} = \kappa_n\vec{g}_n + \kappa_t\vec{W}_t$ at the expense of a sphere on the lower side.

Thus the j-th component of the collisional or nonlocal momentum flux vector through the unit surface area perpendicular to the $\hat{i}$ axis is

$$\begin{aligned} p_{ij}^{NL} &= a^3\int d\vec{v}\int d\vec{\omega}\int d\vec{v}_1\int d\vec{\omega}_1\int d\hat{\lambda}(\vec{g}\cdot\hat{\lambda})\Theta(\vec{g}\cdot\hat{\lambda})Y\left[n(\vec{x}-a\hat{\lambda}/2)\right] \\ &\quad\times f(\vec{x},\vec{v},\vec{\omega})f(\vec{x}_1,\vec{v}_1,\vec{\omega}_1)\lambda_i\Theta(\lambda_i)(\kappa_n\vec{g}_n+\kappa_t\vec{W}_t)_j \\ &= \frac{a^3}{2}\int d\vec{v}\int d\vec{v}_1\int d\vec{\omega}\int d\vec{\omega}_1\int d\hat{\lambda}(\vec{g}\cdot\hat{\lambda})\Theta(\vec{g}\cdot\hat{\lambda})Y\left[n(\vec{x}-a\hat{\lambda}/2)\right] \end{aligned}$$

$$\times f(\vec{x},\vec{v},\vec{\omega})f(\vec{x}-a\hat{\lambda},\vec{v}_1,\vec{\omega}_1)\lambda_i(\kappa_n g_{nj}+\kappa_t W_{tj}). \tag{109}$$

Following the procedure in §**III.3**, we adopt the triaxial distribution (89), change the integration variables from $\vec{v},\vec{v}_1,\vec{\omega},\vec{\omega}_1$ to $\vec{V}_c,\vec{g},\vec{\omega},\vec{s}$, and integrate over $\vec{V}_c$, $\vec{\omega}$ and $\vec{s}$:

$$p_{ij}^{NL}=\frac{a^3}{2}\int d\hat{\lambda}\int d\vec{g}(\vec{g}\cdot\hat{\lambda})\Theta(\vec{g}\cdot\hat{\lambda})Y\left[n(\vec{x}-a\hat{\lambda}/2)\right]n(\vec{x})n(\vec{x}-a\hat{\lambda})$$
$$\times G(\vec{g},\hat{\lambda})\lambda_i\left[\kappa_n\vec{g}_n+\kappa_t(\vec{g}_t+a\vec{\mu}\times\hat{\lambda})\right]_j. \tag{110}$$

The nonlocal momentum flux density tensor is generally not symmetric, although it is symmetric when the spin degrees of freedom are neglected ($\epsilon_t=1$). [1] The total momentum flux density tensor is $p_{ij}^T=p_{ij}+p_{ij}^{NL}$.

From equation (110) we can calculate various interesting quantities:

(i) The kinematic viscosity is defined by

$$\nu^T=\nu+\nu^{NL}=\frac{p_{r\theta}+p_{r\theta}^{NL}}{-r\Omega'(r)n(z)}, \tag{111}$$

where

$$p_{r\theta}=(p_{11}-p_{22})\sin\delta\cos\delta, \tag{112}$$

$$p_{r\theta}^{NL}=(p_{11}^{NL}-p_{22}^{NL})\sin\delta\cos\delta+p_{12}^{NL}\cos^2\delta-p_{21}^{NL}\sin^2\delta. \tag{113}$$

Equation (111) reduces to equation (45) in Goldreich and Tremaine (1978) if the nonlocal momentum flux density tensor is neglected.

(ii) The angular momentum luminosity is the rate of outward transport of angular momentum across the streamline with radius r (Borderies *et al.*, 1985). Since the

[1] For most fluids the pressure tensor is symmetric, since an antisymmetric pressure tensor leads to a net torque on a small fluid element which leads to arbitrarily large angular acceleration as the size of the element shrinks to zero (e.g., Misner *et al.*, 1970, p.141). However, a non-symmetric pressure tensor can arise in simple systems; e.g., a hard sphere gas with polarized spins.

viscous torque exerted on a unit length of streamline due to the material inside it is

$$r \int_{-\infty}^{\infty} p_{r\theta}^{T} dz,$$

the angular momentum luminosity due to viscosity is

$$L^{T}(r) = 2\pi r^{2} \int_{-\infty}^{\infty} (p_{r\theta} + p_{r\theta}^{NL}) dz. \tag{114}$$

(iii) A useful dimensionless number is the ratio R of the viscous stress $p_{r\theta}^{T}$ to the mean pressure $\mathrm{Tr}p^{T}/3$. In a fluid this ratio is $R = -r\Omega'(r)\eta/p$, where p and η are the scalar pressure per unit mass and the dynamic viscosity $n\nu$. In our case

$$R = \frac{3}{2} \frac{n(c_1^2 - c_2^2)\sin 2\delta + 2p_{r\theta}^{NL}}{n(c_1^2 + c_2^2 + c_3^2) + p_{11}^{NL} + p_{22}^{NL} + p_{33}^{NL}}. \tag{115}$$

The ratio R is equivalent to the quantity $\sqrt{2}F_1$ defined by Borderies *et al.* (1985) for Keplerian disks. F_1 or R is generally of order unity in granular flow models of particulate rings (e.g., Haff, 1983).

IV. NUMERICAL RESULTS

Due to the complexity of the complete problem, for the rest of this section we will confine ourselves to the case without spin degrees of freedom, i.e., we set $\epsilon_t = 1$. The case including spin degrees of freedom will be treated in a subsequent paper.

We shall also specialize to the Keplerian rotation law

$$\Omega(r) = \sqrt{\frac{GM}{r^3}}, \tag{116}$$

where G is the gravitational constant and M is the mass of the central planet.

The principal difficulty in solving for the ring structure is in determining the exact vertical equilibrium of the ring. Even in the case where non-local effects are neglected the exact vertical ring equilibrium has not been established (cf. Goldreich and Tremaine, 1978). In fact we have already abandoned the possibility of determining the exact vertical equilibrium self-consistently by our assumption that the velocity ellipsoid is independent of z (cf. §**II.1**). Hence we shall investigate two approximate models for the vertical structure in §**IV.2** and §**IV.3** and estimate our uncertainties by comparing the two models.

IV.1. Equations of Equilibrium

In planetary rings $|z| \ll r$ so that to the first order in z^2/r^2 the potential is given by

$$U(r,z) = -\frac{GM}{\sqrt{r^2+z^2}} \approx -\Omega^2(r)r^2 + \frac{1}{2}\Omega^2(r)z^2. \tag{117}$$

As is shown later $T_r = T_\theta = 0$, so that the horizontal components of Euler's equation are automatically satisfied when $|z| \ll r$. Thus, from (29), the vertical

component of Euler's equation is

$$n\Omega^2 z + 2\pi G m n(z) \int_{-z}^{z} n(z')dz' = T_3 - \frac{\partial p_{33}}{\partial z}. \tag{118}$$

Here we have added the overall self-gravity of disk particles to the left hand side of equation (118). For sufficiently high filling factors velocity dispersions become so small that self-gravity effects are generally important (cf. equation [125]).

Since we have $p_{ii} = n(\vec{x})c_i^2$ from (89), the viscous-stress equation (34) reduces to

$$-\frac{3}{2}\Omega n c_1^2 \sin 2\delta = Q_{11}, \tag{119-1}$$

$$\frac{3}{2}\Omega n c_2^2 \sin 2\delta = Q_{22}, \tag{119-2}$$

$$0 = Q_{33}, \tag{119-3}$$

$$\frac{5 - 3\cos 2\delta}{4}\Omega n c_1^2 - \frac{5 + 3\cos 2\delta}{4}\Omega n c_2^2 = Q_{12}, \tag{119-4}$$

$$0 = Q_{23}, \tag{119-5}$$

$$0 = Q_{31}. \tag{119-6}$$

Next we nondimensionalize equations (118), (119) by introducing the following quantities:

$$z^* = \frac{z}{a}, \quad n^*(z^*) = \frac{n(z)}{n(0)}, \quad g_i^* = \frac{g_i}{\Omega a}, \quad \delta u_i^* = \frac{\delta u_i}{\Omega a},$$

$$c_i^* = \frac{c_i}{\Omega a}, \qquad T_i^* = \frac{T_i}{n(0)a\Omega^2}, \qquad Q_{ij}^* = \frac{Q_{ij}}{n(0)a^2\Omega^3}. \tag{120}$$

Then we have

$$n^* z^* + \frac{3}{4}b(0)G_s n^* \int_0^{z^*} n^*(x)dx = T_3^* - \frac{d}{dz^*}(n^* c_3^{*2}), \tag{121}$$

$$-\frac{3}{2}n^* c_1^{*2} \sin 2\delta = Q_{11}^*, \tag{122-1}$$

$$\frac{3}{2}n^*c_2^{*2}\sin 2\delta = Q_{22}^*, \tag{122-2}$$

$$0 = Q_{33}^*, \tag{122-3}$$

$$\frac{5-3\cos 2\delta}{4}n^*c_1^{*2} - \frac{5+3\cos 2\delta}{4}n^*c_2^{*2} = Q_{12}^*, \tag{122-4}$$

$$0 = Q_{23}^*, \tag{122-5}$$

$$0 = Q_{31}^*. \tag{122-6}$$

In equation (121), $b(0)$ denotes four times the filling factor in the neutral plane (see equation [104]):

$$b(0) = \frac{2}{3}\pi n(0)a^3 = 4FF(0). \tag{123}$$

Also, a factor G_s has been defined by

$$G_s = \frac{8Gm}{\Omega^2 a^3} = \left(\frac{r}{r_S}\right)^3\left(\frac{\rho_P}{\rho_S}\right), \tag{124}$$

where r_S, ρ_S are the radius and volumic density of the planet, and ρ_P is the volumic density of the particle material (this factor is related to the factor F_2 in equation (42) of Borderies *et al.*, 1985: $F_2 = 1 + 3G_s$).

At a typical location in the Saturnian B ring we have $r_S = 6.03 \times 10^9$ cm, $\rho_S = 0.618$ g cm^{-3}, $r = 1.04 \times 10^{10}$ cm, $\rho_P = 0.9$ g cm^{-3} so that $G_s = 7.4$. From equation (121), the condition that the self-gravity term can be neglected as compared with the first term is given by

$$3G_sFF(0)\frac{1}{z^*}\int_0^{z^*} n^*(x)dx \approx G_sFF(0) \ll 1, \tag{125}$$

which is violated even for $FF(0) = 0.1$ when $G_s = 7.4$.

When the spin degrees of freedom are neglected, equations (100) and (102) become

$$T_i^* = \frac{n(0)a^3\kappa_n}{(4\pi)^{3/2}c_1^*c_2^*c_3^*}\int d\hat{\lambda}\int d\vec{g}^*Y\left[n^*(z^*-\lambda_3/2)\right]n^*(z^*)n^*(z^*-\lambda_3)e^{-Z}$$
$$\times(\vec{g}^*\cdot\hat{\lambda})^2\Theta(\vec{g}^*\cdot\hat{\lambda})\lambda_i, \tag{126}$$

$$Q_{ij}^* = \frac{n(0)a^3\kappa_n}{(4\pi)^{3/2}c_1^*c_2^*c_3^*}\int d\hat{\lambda}\int d\vec{g}^* Y\left[n^*(z^*-\lambda_3/2)\right]n^*(z^*)n^*(z^*-\lambda_3)e^{-Z}$$
$$\times(\vec{g}^*\cdot\hat{\lambda})^2\Theta(\vec{g}^*\cdot\hat{\lambda})\left[\frac{\delta u_i^*-g_i^*}{2}\lambda_j+\frac{\delta u_j^*-g_j^*}{2}\lambda_i+\kappa_n(\vec{g}^*\cdot\hat{\lambda})\lambda_i\lambda_j\right], \quad (127)$$

where

$$Z=\sum_{k=1}^{3}\left(\frac{g_k^*-\delta u_k^*}{2c_k^*}\right)^2.$$

In equations (126) and (127) we have assumed that the scale of horizontal density variations is much larger than that of vertical density variations so that the radial dependence of the density can be neglected.

The $|\vec{g}^*|$ integration can be carried out analytically. The results are

$$T_i^* = \frac{n(0)a^3\kappa_n}{(4\pi)^{3/2}c_1^*c_2^*c_3^*}\int_0^{\pi}d\vartheta_\lambda\sin\vartheta_\lambda\int_0^{2\pi}d\varphi_\lambda Y\left[n^*(z^*-\cos\vartheta_\lambda/2)\right]$$
$$\times n^*(z^*)n^*(z^*-\cos\vartheta_\lambda)e^{-C}$$
$$\times\lambda_i\int_0^{\pi/2}d\vartheta\sin\vartheta\cos^2\vartheta\int_0^{2\pi}d\varphi A^{-5/2}f_5(\zeta), \quad (128)$$

$$Q_{ij}^* = \frac{n(0)a^3\kappa_n}{(4\pi)^{3/2}c_1^*c_2^*c_3^*}\int_0^{\pi}d\vartheta_\lambda\sin\vartheta_\lambda\int_0^{2\pi}d\varphi_\lambda Y\left[n^*(z^*-\cos\vartheta_\lambda/2)\right]$$
$$\times n^*(z^*)n^*(z^*-\cos\vartheta_\lambda)e^{-C}$$
$$\times\int_0^{\pi/2}d\vartheta\sin\vartheta\cos^2\vartheta\int_0^{2\pi}d\varphi\left[D_{ij}A^{-3}f_6(\zeta)+E_{ij}A^{-5/2}f_5(\zeta)\right], \quad (129)$$

where

$$\gamma_1=\sin\vartheta\cos\varphi\sin\varphi_\lambda+\sin\vartheta\sin\varphi\cos\vartheta_\lambda\cos\varphi_\lambda+\cos\vartheta\sin\vartheta_\lambda\cos\varphi_\lambda,$$
$$\gamma_2=-\sin\vartheta\cos\varphi\cos\varphi_\lambda+\sin\vartheta\sin\varphi\cos\vartheta_\lambda\sin\varphi_\lambda+\cos\vartheta\sin\vartheta_\lambda\sin\varphi_\lambda,$$
$$\gamma_3=-\sin\vartheta\sin\varphi\sin\vartheta_\lambda+\cos\vartheta\cos\vartheta_\lambda, \quad (130)$$

$$A(\vartheta,\varphi,\vartheta_\lambda,\varphi_\lambda)=\frac{1}{2}\sum_{k=1}^{3}\left(\frac{\gamma_k}{c_k^*}\right)^2,$$

$$B(\vartheta,\varphi,\vartheta_\lambda,\varphi_\lambda) = -\frac{1}{2}\sum_{k=1}^{3}\frac{\gamma_k \delta u_k^*}{c_k^{*2}},$$

$$C(\vartheta_\lambda,\varphi_\lambda) = \frac{1}{4}\sum_{k=1}^{3}\left(\frac{\delta u_k^*}{c_k^*}\right)^2,$$

$$D_{ij}(\vartheta,\varphi,\vartheta_\lambda,\varphi_\lambda) = \kappa_n \cos\vartheta\lambda_i\lambda_j - \frac{1}{2}(\gamma_i\lambda_j + \gamma_j\lambda_i),$$

$$E_{ij}(\vartheta_\lambda,\varphi_\lambda) = \frac{1}{2}(\delta u_i^*\lambda_j + \delta u_j^*\lambda_i), \tag{131}$$

$$f_5(\varsigma) = -\varsigma^3 - 5\varsigma + \sqrt{\frac{\pi}{2}}\exp\left(\frac{\varsigma^2}{2}\right)\mathrm{erfc}\left(\frac{\varsigma}{\sqrt{2}}\right)(\varsigma^4 + 6\varsigma^2 + 3),$$

$$f_6(\varsigma) = \varsigma^4 + 9\varsigma^2 + 8 - \sqrt{\frac{\pi}{2}}\exp\left(\frac{\varsigma^2}{2}\right)\mathrm{erfc}\left(\frac{\varsigma}{\sqrt{2}}\right)(\varsigma^5 + 10\varsigma^3 + 15\varsigma), \tag{132}$$

$$\varsigma = \frac{B}{\sqrt{A}}, \tag{133}$$

$$\mathrm{erfc}(x) = \frac{2}{\sqrt{\pi}}\int_x^\infty e^{-t^2}dt.$$

If we neglect the nonlocal effects in equation (129), its off-diagonal components are zero and its diagonal components reduce to equation (33) of Goldreich and Tremaine (1978) or equation (17) of Borderies *et al.* (1983).

From equations (126) and (127) we can show analytically that

$$T_1^* = T_2^* = Q_{23}^* = Q_{31}^* = 0,$$

and that $T_3^*$is an odd function of z^*. These results are independent of the form of $n^*(z^*)$ so long as it is even. Therefore, particularly, we have

$$\overline{T_3^*} = 0,$$

where we denote the vertical integration of a quantity $q(z^*)$ by

$$\overline{q} = \int_{-\infty}^{\infty} q(z^*)dz^*.$$

In principle, equation (121) can be solved to determine $n^*(z^*)$ directly. However, the computational procedure is rather involved since each evaluation of T_3^* requires the values of $n^*(z^*)$ at many different heights. Therefore, we look at two simple approximate models. In the first model $n^*(z^*)$ is assumed to have a Gaussian profile. This is certainly valid when the collision frequency is low and this model should serve as a reasonable approximation at low optical depths. In the second model we consider the high collision frequency limit, where the velocity ellipsoid is determined independently of the density profile.

IV.2. Gaussian Model

We assume that $n^*(z^*)$ follows a Gaussian profile

$$n^*(z^*) = \exp\left(-\frac{z^{*2}}{2H^{*2}}\right), \tag{134}$$

where H^* is the scale of the disk thickness in units of a. Since $Q_{23}^* = Q_{31}^* = 0$ identically, we may integrate equations (122) over z^* to obtain four equations:

$$-\frac{3}{2}\sqrt{2\pi}H^* c_1^{*2}\sin 2\delta = \overline{Q_{11}^*}, \tag{135-1}$$

$$\frac{3}{2}\sqrt{2\pi}H^* c_2^{*2}\sin 2\delta = \overline{Q_{22}^*}, \tag{135-2}$$

$$0 = \overline{Q_{33}^*}, \tag{135-3}$$

$$\frac{\sqrt{2\pi}}{4}H^*\left[(5-3\cos 2\delta)c_1^{*2} - (5+3\cos 2\delta)c_2^{*2}\right] = \overline{Q_{12}^*}. \tag{135-4}$$

A simple integration of equation (121) would yield the trivial result $\overline{T_3^*} = 0$. Hence we first multiply by z^* and then integrate over z^*:

$$\sqrt{2\pi}H^*\left[H^{*2} - c_3^{*2} + \frac{3\sqrt{2}}{2}G_s H^{*2} FF(0)\right] = \overline{T_3^* z^*}, \tag{136}$$

where the normal optical depth is defined by

$$\tau = \pi\left(\frac{a}{2}\right)^2 \int_{-\infty}^{\infty} n(z)dz = \frac{\pi}{4}n(0)a^3 \int_{-\infty}^{\infty} n^*(z^*)dz^*. \tag{137}$$

Equations (135) and (136) give a system of five algebraic equations which may be solved for $(c_1^*, c_2^*, c_3^*, \delta, H^*)$ at given values of the normal restitution coefficient ϵ_n and filling factor in the neutral plane $FF(0) = b(0)/4$. The vertical integration may be carried out analytically as follows: From equations (104), (120) and (134) we find

$$b(z^*) = b(0)\exp\left(-\frac{z^{*2}}{2H^{*2}}\right). \tag{138}$$

Substituting equation (138) into equation (108), multiplying by $n^*(z^*)n^*(z^* - \cos\vartheta_\lambda)$, and integrating over z^*, we find

$$\overline{Y\left[n^*(z^* - \cos\vartheta_\lambda/2)\right]n^*(z^*)n^*(z^* - \cos\vartheta_\lambda)} = \sqrt{\pi}H^*\exp\left[-\left(\frac{\cos\vartheta_\lambda}{2H^*}\right)^2\right]S, \tag{139}$$

where

$$S\left[b(0)\right] = \sum_{m=2}^{7}\sqrt{\frac{2}{m}}D_m\left[b(0)\right]^{m-2}. \tag{140}$$

Thus,

$$\overline{Q_{ij}^*} = \frac{\sqrt{\pi}\tau\kappa_n S}{(2\pi^2)^{3/2}c_1^*c_2^*c_3^*}\int_0^\pi d\vartheta_\lambda \sin\vartheta_\lambda \exp\left[-\left(\frac{\cos\vartheta_\lambda}{2H^*}\right)^2\right]\int_0^{2\pi} d\varphi_\lambda e^{-C}$$
$$\times\int_0^{\pi/2} d\vartheta \sin\vartheta\cos^2\vartheta\int_0^{2\pi} d\varphi\left[D_{ij}A^{-3}f_6(\zeta) + E_{ij}A^{-5/2}f_5(\zeta)\right]. \tag{141}$$

Similarly,

$$\overline{T_3^* z^*} = \frac{\sqrt{\pi}\tau\kappa_n S}{2(2\pi^2)^{3/2}c_1^*c_2^*c_3^*}\int_0^\pi d\vartheta_\lambda \sin\vartheta_\lambda\cos^2\vartheta_\lambda \exp\left[-\left(\frac{\cos\vartheta_\lambda}{2H^*}\right)^2\right]\int_0^{2\pi} d\varphi_\lambda e^{-C}$$
$$\times\int_0^{\pi/2} d\vartheta \sin\vartheta\cos^2\vartheta\int_0^{2\pi} d\varphi A^{-5/2}f_5(\zeta). \tag{142}$$

Our aim is now to solve the system of five nonlinear algebraic equations for given values of ϵ_n and $FF(0)$. The greatest problem lies in evaluating the collision integrals on the right hand sides of equations (135) and (136), each of which is a four dimensional integral. We begin by tabulating the complementary error function which appears in $f_5(\zeta)$ and $f_6(\zeta)$. From this table we find necessary

values of the function by the 4-point Lagrangian interpolation formula. The φ and φ_λ integrations are first carried out by the m-point trapezoidal rule. Since the integrands are periodic functions with period 2π, the trapezoidal rule yields results with excellent accuracy. The remaining ϑ and ϑ_λ integrations are done by the n-point Gaussian quadrature formula. Here the symmetry of the integrand with respect to $\vartheta_\lambda = \pi/2$ is taken into account in the ϑ_λ integration. For $m = n = 10$ we attain four-digit accuracy. Therefore, about 10000 evaluations of the integrand are required to find a value of the collision integral, which corresponds to about 6 CPU seconds on VAX 11/780 computers. Once we know how to evaluate collision integrals, we can use the five-dimensional Newton's method to find solutions to the system of equations.

We solved the system of equations (135) for various values of ϵ_n with and without the effect of self-gravity. The numerical results for $\epsilon_n = 0$ with self-gravity are presented in Figure 2. This is the most extreme case in the sense that the particle disk has the least thickness (both the completely inelastic collisions and self-gravity contribute to the small thickness). In general the velocity dispersions are decreasing functions of the central filling factor $FF(0)$ and in general $c_2^* < c_3^* < c_1^*$. At $FF(0) = 0$ where the particle collisions are completely neglected, we have numerically verified that $\delta = 0$ and $c_1^* = 2c_2^*$, a well-known fact for a collisionless disk in a Keplerian force field (Chandrasekhar, 1960). Only at $FF(0) = 0$ is the root mean square disk thickness equal to $H = H^* a = c_3^* a = c_3/\Omega$ and at higher filling factors the difference between H^* and c_3^* becomes significant. The tilt angle of the velocity ellipsoid δ increases with increasing filling factor. Since we are only interested in the liquid phase of the hard sphere system, we cut off the range of the filling factor at the crystallization point $FF(0) = 0.50$. We note here that this crystallization point was determined for a system of perfectly elastic hard spheres. (There have been no molecular dynamics data for inelastic hard spheres, but the

filling factor at the crystalization point for the latter system is probably lower than 0.50.) The optical depth is also plotted as a function of the filling factor. Within the assumptions of this model we conclude that the solid phase must exist in the system if the optical depth is larger than the critical value $\tau(0.50) = 0.28$. The critical optical depth actually depends on the choice of ϵ_n ($\tau[0.50] = 0.48$ for $\epsilon_n = 0.25$, 0.93 for $\epsilon_n = 0.50$) and it is larger if the self-gravity is neglected. The above conclusion provides the first quantitative prediction for the possible existence of the solid phase in the Saturnian B ring.

IV.3. High Collision Rate Limit

It is rather involved to solve the system of equations (121) and (122) to determine the vertical structure of the particle disk in general, but it is possible to solve equations (122) for $(c_1^*, c_2^*, c_3^*, \delta)$ in the formal limit when the density is near the close-packed density. In this limit the Enskog factor Y becomes very large, and if we neglect variations in the Enskog factor over distances of the order of the particle size, then equations (122) can only be solved if

$$R_{11} = R_{22} = R_{33} = R_{12} = 0, \tag{143}$$

where

$$R_{ij} = \int_0^{\pi} d\vartheta_\lambda \sin\vartheta_\lambda \int_0^{2\pi} d\varphi_\lambda e^{-C} \times \int_0^{\pi/2} d\vartheta \sin\vartheta \cos^2\vartheta \int_0^{2\pi} d\varphi \left[D_{ij} A^{-3} f_6(\zeta) + E_{ij} A^{-5/2} f_5(\zeta) \right]. \tag{144}$$

In practice the formal limit $Y \gg 1$ is not attained because a phase transition occurs first; however, at the phase transition $Y = 5.84$ is substantially larger than unity, which suggests that equations (143) provide a useful first approximation to

the behavior of densely packed rings. We shall call this the "high collision rate" limit. The system of equations (143) involves four unknowns $(c_1^*, c_2^*, c_3^*, \delta)$ and a parameter ϵ_n. The numerical solution to (143) is given in Figure 3. The value of δ is within 0.007% of $\pi/4$ for all ϵ_n and it seems likely that $\delta = \pi/4$ exactly. The inequality $c_2^* < c_3^* < c_1^*$ holds except in the vicinity of $\epsilon_n = 0$ and as ϵ_n approaches unity the velocity dispersions tend to diverge. In the limiting case of perfectly inelastic collisions $\epsilon_n = 0$, we find

$$c_1^* = 0.2999, \quad c_2^* = 0.2262, \quad c_3^* = 0.2245, \quad \delta = 0.7854. \tag{145}$$

It is to be noticed that this solution is valid at any height z^* so long as the approximations leading to equations (143) are valid. The value of δ is consistent with the value for a fluid ring when non-local effects are neglected ($\delta = \pi/4$, Goldreich and Tremaine, 1978), but in contrast to the fluid model the velocity dispersion tensor is not isotropic. The velocity ellipsoid is independent of height, consistent with the assumption (iv) of §**II.1**.

Substituting (145) into equation (121), we now determine the vertical density profile in the limit of high collision rate. Since the variation in density across a particle diameter is assumed to be slow, we have

$$\begin{aligned} &Y\left[n^*(z^* - \cos\vartheta_\lambda/2)\right] n^*(z^* - \cos\vartheta_\lambda) \\ \approx &Y\left[n^*(z^*)\right] n^*(z^*) - \cos\vartheta_\lambda \left\{ \frac{n^*(z^*)}{2} \frac{dY}{dn^*} + Y\left[n^*(z^*)\right] \right\} \frac{dn^*}{dz^*}. \end{aligned} \tag{146}$$

Upon integrating over ϑ_λ, the contribution from the first term vanishes so that we are led to the equation

$$z^* + \frac{3}{4} b(0) G_s \int_0^{z^*} n^*(x)dx = K \left\{ \frac{n^*(z^*)}{2} \frac{dY}{dn^*} + Y\left[n^*(z^*)\right] \right\} \frac{dn^*}{dz^*} - \frac{c_3^{*2}}{n^*} \frac{dn^*}{dz^*}, \tag{147}$$

where

$$\begin{aligned} K = &\frac{-n(0)a^3\kappa_n}{(4\pi)^{3/2} c_1^* c_2^* c_3^*} \int_0^\pi d\vartheta_\lambda \sin\vartheta_\lambda \cos^2\vartheta_\lambda \int_0^{2\pi} d\varphi e^{-C} \\ &\times \int_0^{\pi/2} d\vartheta \sin\vartheta \cos^2\vartheta \int_0^{2\pi} d\varphi A^{-5/2} f_5(\zeta). \end{aligned} \tag{148}$$

We differentiate equation (147) with respect to z^* to obtain a second order differential equation

$$1+\frac{3}{4}b(0)G_s n^*(z^*)=\frac{d^2}{dz^{*2}}\left[\frac{K}{2b(0)}\sum_{i=2}^{7}\frac{i}{i-1}D_i b^{i-1}(0)n^{*i-1}-c_3^{*2}\ln n^*\right], \quad (149)$$

which can be solved numerically with the boundary conditions $n^*(0)=1$ and $n^{*\prime}(0)=0$. In the limit where the self-gravity is negligible ($G_s=0$) the solution is analytic.

The resulting vertical density profile was computed by the fourth order Runge-Kutta method. The results are shown in Figure 4. Five curves correspond to the various choices of central filling factors $FF(0)$=0.1, 0.2, 0.3, 0.4, 0.5. We have included low values of $FF(0)$ for comparison even though the approximations leading to equations (143) and (144) are not accurate there. As $FF(0)$ increases, the deviation of the profile from Gaussian becomes significant. The density profile depends on the choice of ϵ_n and on whether the effect of overall self-gravity is included. In general larger $FF(0)$ and ϵ_n yield thicker disks. By switching off the self-gravity we can have even larger thickness. Once we have the density profile $n^*(z^*)$, we can determine the optical depth (equation [137]) and the disk thickness $\langle z^{*2}\rangle^{1/2}$, where

$$\langle z^{*2}\rangle=\frac{\overline{z^{*2}n^*}}{\overline{n^*}}. \quad (150)$$

For the Gaussian profile (134), $\langle z^{*2}\rangle^{1/2}=H^*$. The results are shown in Figure 5. For comparison, the corresponding results for the Gaussian model are also shown. In the low filling factor limit the Gaussian model is good, whereas it becomes progressively more inaccurate with increasing filling factor and the results in the high collision rate limit should provide a better approximation. It is encouraging that the two methods agree fairly well for intermediate values of the filling factor.

Finally, in Figure 6 the height-integrated kinematic viscosity in units of Ωa^2, the angular momentum luminosity in units of $3\pi r^2\Omega^2 a^2 n(0)$ and the height-

integrated ratio $\overline{R}$ (cf. equation [115]) are plotted as a function of $FF(0)$. These are explicitly given by

$$\overline{\nu^{T^*}} = \frac{\overline{\nu^T}}{\Omega a^2} = \frac{2}{3}\frac{\overline{p_{r\theta}^{T^*}}}{\overline{n^*}}, \tag{151}$$

$$L^{T^*} = \frac{L^T}{3\pi r^2(\Omega a^2)^2 n(0)} = \frac{2}{3}\overline{p_{r\theta}^{T^*}}, \tag{152}$$

$$\overline{R} = \frac{3\overline{p_{r\theta}^{T^*}}}{\overline{n^*}(c_1^{*2} + c_2^{*2} + c_3^{*2}) + \overline{p_{11}^{NL^*}} + \overline{p_{22}^{NL^*}} + \overline{p_{33}^{NL^*}}}, \tag{153}$$

where

$$2\overline{p_{r\theta}^{T^*}} = \overline{n^*}(c_1^{*2} - c_2^{*2})\sin 2\delta + (\overline{p_{11}^{NL^*}} - \overline{p_{22}^{NL^*}})\sin 2\delta + 2\overline{p_{12}^{NL^*}}\cos 2\delta. \tag{154}$$

In the low filling factor limit the results for the high collision rate limit do not vanish, but approach finite values, which correspond to the values given by equations (151)–(154) when the nonlocal pressure tensor is set to zero and c_i^* and δ are given by equation (145). As for the angular momentum luminosity and height-integrated kinematic viscosity, there is a general agreement between the two models in the intermediate filling factor range; we expect that the Gaussian model becomes more accurate at lower filling factors, while the results from the high collision rate limit should be more accurate at higher filling factors. The height-integrated ratio shows a fairly large disagreement at lower filling factors, but in the higher filling factor range where this ratio is more meaningful the two models seem to show a better agreement (relative error is 16% at $FF(0) = 0.5$).

Using an α-model for viscosity, Lightman and Eardley (1974) demonstrated that the inner region of a gaseous accretion disk around a compact object was unstable to clumping into rings. It has been conjectured that there may also be viscous instabilities in particle disk systems since there are regions where the angular momentum luminosity decreases with increasing optical depth (Lin and Bodenheimer, 1981; Lukkari, 1981; Ward, 1981), but the analytic and numerical

treatments by these authors are based on the assumption that $FF(0) \ll 1$. In our study the angular momentum luminosity is always an increasing function of $FF(0)$ and τ due to the presence of the nonlocal momentum flux density tensor which dominates the pressure tensor at higher densities. Therefore, we conclude that within the assumptions of our model there is no viscous instability and that it is not responsible for the multi-ringlet structure of the Saturnian B ring.

V. DISCUSSION

This work represents an attempt to apply the theory of liquids and dense gases to differentially rotating disks of inelastic particles. Our results are based on Enskog's (1922) theory, which has had only limited success in molecular dynamics because molecules are not hard spheres; however it is well suited for the study of particle disks.

Within the context of Enskog's theory the only major approximation is in the treatment of the vertical structure of the disk. We have investigated two models, which should be accurate in the limit of low and high filling factors. The models generally agree well at intermediate values of the filling factors (cf. Figures 5 and 6).

Our results confirm Brahic's (1977) claim that even disks of completely inelastic particles maintain a thickness which is of the order of the particle radius. We find that for completely inelastic particles the root mean square z-dispersion of the particle centers in units of the particle diameters is $\sqrt{\langle z^{*2} \rangle} = 0.2 - 0.3$ for value of the self-gravity parameter $G_s = 7.4$ which is appropriate for Saturn's B ring (Figure 5).

We find that the angular momentum luminosity is an increasing function of optical depth in rings composed of inelastic particles and hence there is no viscous instability.

We find that a dense ring can have filling factors which are large enough that a transition to the solid phase should occur (at least according to molecular dynamics experiments on elastic hard spheres). This result suggests that part of the Saturnian B ring may be in the solid phase. Naturally the whole B ring cannot be solid because on macroscopic scales it must rotate differentially with the Kepler shear. However, it may be that the complex ringlet structure in the B

ring represents adjacent solid and liquid phases. A system of this kind might well be stable, since if a solid annulus begins to grow, the shear in the adjacent liquid annuli increases, so that the liquid annuli are heated more strongly by viscous dissipation and tend to "melt" the edges of the solid annulus.

It is easy to imagine many ways in which the present work can be extended and improved. Particle spins (Shukhman, 1984), a particle size distribution (Shu and Stewart, 1985), a velocity-dependent restitution coefficient and gravitational scattering beween particles must all be included before a quantitative comparison with ring observations will be possible.

However, the present work at least provides a kinetic theory model which includes the effects of finite particle size and which can serve as a basis for comparison with numerical models of particle disks.

ACKNOWLEDGEMENTS

This research was supported in part by NSF grant AST-8412365. We thank Peter Goldreich for discussions. Our work was strongly influenced by the receipt of the preprint of the work of Shukhman (1984).

REFERENCES

BOGOLYUBOV, N. N. (1962). Problems of a Dynamical Theory in Statistical Physics. In *Studies in Statistical Mechanics* (J. de Boer and G. E. Uhlenbeck, Eds.), vol. **1**, pp. 1–118. North-Holland Publishing Company, Amsterdam.

BORDERIES, N., P. GOLDREICH, AND S. TREMAINE (1983). Perturbed Particle Disks. *Icarus* **55**, 124–132.

BORDERIES, N., P. GOLDREICH, AND S. TREMAINE. (1985). A Granular Flow Model for Planetary Rings. *Icarus*. To be published.

BRAHIC, A. (1977). Systems of Colliding Bodies in a Gravitational Field: I — Numerical Simulation of the Standard Model. *Astron. Astrophys.* **54**, 895–907.

CARNAHAN, N. F., AND K. E. STARLING (1969). Equation of State for Nonattracting Rigid Spheres. *J. Chem. Phys.* **51**, 635–636.

CHANDRASEKHAR, S. (1960). *Principles of Stellar Dynamics*, p. 159. Dover, New York.

CHAPMAN, S., AND T. G. COWLING. (1970). *The Mathematical Theory of Non-uniform Gases* (3rd Ed.), pp. 297–321. Cambridge University Press, Cambridge.

COHEN, E. G. D. (1983). Kinetic Theory of Non-equilibrium Fluids. *Physica* **118A**, 17–42.

COOK, A. F., AND F. A. FRANKLIN (1964). Rediscussion of Maxwell's Adams Prize Essay on the Stability of Saturn's Rings. *Astron. J.* **69**, 173–200.

DE LLANO, M., AND S. RAMÍREZ (1975). On the Fluid-Solid Transition of Hard Spheres. *J. Chem. Phys.* **62**, 4242–4243.

DEVORE, J. A. (1984). A Pressure Consistent BGY Equation: Virial Coefficients for Rigid Disks and Spheres. *J. Chem. Phys.* **80**, 1304–1308.

ENSKOG, D. (1922). Kinetische Theorie der Wärmeleitung, Reibung und Selbstdiffusion in gewissen verdichteten Gasen und Flüssigkeiten. *Kungliga Svenska Vetenskaps Akademiens Handlinger* **63**, No. 4.

GOLDREICH, P., AND S. TREMAINE (1978). The Velocity Dispersion in Saturn's Rings. *Icarus* **34**, 227–239.

HAFF, P. K. (1983). Grain Flow as a Fluid-Mechanical Phenomenon. *J. Fluid Mech.* **134**, 401–430.

HOOVER, W. G., AND F. H. REE (1968). Melting Transition and Communal Entropy for Hard Spheres. *J. Chem. Phys.* **49**, 3609–3617.

KIRKWOOD, J. G., E. K. MAUN, AND B. J. ALDER (1950). Radial Distribution Functions and the Equation of State of a Fluid Composed of Rigid Spherical Molecules. *J. Chem. Phys.* **18**, 1040–1047.

LIGHTMAN, A. P., AND D. M. EARDLEY (1974). Black Holes in Binary Systems: Instability of Disk Accretion. *Astrophys. J. Lett.* **187**, L1–L3.

LIN, D. N. C., AND P. BODENHEIMER (1981). On the Stability of Saturn's Rings. *Astrophys. J. Lett.* **248**, L83–L86.

LUKKARI, J. (1981). Collisional Amplification of Density Fluctuations in Saturn's Rings. *Nature* **292**, 433–435.

MAXWELL, J. C. (1890). On the Stability of the Motion of Saturn's Rings. In *The Scientific Papers of James Clerk Maxwell* (W. D. Niven, Ed.), vol. **1**, pp. 288–376. Cambridge University Press, Cambridge.

MISNER, C. W., K. S. THORNE, AND J. A. WHEELER. (1970). *Gravitation*, pp. 141–142. W. H. Freeman and Company, San Francisco.

REE, F. H., AND W. G. HOOVER (1967). Seventh Virial Coefficients for Hard Spheres and Hard Disks. *J. Chem. Phys.* **46**, 4181–4197.

SHU, F. H., AND G. R. STEWART. (1985). The Collisional Dynamics of Particulate Disks. Preprint.

SHUKHMAN, I. G. (1984). Collisional Dynamics of Particles in Saturn's Rings. *Astr. Zh.* **61**, 985–1004. Translated in *Sov. Astron. AJ* **28**, 574–585.

STEWART, G. R., D. N. C. LIN, AND P. BODENHEIMER. (1984). Collision-induced Transport Processes in Planetary Rings. In *Planetary Rings* (R. Greenberg and A. Brahic, Eds.), pp. 447–512. University of Arizona Press, Tucson.

TRULSEN, J. (1971). Towards a Theory of Jet Streams. *Astrophys. Space Sci.* **12**, 329–348.

WARD, W. R. (1981). On the Radial Structure of Saturn's Rings. *Geophys. Res. Letters* **8**, 641–643.

YOUNG, D. A., AND B. J. ALDER (1980). Studies in Molecular Dynamics. XVIII. The Square-well Phase Diagram. *J. Chem. Phys.* **73**, 2430–2435.

FIGURE CAPTIONS

Figure 1:— The definition of the Euler angles which give the configuration of the body system $(\hat{x}_b, \hat{y}_b, \hat{z}_b)$ relative to the fixed system $(\hat{x}, \hat{y}, \hat{z})$ whose origin is located at the center of the planet and whose $\hat{z}$ axis is normal to the ring plane.

Figure 2:— Solution to the system of five equations (135) and (136) when the normal restitution coefficient $\epsilon_n = 0$ and the overall self-gravity ($G_s = 7.4$) is included. The velocity dispersions c_1^*, c_2^*, c_3^*, transformation angle δ, disk thickness H^* (all solid lines) and the optical depth τ (dotted line) are plotted against the filling factor in the neutral plane $FF(0)$.

Figure 3:— Solution to the system of four equations (143) in the high collision rate limit. The velocity dispersions c_1^*, c_2^*, c_3^* and transformation angle δ are plotted against ϵ_n.

Figure 4:— The vertical density profile in the high collision rate limit when $\epsilon_n = 0$ and the overall self-gravity ($G_s = 7.4$) is included. The number density n^* is plotted against z^* for five cases: $FF(0) = 0.1, 0.2, 0.3, 0.4, 0.5$. The horizontal scale is in units of the particle diameter.

Figure 5:— Comparison between the Gaussian model and the high collision rate limit when the self-gravity factor is $G_s = 7.4$. The disk thickness and optical depth are plotted against $FF(0)$. The Gaussian model is dashed at high values of $FF(0)$ and the high collision rate limit is dashed at low values of $FF(0)$, to indicate schematically the region of validity of each model.

Figure 6:— Comparison between the Gaussian model and the high collision rate limit when the self-gravity factor is $G_s = 7.4$. The kinematic viscosity $\overline{\nu^{T^*}}$, angular momentum luminosity L^{T^*} and the ratio $\overline{R}$ are plotted against $FF(0)$. The Gaussian model is dashed at high values of $FF(0)$ and the high collision rate limit is dashed at low values of $FF(0)$, to indicate schematically the region of

validity of each model.

Figure 1

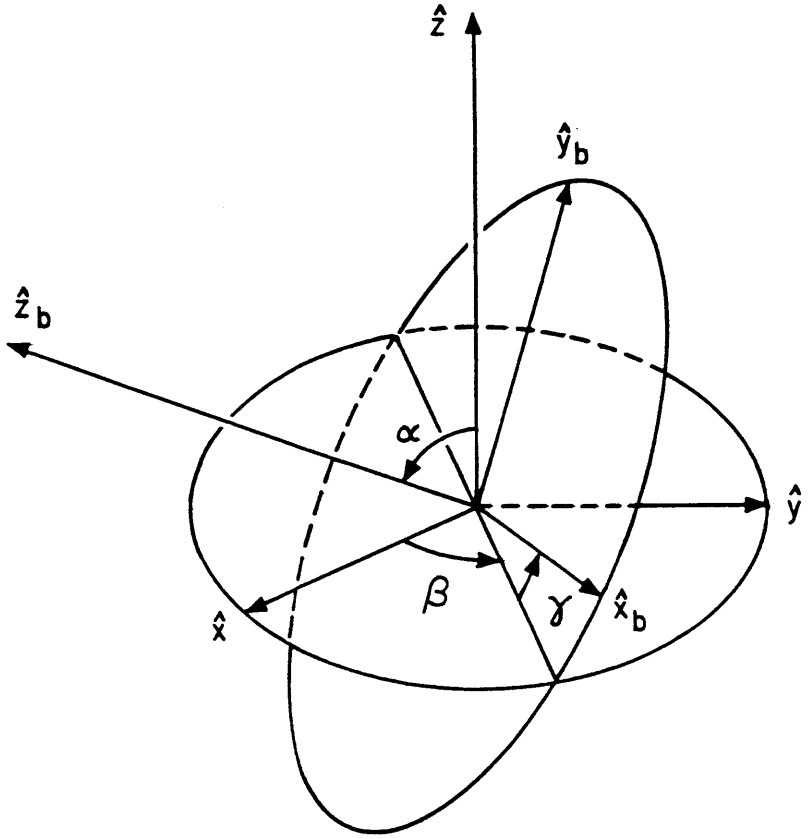

Figure 2

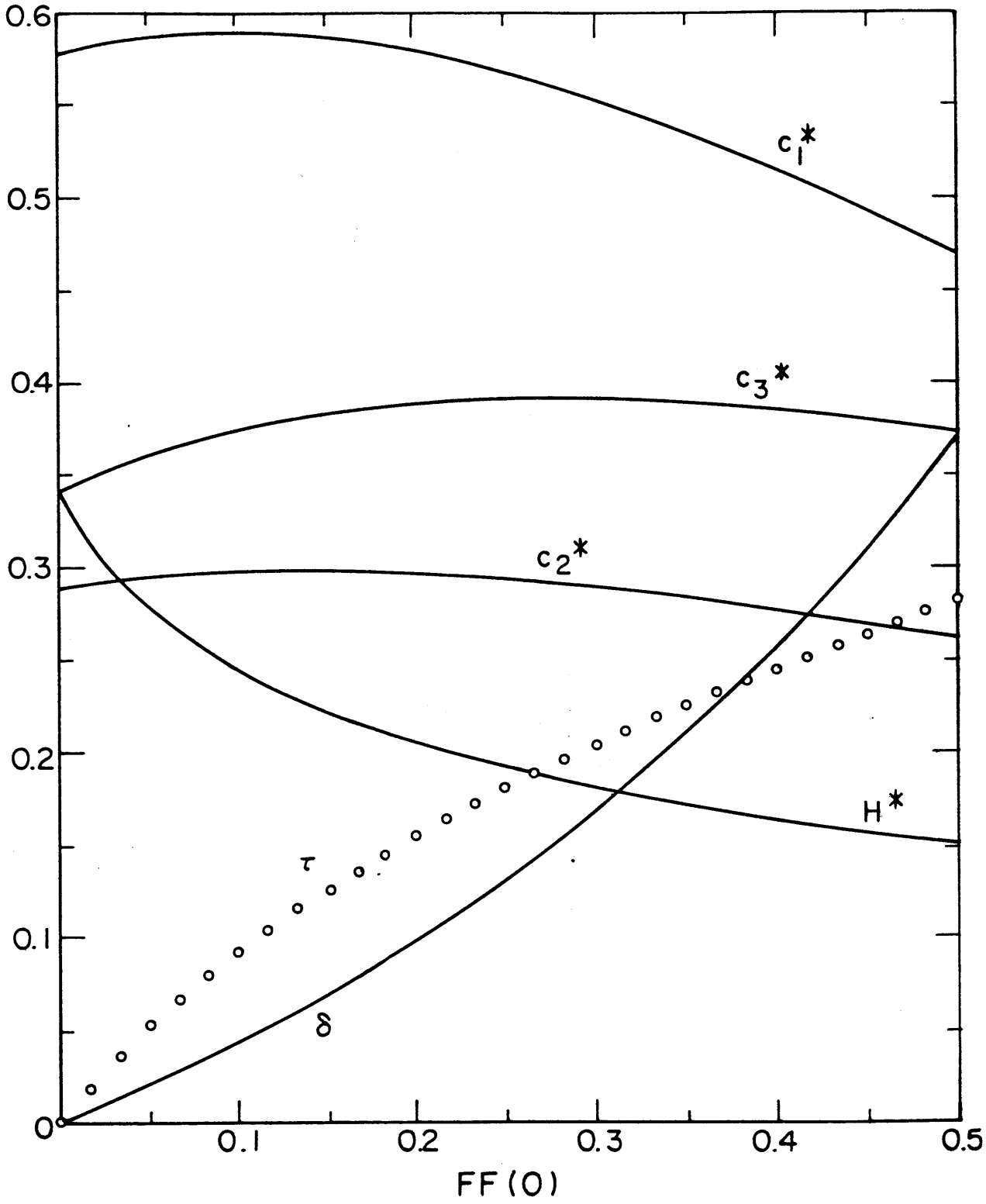

Figure 3

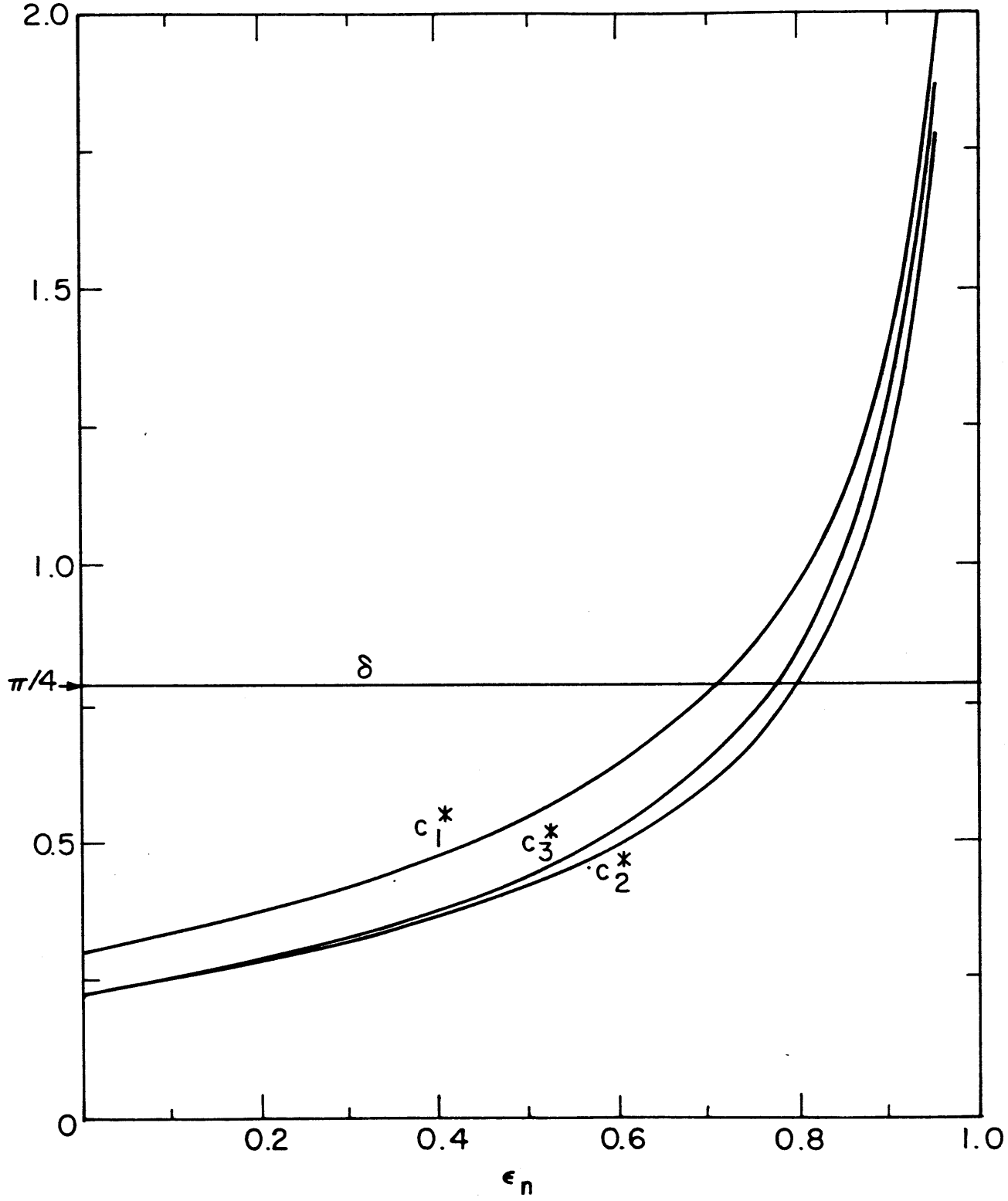

Figure 4

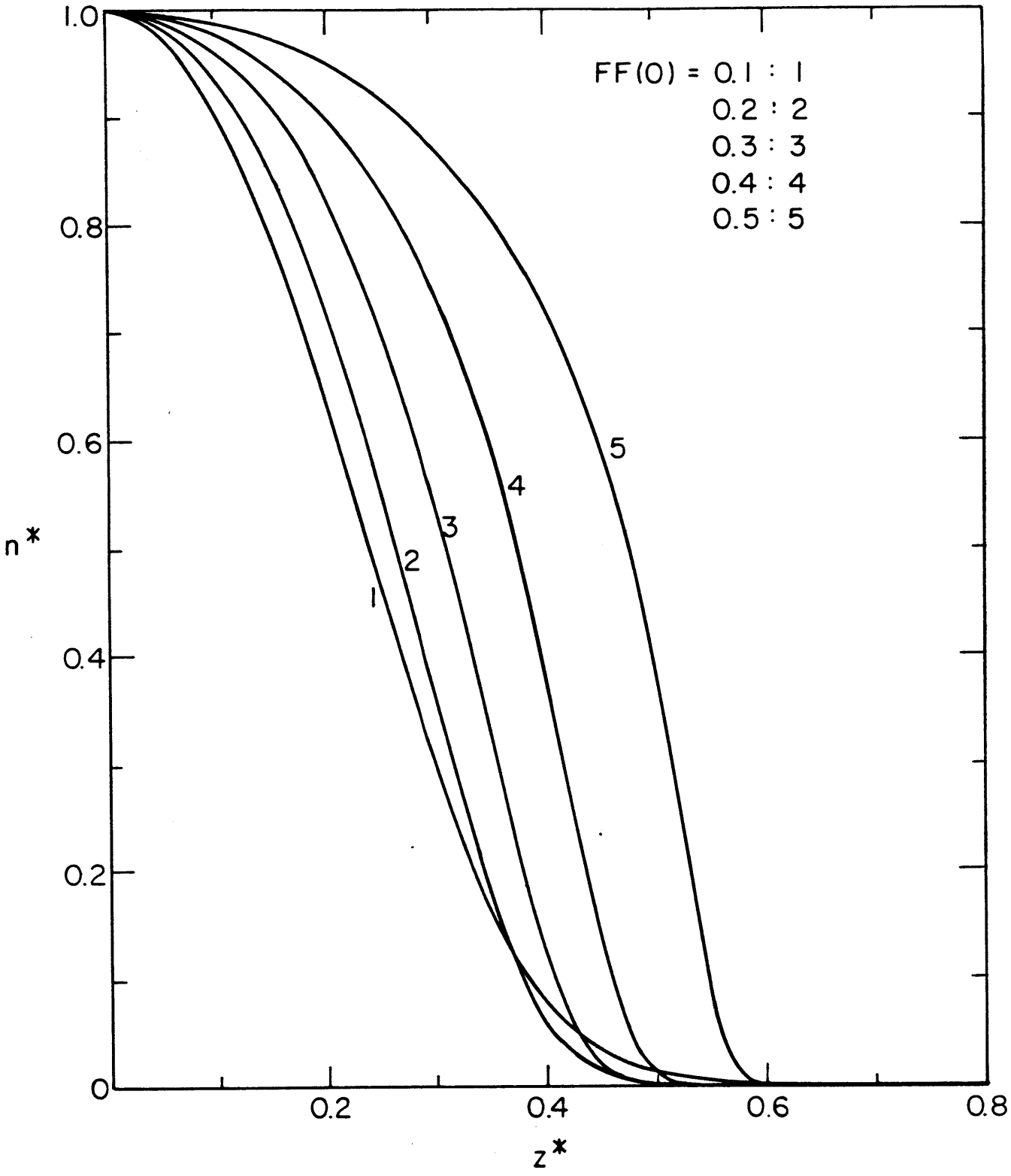

Figure 5

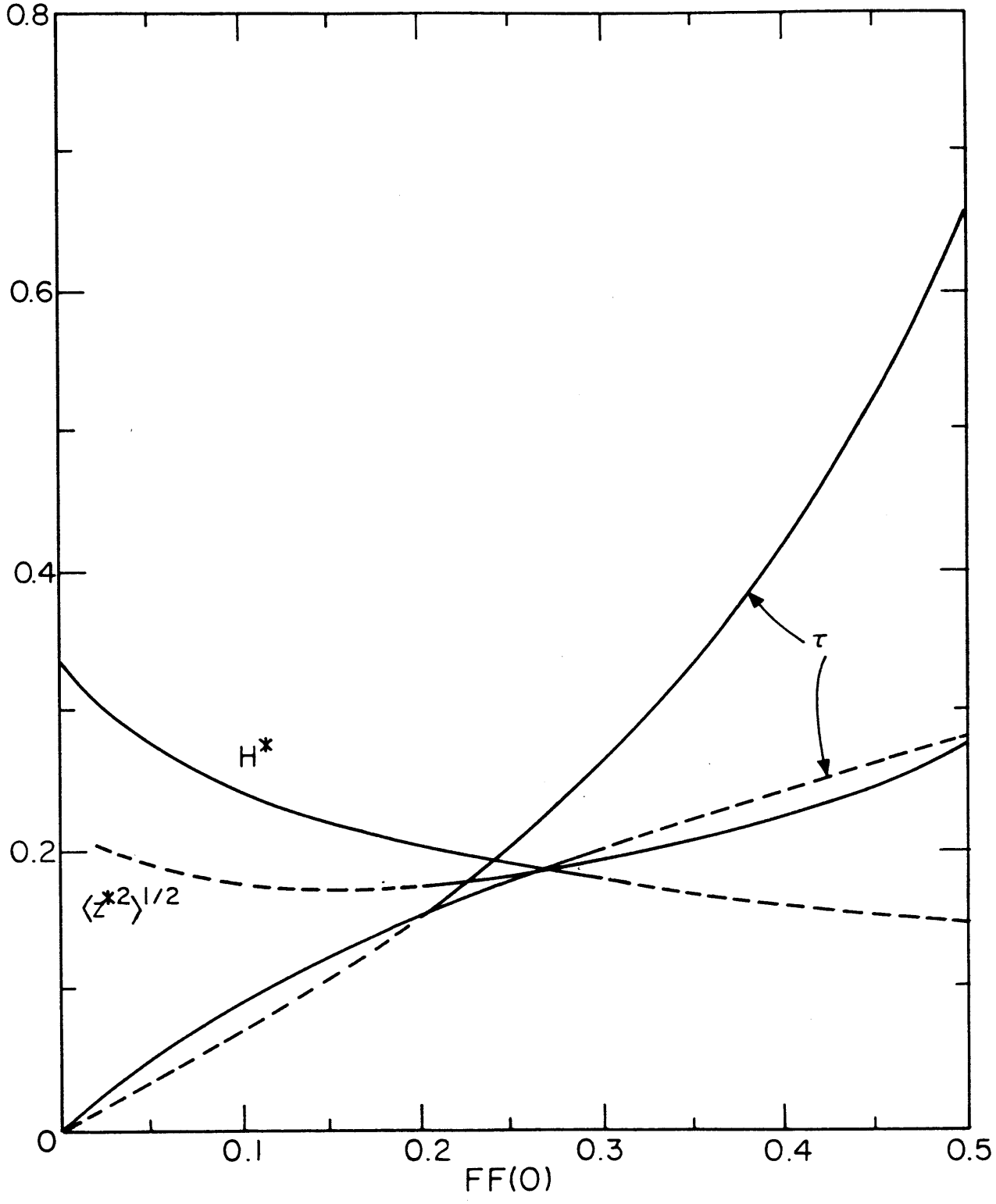

Figure 6

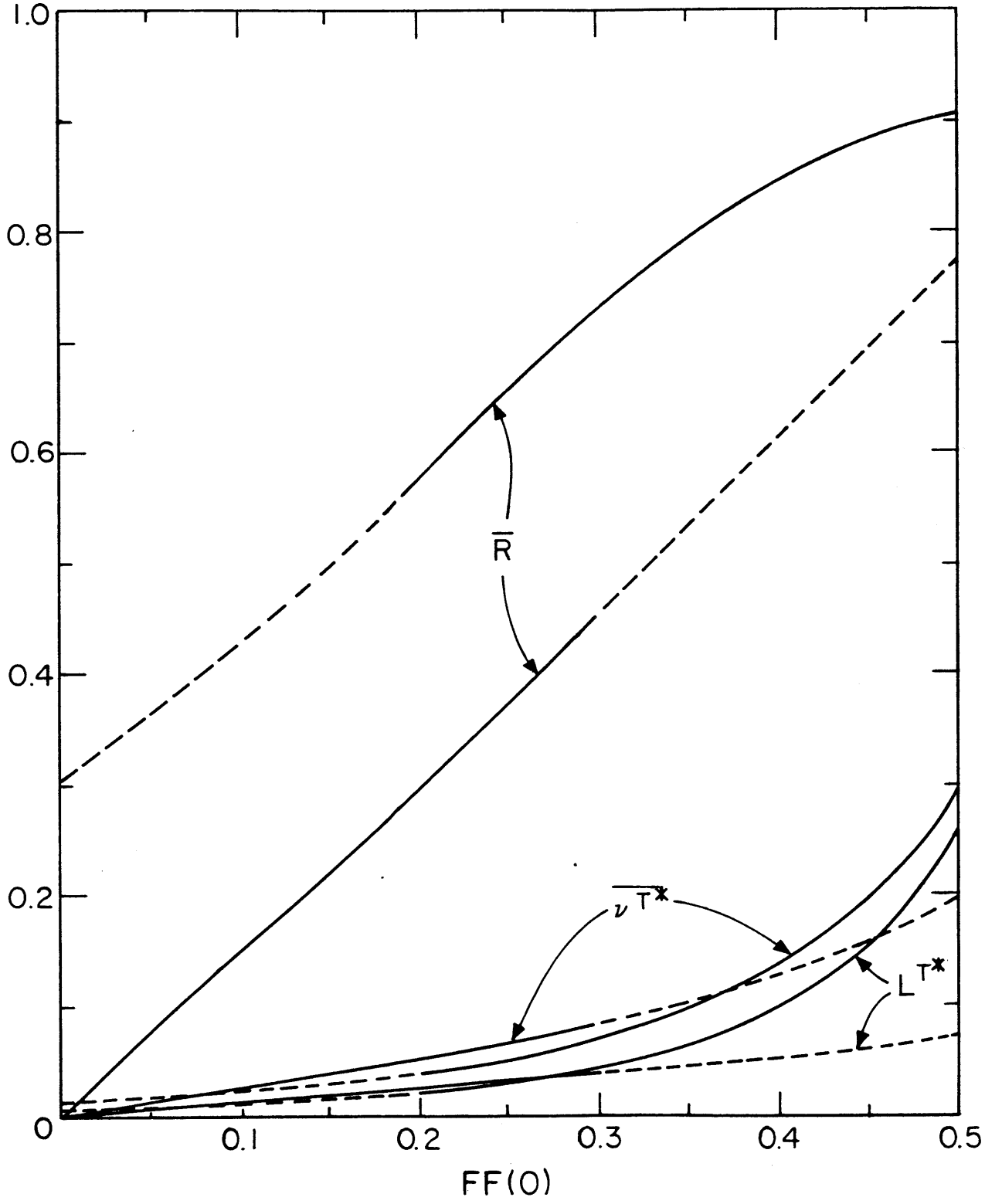

ACKNOWLEDGEMENTS

All of the work in this thesis began with suggestions by Professor Scott Tremaine and ended with his critical and patient reading of manuscripts written in my rather awkward English. It has been a pleasure having him as my thesis supervisor since March 5, 1982. Above all I have learned from him two important things: violation of time-reversal invariance in human life, i.e., how efficiently time should be spent, and how to write a paper. I am also grateful for the practical introduction to numerical analysis cordially provided by Professor Alar Toomre while I was engaged in the second project which had originally been initiated by himself some years ago. The work described in this thesis would have gone far more slowly and far less pleasantly had it not been for the support from these advisors.

I wish to thank my office-mates for bearing with me during periods of paper preparation, and especially Fran Justice for her efficient and thoughtful secretarial work.

I would like to thank the Rotary Foundation of Rotary International for a fellowship without which my graduate study at MIT would never have been initiated, and the MIT Physics Department for staff positions as teaching and research assistants which provided me with the major support for the past five years.

During my graduate school career Hideichi and Hideko Araki, and Katsutoshi and Chizuko Akagi have all contributed immeasurably to the health and well-being of my family. Finally I thank my girls Sayaka and Misato for cheerful encouragement, and my wife Yoko for reminding me, especially at difficult times, that we all walk by thanking the people we meet and that indeed we have been supported by Jun Araki, a great mountaineer, before and after his death.